UNIVERSITA' DEGLI STUDI DI PADOVA

Sede Amministrativa: Università degli Studi di Padova

Dipartimento di Tecnica e Gestione dei Sistemi Industriali

SCUOLA DI DOTTORATO DI RICERCA IN: INGEGNERIA INDUSTRIALE

INDIRIZZO: MECCATRONICA E SISTEMI INDUSTRIALI

XX° CICLO

CORRELATION BETWEEN PROCESSING AND QUALITY OF ALUMINIUM ALLOY CASTINGS

CORRELAZIONE TRA PARAMETRI DI PROCESSO DI FONDERIA E QUALITA' DEI PRODOTTI

Direttore della Scuola: Ch.mo Prof. Paolo F. Bariani

Supervisore: Ch.mo Prof. Franco Bonollo

Dottorando: Giulio Timelli

31 GENNAIO 2008

To my Mum with love

"…Così tra quest'immensità s'annega il pensier mio:
e il naufragar m'è dolce in questo mare."
G. Leopardi, "L'infinito", 1819

PREFACE

This doctoral thesis is the result of three years full-time studies, including courses and research at the University of Padova from January 2005 to December 2007. The experimental work was carried out at the Department of Management and Engineering (DTG), Vicenza (Italy), and at the Department of Materials Science and Engineering at Norwegian University of Science and Technology (NTNU), Trondheim (Norway), during a six months visit from March to August 2006.

Professor Franco Bonollo was the principal supervisor. Prof. Otto Lohne and Prof. Lars Arnberg were supervisors during the research period at NTNU.

The results were reported and published throughout the three years period and the articles included in the thesis are presented in the form they were submitted for publication or printed. The thesis consists of two parts:

PART 1 is intended to give the reader sufficient background on the influence of processing and process parameters on the quality of aluminium alloy castings, physical fundamentals and literature review as well as industrial challenges, motivation and goals.

PART 2 is a collection of six articles dealing with different aspects of aluminium foundry. The manuscript included in this section are:

Article 1
The effects of modification and solidification rate on aluminium-silicon cast alloys
A. Manente, G. Timelli and F. Bonollo, Submitted for publication in Journal of Materials Science, 2007.

Article 2
On the fluidity of aluminium alloy diecastings
G. Timelli and F. Bonollo, Submitted for publication in International Journal of Cast Metals Research, 2007.

Article 3
Permanent mold casting of aluminium alloys: correlation among processing, microstructure and simulation
F. Bonollo, G. Timelli, N. Gramegna and B. Molinas, Proceeding of 3rd International Conference High Tech Die Casting, Vicenza, Italy, September 21-22, 2006.

Article 4
Impact behaviour of A356 alloy for low pressure die casting automotive wheels
M. Merlin, G. Timelli, F. Bonollo and G.L. Garagnani, Submitted for publication in Journal of Materials Processing Technology, 2007.

Article 5
Quality mapping of aluminium alloy diecastings
G. Timelli and F. Bonollo, Presented at the 3rd International Conference High Tech Die Casting,Vicenza, Italy, September 21-22, 2006. Also submitted for publication in Metallurgical Science and Technology, 2007.

Article 6
Effect of solution heat treatments on the microstructure and mechanical properties of a die-cast AlSi7Mg alloy
G. Timelli, O. Lohne, L. Arnberg and H.I. Laukli, Submitted for publication in Metallurgical and Materials Transactions A, 2007.

In addition to the articles included in the thesis, parts were presented in the following publications:

1. **Microstructure, defects and properties in aluminium alloys casting: a review**, G. Timelli and F. Bonollo, Proc. 6th World Aluminium Two Thousand Congress, Firenze, Italy, March 13-17, 2007.

2. **Influence of microstructure and casting parameters on impact strength of low-pressure cast A356 wheels**, G. L. Garagnani, F.Piasentini, M.Merlin, F.Bonollo and G.Timelli, Presented at the 3rd International Conference High Tech Die Casting, Vicenza, Italy, September 21-22, 2006.

3. **Effect of mechanical mould vibration on the characteristics of cast metal matrix composites**, G. Timelli, P. Ferro and F. Bonollo, Presented at the 8th Seminar on Experimental Techniques and Design in Composite Materials (ETDCM8), Sant'Elmo Beach Hotel – Castiadas – Costa Rei, Italy, October 3-6, 2007.

4. **Numerical and experimental investigations of high-pressure die-cast aluminium matrix composites**, N. Gramegna, F. Bonollo and G. Timelli, Presented at the 8th Seminar on Experimental Techniques and Design in Composite Materials (ETDCM8), Sant'Elmo Beach Hotel – Castiadas – Costa Rei, Italy, October 3-6, 2007.

5. **Microstructural evolution in semi-solid A356 alloy during partial remelting**, E. Della Rovere, F. Bonollo, G. Timelli and Sergio Lupi, Presented at the European Congress on Advanced Materials and Process (EUROMAT 2007), Nürnberg, Germany, September 10-13, 2007.

6. **Die cast Aluminium automotive components: mapping of the quality**, F. Bonollo, G. Timelli, N. Gramegna, E.W. Blümcke, S. Nissle, E. Hepp, P. Bernbeck, V. Seefeldt and U. Weiss, Presented at the International Conference on CAE and Computational Technologies for Industry, Lecce, Italy, October 5-8, 2005.

7. **Sistema integrato di provini per lo studio della microstruttura e del comportamento meccanico di leghe leggere pressocolate**, G. Timelli, F. Grosselle, F. Bonollo, F. Voltazza, L. Capra, N. Gramegna and E. Della Corte, Presented at Alumotive 2007, Modena, Italy, October 18-20, 2007.

8. **La simulazione numerica dei trattamenti termici**, P. Ferro, A. Tiziani, F. Bonollo, G. Timelli, Submitted for publication in Trattamenti e finiture, 2007.

In addition, the following M.S. thesis have been supervised:

1. M. Barutta, **Meccanismi di frattura nelle leghe Al-Si da fonderia**, supervisors: F. Bonollo, G. Timelli, A.A. 2005-2006.

2. M. Ceolato, **Rassegna delle caratteristiche a fatica delle leghe di alluminio da fonderia**, supervisors: F. Bonollo, G. Timelli, A.A. 2007-2008.

3. C. Dal Bianco, **Rassegna delle caratteristiche termiche ed elettriche delle leghe di alluminio**, supervisors: F. Bonollo, G. Timelli, A.A. 2004-2005.

4. B. Faresin, **Influenza di Stagno e Piombo sulle proprietà di leghe d'alluminio (6XXX) estruse**, supervisors: F. Bonollo, G. Timelli, C. Fantinel, A.A. 2004-2005.

5. F. Groppo, **Caratterizzazione meccanica e microstrutturale di una lega pressocolata di alluminio eutettica degasata**, supervisors: F. Bonollo, G. Timelli, A.A. 2007-2008.

6. O. Panozzo, **Caratterizzazione meccanica e microstrutturale di getti pressocolati in lega di alluminio**, supervisors: F. Bonollo, G. Timelli, A.A. 2007-2008.

7. M. Sadocco, **Pressocolata di leghe di alluminio: validazione delle simulazioni di processo e sviluppo di modelli per il riconoscimento delle porosità**, supervisors: F. Bonollo, G. Timelli, A.A. 2004-2005.

8. M. Scandiuzzi, **Al-alloy casting: evaluation of the external costs during the life cycle of a product**, supervisors: F. Bonollo, G. Timelli, A.A. 2005-2006.

9. N. Tomanin, **Messa a punto del ciclo produttivo di una ruota in lega AlSi7Mg0.3**, supervisors: F. Bonollo, G. Timelli, G. Marangoni, A.A. 2005-2006.

10. A. Urbani, **Correlazioni tra parametri di processo e proprietà meccaniche di getti pressocolati in leghe di alluminio**, supervisors: F. Bonollo, G. Timelli, A.A. 2006-2007.

11. J. Zennari, **Sviluppo di un database sulle caratteristiche a fatica di leghe di alluminio da fonderia**, supervisors: F. Bonollo, G. Timelli, A.A. 2007-2008.

SUMMARY

The influence of processing and process parameters plays a key role for the Aluminium foundry and transport industries as it affects the *quality* and soundness of the cast products. Particularly, the choice of a process chain in Aluminium foundry, otherwise of process parameters, influences the reject rates, hence casting costs, the process yield and the production rate. The process chain in Aluminium foundry is a complex sequence of processes and the final casting quality depends on many parameters. Several aspects of this subject are still not fully understood. The motivation of the research presented in this doctoral thesis work was, therefore, to fill this gap in knowledge. The study has aimed at understanding the influence of various process and process parameters of foundry on the *quality* of aluminium alloy castings and, in particular, Al-Si based castings.

A literature review and a sufficient background of previously reported results on the influence of processing and process parameters on the *quality* of aluminium alloy castings, physical fundamentals as well as industrial challenges, motivation and goals were carried out.

Special attention in Aluminium process chain has been given to:

The modification of aluminium-silicon cast alloys: before casting aluminium alloys, the molten metal can be treated in order to improve the microstructure and properties of alloys by addition of small quantities of certain “modifying” elements.

The pouring of molten metal into the mould: this is one of the critical steps in foundry technology, since the behaviour of the liquid and its subsequent solidification and cooling determine whether the cast shape will be properly formed, internally sound and free from defects.

The chill casting processes, such as gravity, low-pressure and high-pressure die casting processes: the essential feature of chill casting is the use of permanent metal moulds, into which the molten alloy is either poured directly or injected under pressure, giving rise to the separate processes of gravity and low/high pressure die casting. Permanent moulds offer obvious advantages in terms of simplicity of production for large quantities of parts, but are subject to limitations yet to be discussed.

The heat treating process applied to high-pressure die castings: conventional die castings are utilised to produce many products but unfortunately the presence of porosity limits the application. In addition to porosity, the microstructure inherent with conventional die casting could not meet the mechanical requirements needed for many applications. Subsequent heat treating, which can positively alter the microstructure, is rarely possible due to defects that emerge during thermal processing, such as blistering.

SOMMARIO

L'influenza del processo e dei corrispondenti parametri utilizzati giocano un ruolo chiave nella Fonderia d'alluminio e nell'industria dei trasporti in genere, poiché influenzano la *qualità* e l'integrità dei getti prodotti. In particolare, le scelte di una determinata catena produttiva nella fonderia di alluminio o dei parametri di processo influenzano la quantità di scarti e di conseguenza il costo finale del getto, la resa del processo e la cadenza produttiva. La catena di processo in fonderia è una sequenza complessa di processi e la qualità finale dei getti dipende da molti parametri; infatti, molti aspetti non sono ancora del tutto noti. Obiettivo di questo lavoro di dottorato di ricerca era perciò supplire a queste lacune. Scopo del presente lavoro è studiare l'influenza di vari processi e parametri di processo nella fonderia d'alluminio sulla *qualità* dei getti realizzati e in particolare getti realizzati in lega Alluminio-Silicio.

In prima analisi, è stata condotta una recensione della letteratura sull'influenza del processo e dei parametri di processo sulla qualità di getti in lega d'alluminio, sugli aspetti fisico-metallurgici così come su quelli industriali.

Nel presente lavoro è stata posta particolare attenzione a:

La modifica delle leghe alluminio-silicio da fonderia: prima della colata, il metallo liquido può essere trattato al fine di migliorare la microstruttura e le proprietà finali della lega attraverso l'aggiunta di piccole quantità di elementi "modificanti".

La colata del metallo liquido all'interno di uno stampo: questo è uno degli aspetti critici in fonderia, poiché il comportamento del metallo liquido e la sua successiva solidificazione determinano se il getto finale sarà stato completamente definito, integro ed esente da difetti.

I processi di colata in gravità, bassa pressione e pressocolata delle leghe d'alluminio: una tecnica frequentemente utilizzata nella fonderia delle leghe leggere è l'utilizzo di stampi in acciaio/ghisa, nei quali il metallo liquido può essere direttamente colato o iniettato sotto pressione; il diverso metodo utilizzato nel colare il metallo all'interno dello stampo dà vita a differenti processi di colata, rispettivamente a gravità, bassa pressione e pressocolata. L'utilizzo di stampi permanenti in acciaio/ghisa offre vantaggi in termini di elevati volumi produttivi, ma è soggetto ad alcune limitazioni discusse nel presente lavoro.

Il trattamento termico applicato a getti pressocolati in lega di alluminio: la pressocolata è utilizzata nella produzioni di massa ma sfortunatamente l'elevata presenza di porosità all'interno dei getti ne limita l'applicazione. In aggiunta alle porosità, la microstruttura di getti pressocolati potrebbe non garantire i requisiti meccanici richiesti in molte applicazioni. Il trattamento termico (solubilizzazione, tempra e invecchiamento), che alterando la microstruttura, migliora le caratteristiche meccaniche finali, è raramente applicabile a getti pressocolati a causa della presenza di porosità, soprattutto di natura gassosa, che espandendosi durante il trattamento termico (*blistering*) compromettono la qualità superficiale del getto stesso.

CONTENTS

PART 1

INTRODUCTION

INTRODUCTION

Aluminium is one of the few metals that can be cast by all of the processes used in casting metals. These processes, in decreasing order of amount of aluminium casting, are: die casting, permanent mould casting, sand casting (green sand and dry sand), plaster casting, investment casting, and continuous casting. Other processes such as lost foam, squeeze casting, and hot isostatic pressing are also mentioned.

There are many factors that affect selection of a casting process for producing a specific aluminium alloy part. The most important factors for all casting processes are:

- *Feasibility* and *cost* factors;
- *Quality* factors.

In terms of feasibility, many aluminium alloy castings can be produced by any of the available methods. For a considerable number of castings, however, dimensions or design features automatically determine the best casting method. Because metal moulds weigh from 10 to 100 times as much as the castings they are used in producing, most very large cast products are made as sand castings rather than as die or permanent mould castings. Small castings usually are made with metal moulds to ensure dimensional accuracy.

Quality factors are also important in the selection of a casting process. When applied to castings, the term *quality* refers to both degree of soundness (freedom from porosity, cracking, and surface imperfections) and levels of mechanical properties (strength and ductility). However, it should be kept in mind that in die casting, although cooling rates are very high, air tends to be trapped in the casting, which gives rise to appreciable amounts of porosity. Extensive research has been conducted to find ways of reducing such porosity; however, it is difficult if not impossible to eliminate completely, and die castings often are lower in strength than low-pressure or gravity-fed permanent mould castings, which are more sound in spite of slower cooling.

The objective of this doctoral thesis is to develop new knowledge on the influence of processing and process parameters on the quality of aluminium alloy castings. Special attention has been given to:

- *The modification of aluminium-silicon cast alloys*; before casting aluminium alloys, the molten metal can be treated in order to improve the microstructure and properties of alloys by addition of small quantities of certain “modifying” elements.

- *The pouring of molten metal into the mould*; this is one of the critical steps in foundry processes, since the behaviour of the liquid and its subsequent solidification and cooling determine whether the cast shape will be properly formed, internally sound and free from defects.

- *The gravity, low-pressure and high-pressure die casting processes*; the essential feature of die casting is the use of permanent metal moulds, into which the molten alloy is either poured directly or injected under pressure,

giving rise to the separate processes of gravity, low- and high-pressure die casting. Permanent moulds offer obvious advantages in terms of simplicity of production for large quantities of parts, but are subject to limitations yet to be discussed.

- *The heat treating process applied to high-pressure die castings*; conventional die casting is utilised to produce many products but unfortunately the presence of porosity limits the application. In addition to porosity, the microstructure inherent with conventional die casting could not meet the mechanical requirements needed for many applications. Subsequent heat treating, which can alter the microstructure, is rarely possible due to defects that emerge during thermal processing, such as blistering.

To accomplish this, a theoretical and literature background of previous investigations have been briefly reported in order to establish a basis for the present studies.

1. THEORETICAL AND LITERATURE BACKGROUND

1.1. Aluminium casting alloys

Aluminium casting is dominated by the automotive industry.[1,2] Roughly two thirds of all aluminium castings are automotive where the use of aluminium castings continues to grow at the expense of iron castings.[3] Although aluminium castings are significantly more expensive than ferrous castings, there is a continuing market requirement to reduce vehicle weight and to increase fuel efficiency.[1-3] It is this requirement which drives the replacement of ferrous parts by aluminium.

Aluminium castings are widely used in cars for engine blocks, heads, piston, inlet manifolds, steering boxes, brackets, wheels etc. The potential for further use of aluminium in automotive applications is considerable. European cars in 1992 had 50-60 kg Al castings and this doubles by year 2000.[4]

When aluminium alloys are cast, there are many potential sources of defects which can harm the quality of the cast part.[5-8] All aluminium alloys are subject to:

- Shrinkage defects; Al alloys shrink by 3.5-6% during solidification (depending on alloy type).
- Gas porosity; molten Al readily picks up hydrogen which is expelled during solidification giving rise to porosity.
- Oxide inclusions; molten Al exposed to air immediately oxides forming a skin of oxide which may be entrained into the casting.

Because of these potential problems aluminium castings, like all castings, suffer from variable mechanical properties which can be described by a distribution curve.[6,7,9-11] The mechanical properties used by the designer of the casting must take the distribution curve into account. If, for example, the process mean tensile strength for a cast alloy is 200 MPa, the designer must use a lower value, taking into account the variability of properties. If the spread of the distribution curve is reduced, then a higher design strength can be used, considering a higher reproducibility of casting process. The strength of castings does not follow the normal bell-shaped distribution curve.[6,9] Figure 1 shows the range of tensile strengths found in an AlSi7Mg alloy cast using various pouring methods.[12,13] In all cases the process mean tensile strength is about 260 MPa, but the distribution is different.

Examination of the fracture surface of the low strength bars showed massive oxide fragments indicating that inclusions in the unfiltered castings were responsible for the low mechanical properties. Filtration of the metal eliminates the inclusions allowing the design strength to be increased to around 230 MPa. The double band appearance of the histrograms is interpreted as indicating that more than one defect type is acting to control the behaviour at the fracture.

It is by reducing the variability of properties of castings that the greatest progress has been made in recent years. This has allowed designers to have greater confidence in castings so that thinner sections and lower weight components can be used. The stages where the greatest improvements have been and can be made are:

- The pouring of molten metal into the mould;
- The treatment of molten metal;
- The casting technology, involving gravity, low-pressure and high-pressure die casting processes;
- The heat treating processes.

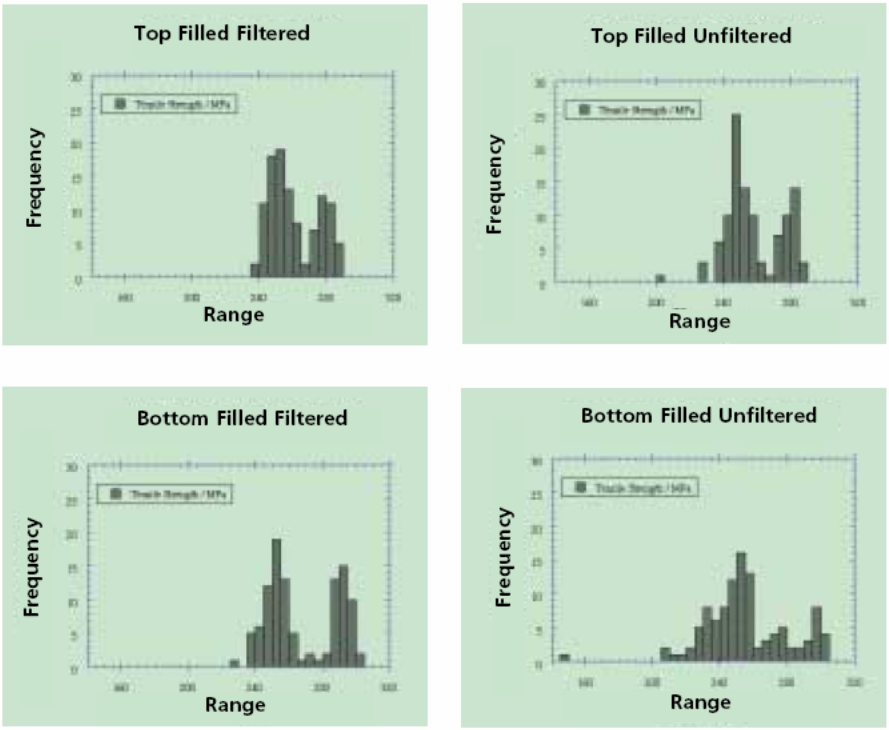

Fig. 1. Histrograms showing the distribution of tensile strength of AlSi7Mg alloy cast in various ways.[12]

Chill casting (into metal moulds) has inherently a greater possibility of producing higher quality than sand casting because the higher rate of solidification reduces pore size and refines grain size.[14-16] The highest quality components are produced using filtered metal, non-turbulently introduced into metal moulds and solidified under high external pressure to minimise porosity. While it is not always possible to use high external pressure during solidification, the understanding of the origins of defects in aluminium castings and their reduction by attention to degassing, metal treatment and filtration has greatly improved the general quality of castings in recent years.[10-13]

1.2. Casting alloys

There is a large and confusing range of casting alloys in use worldwide, defined by the National Specifications of the major industrial countries. Unfortunately there is little correspondence between the Standard Alloys used in different countries.
The European Standard for Aluminium Casting Alloys is the EN 1706 standard.[17] UNI EN 1706:1999 specifies the chemical composition of 37 alloys. For each alloy, mechanical properties are specified only for the commonly used methods of casting and for commonly used tempers.[17] Refer to UNI EN 1706:1999 for full details.
While Table 1 lists the alloy designation of alloys commonly used for chill casting, Table 2 shows mechanical properties of some alloys.

Table 1: UNI EN 1706:1999 alloys commonly used for chill casting.[17]

Alloy group	*Alloy designation*	
	Numerical	*Chemical symbols*
Al Cu	EN AC-21000	EN AC-Al Cu4MgTi
	EN AC-21100	EN AC-Al Cu4Ti
Al SiMg Ti	EN AC-41000	EN AC-Al Si2MgTi
Al Si7Mg	EN AC-42000	EN AC-Al Si7MgTi
	EN AC-42100	EN AC-Al Si7Mg0.3
	EN AC-42200	EN AC-Al Si7Mg0.6
Al Si10M	EN AC-43000	EN AC-Al Si10Mg(a)
	EN AC-43100	EN AC-Al Si10Mg(b)
	EN AC-43200	EN AC-Al Si10Mg(Cu)
	EN AC-43300	EN AC-Al Si9Mg
Al Si	EN AC-44000	EN AC-Al Si11
	EN AC-44100	EN AC-Al Si12(b)
	EN AC-44200	EN AC-Al Si12(a)
AlSi5Cu	EN AC-45000	EN AC-Al Si6Cu4
	EN AC-45200	EN AC-Al Si5Cu3Mn
	EN AC-45300	EN AC-Al Si5Cu1Mg
Al Si9Cu	EN AC-46200	EN AC-Al Si8Cu3
	EN AC-46400	EN AC-Al Si9Cu1Mg
	EN AC-46600	EN AC-Al Si7Cu2
Al Si(Cu)	EN AC-47000	EN AC-Al Si12(Cu)
Al Mg	EN AC-51000	EN AC-Al Mg3(b)
	EN AC-51100	EN AC-Al Mg3(a)
	EN AC-51300	EN AC-Al Mg5
	EN AC-51400	EN AC-Al Mg5(Si)
Al ZnMg	EN AC-71000	EN AC-Al Zn5Mg

Table 2: Mechanical properties of commonly used UNI EN 1706:1999 alloys.[17]

Alloy designation *Numerical*	*Chemical Symbols*	*Casting method*	*Temper*	*Tensile strength (MPa)*	*Proof stress (MPa)*	*Elong. (%)*	*Brinell HBS*
EN AC-42000	AlSi7Mg	sand	F	140	80	2	50
		sand	T6	220	180	1	75
		chill	F	170	90	2.5	55
		chill	T6	260	220	1	90
		sand	T64	240	200	2	80
EN AC-44100	AlSi12(b)	sand	F	150	70	4	50
		chill	F	170	80	5	55
EN AC-45200	AlSi5Cu3Mn	sand	F	140	70	1	60
		sand	T6	230	200	<1	90
		chill	F	160	80	1	70
		chill	T6	280	230	<1	90
EN AC-46600	AlSi7Cu2	sand	F	150	90	1	60
		chill	F	170	100	1	75
EN AC-46500	AlSi9Cu3(Fe)(Zn)	pressure d/c	F	240	140	<1	80

1.3. The effect of alloying elements

Silicon

Pure aluminium melts at 660.4°C, it is not suitable for casting and is only used for electrical applications (where high conductivity is essential), and a few other special applications. Most casting alloys contain silicon as the major alloying element. Silicon forms an eutectic with aluminium at 12.6%, 577°C.[18] Silicon additions improve casting characteristics by improving fluidity, feeding and hot tear resistance. The silicon-rich phase is hard, so the hardness of the alloy is increased with Si content but ductility and machinability are reduced.
Typical silicon levels of popular casting alloys are:

Alloy	*Si content*	*Typical freezing range (°C)*
Low silicon	4–6%	625–525
Medium silicon	7.5–9.5%	615–550
Eutectic alloys	10–13%	575–565
Special hypereutectic alloys	> 16%	650–505

The eutectic alloys, having a short freezing range, solidify with primary shrinkage. They are good for thin section castings. Where higher strength is needed, the lower silicon alloys are used. The hypereutectic alloys are difficult to machine, they are used for wear-resistant applications such as pistons.

Copper

Improves strength, hardness, machinability and thermal conductivity. Heat treatment is most effective with 4-6% Cu alloys. Copper decreases castability and hot tear resistance together with corrosion resistance.

Magnesium

Small additions of 0.25-0.5% Mg allow Al-Si alloys to be hardened by heat treatment, improving mechanical properties through the precipitation of Mg_2Si in a finely dispersed form.[18] Their proof stress can be almost doubled. Mg is used at levels of around 1% in high silicon piston alloys. Higher levels still, around 3-6% Mg, are used in low silicon alloys to improve the anodising characteristics and give a bright surface finish for decorative components. Magnesium content is kept low in pressure die casting alloys to avoid embrittlement. The presence of magnesium increases the oxidation losses of liquid aluminium.

Iron

Levels of 0.9-1.0% Fe are used in pressure die casting alloys to prevent die sticking.[19] High Fe contents decrease ductility, shock resistance and machinability. Castability is decreases by Fe due to the formation of sludge phases with manganese and chromium etc., so alloys for processes other than pressure die casting are limited to less than 0.8% Fe.

Manganese

Improves casting soundness at levels over 0.5%. Mn controls the intermetallic form of iron in the alloy, leading to improved ductility and shrinkage characteristics.

Nickel
When combined with copper, enhanced strength and hardness at elevated temperature.

Zinc
When combined with copper and magnesium, heat treatment and natural ageing characteristics are improved. The fluidity is increased but shrinkage problems may occur.

Lead
Improves machinability at levels over 0.1%.[20,21]

Titanium
Refines the grain structure when combined with boron.

Phosphorus
Refines the primary Si phase in hypereutectic alloys. In hypoeutectic alloys, low levels of phosphorus coarsen the eutectic structure and reduce the effect of Na and Sr eutectic modifiers.

Strontium
Levels of 80-400 ppm Sr modify the Al-Si eutectic structure.

Sodium
Used to modify the eutectic structure.

Lithium
While lithium up to 3% may be used to improve the properties of wrought aluminium alloys, it has a generally harmful effect on casting properties by reducing the effectiveness of Na or Sr modifiers at levels above 0.5%. At even lower levels, above 0.01%, porosity problems are experienced. It is recommended that Li levels below 0.003% are used for casting alloys.

1.4. Melting aluminium alloys

Aluminium and aluminium alloys are melted for conversion into castings, ingots for subsequent fabrication or remelting. The components of the charge – ingot, alloying ingredients and scrap – may contain gas, oxides and other inclusions that could be detrimental to the product. By careful melting, fluxing (or other metal treatment) and handling during transfer, oxide content can be reduced and gas content adjusted to achieve metal of acceptable quality.[22-24] Alloying elements are added to molten metal to produce alloys of the desired composition and quality.
The successful casting of aluminium alloys requires attention to a number of special factors:

Effect of oxides in melting
The tenacious oxide film formed on the surface of molten aluminium protects the metal from further rapid reaction, even though, as is well known, aluminium is highly reactive with oxygen. This protection is effective at melting temperatures, and it is not necessary to use cover fluxes during melting or transfer. The oxide skin has a

protective effect, preventing catastrophic oxidation of the melt but it causes problems during melting and also during casting.[7,9-11] An oxide film can form even as the metal is filling the mould and can give rise to entrained oxide in the casting compromising the physical and mechanical properties of castings.[5-7,9,10,13,25-27]
Oxide inclusions in aluminium alloys are of Al_2O_3 or $MgO{\cdot}Al_2O_3$ which have a density only 5% less than that of liquid aluminium so flotation of oxide inclusions takes place slowly. For inclusion-free castings it is advisable to use metal filters to clean the metal as it enters the mould.[7,10,23] Fluxes are used during melting to drag oxides from the melt, to remove elements such as magnesium or sodium, or to recover metal from the skim form in melting.

Source and solubility of Hydrogen

Solubility of hydrogen in molten aluminium alloys is an important factor in melting operations.[16] Hydrogen is the only gas having any measurable solubility in aluminium (Figure 2).[22,28]

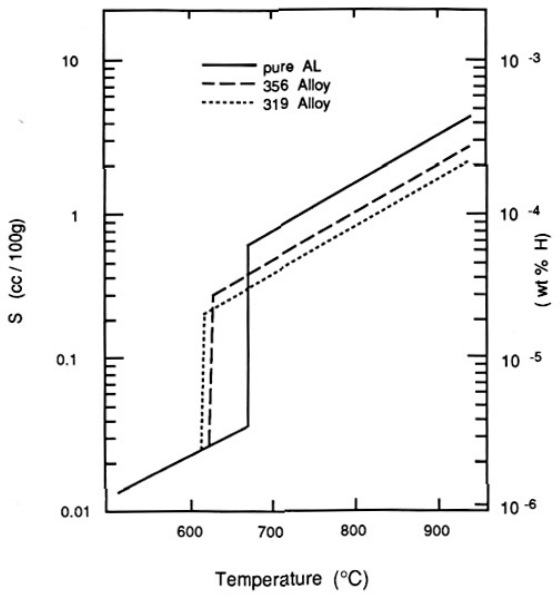

Fig. 2. Solubility of Hydrogen in pure aluminium and in EN AB-42000 (A356) and 45400 (A319) alloys.[22]

Hydrogen occurs in aluminium-base alloys through reaction of the aluminium with moisture in the melting environment. Source of moisture in melting are:[16,28]

- *Natural occurrence in air*;
- *Products of combustion of fuel*;
- *Moisture absorbed on the surfaces of charge components*;
- *Residual lubricants on scrap*;
- *Moisture absorbed on furnace tools*;
- *Moisture absorbed or chemically combined in solid fluxes or flux residues*;
- *Incompletely dried refractory coatings*;
- *Gases*.

Each is an important source of hydrogen and practises should be designed to minimise them. Since both hydrogen pickup and oxide formation increase with temperature, furnace temperature should be controlled to a minimum.[22,29,30]
In addition to hydrogen pickup during melting, hydrogen can enter aluminium by reaction of the liquid metal with moisture in the air during transfer or pouring, especially if the oxide film on the metal surface is broken by turbulence during these operations. It should be emphasized that the hydrogen pick up is relatively slow when the surface oxide of the melt is undisturbed.
Liberation of hydrogen and its entrapment during solidification can cause porosity in the cast metal.

Heat sources and Furnaces for melting and remelting

The choice of a furnace for melting aluminium is influenced primarily by (*a*) amount of molten metal required; (*b*) capital investment necessary; (*c*) forms and types of charge materials; (*d*) melt rate and temperature control desired; (*e*) economics of melting, including repair and maintenance; (*f*) melt quality necessary; and (*g*) method of pouring and type of product or products contemplated.[15,16,31]
Although furnaces can also be heated with coke, coal or electricity, gas-fired or oil-fired furnaces melt the greatest tonnages. The main types of furnaces are:

- *Reverberatory furnaces*, generally employed to melt large volumes of metal for use in foundry holding furnaces, permanent mould dip wells, foundry and fabricating ingot production, and scrap remelting;
- *Dry-hearth furnaces*, another form of reverberatory, employed to melt aluminium for either reclamation or casting operations;
- *The crucible or pot furnace*, with capacities from 10 to 500 kg, employed for melting of holding or both;
- *Core-type low-frequency induction furnaces*, used in die, permanent mould and sand casting;
- *High-frequency induction furnaces* have limited commercial application for aluminium because of their high initial cost and relatively small capacity.

Charging materials

Foundries usually purchase pre-alloyed ingots from specialist suppliers. These rich alloys are produced by adding the hardening elements directly to primarily aluminium and the high temperature and turbulence facilitate their easy solution. Although relatively pure metals are generally employed to prepare rich alloy or casting alloy ingot, scrap is a major component charged into melting or remelting furnaces in preparing aluminium alloys. If the scrap is contaminated with more than the normal dirt, oxide, or miscellaneous materials not easily separated and not conducive to the production of high-quality ingot, some preliminary cleaning process must be utilised.[22-24,32,33] Scrap metal is carefully sorted by the supplier using spectroscopic analysis and melted in large induction or gas-fired furnaces. Scrap is classified into several grades: (*a*) remelt scrap ingot; (*b*) segregated briquettes or too heavy to briquette; (*c*) segregated, baled or packaged; (*d*) segregated loose; (*e*) nonsegregated; (*f*) borings and turnings; and (*g*) skimmings.[16,18]
The value of the various grades of scrap is governed by the ease with which they can be converted into useful molten metal. Well-segregated scrap is of course, most easily used; remelting and ingot casting facilities are thus generally located at a large

fabricating plant. The heavier grades of scrap or tightly briquetted material, which can be submerged without special effort, are preferred, because of the minimum oxidation occurring during the melting operation. Turnings and borings and various grades of finely divided scrap are relatively poor materials for melting purposes, because they may oxidise excessively due to the large percentage of surface area exposed during melting.

1.5. Treatment of aluminium alloy melts

Before casting aluminium alloys, the molten metal must be treated in order to:[14-16,18,22,23,31]

Degas	Molten aluminium contains undesirable amounts of hydrogen which will cause porosity defects in the casting unless removed.
Grain refine	Mechanical properties of the casting can be improved by controlling the grain size of the solidifying metal.
Modify	The microstructure and properties of alloys can be improved by the addition of small quantities of certain modifying elements (Na, Sr, Sb, etc.).

Among these treatments, the modification in Al-Si alloys is briefly treated here, to give the reader sufficient background in the interpretation of the results in the appended articles.

The refinement of primary aluminium grains and degassing technology have been reviewed by other authors and are not reviewed here.[14-16,18,22,23,31,34,35]

1.5.1. Modification

1.5.1.1. The Al-Si phase diagram and Equilibrium cooling

Aluminium-Silicon system is a simple binary eutectic with limited solubility of aluminium in silicon and limited solubility of silicon in aluminium. There is an equilibrium eutectic reaction at approximately 12.6 wt% silicon and 577°C and at this temperature the solubilities of silicon in aluminium and aluminium in silicon are 1.65 wt% and 0.5 wt%, respectively. The binary aluminium-silicon equilibrium phase diagram is shown in Figure 3.[36] There is only one invariant reaction in this diagram, namely

$$L \rightarrow \alpha + \beta \quad \text{(eutectic)} \qquad (1)$$

In equation (1), L is the liquid phase, α is predominantly aluminium, and β is predominantly silicon. Figure 3 shows that the aluminium-silicon eutectic can form as follows:

1. Directly from the liquid in the case of a silicon concentration of 12.6% (i.e., for a eutectic aluminium-silicon alloy),
2. In the presence of primary aluminium in the case of silicon contents <12.6% (i.e., for hypoeutectic aluminium-silicon alloys), and

3. In the presence of primary silicon crystals in the case of silicon contents >12.6% (for hypereutectic aluminium-silicon alloys).

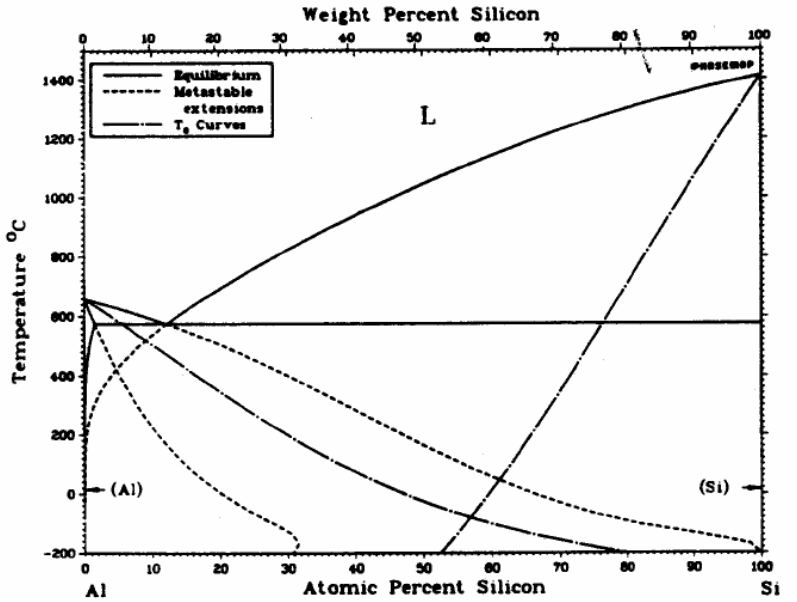

Fig. 3. Equilibrium diagram for the Al-Si system showing metastable extensions of liquidus and solidus lines.[36]

Typical eutectic structures of binary alloys form by the simultaneous growth of two phases from the liquid; therefore they may exhibit a variety of microstructures that can be classified according to two criteria:

- Lamellar vs. fibrous morphology of the individual phases, and
- Regular vs. irregular growth of the individual phases.

Figure 4 shows the microstructure of the aluminium-silicon eutectic.[37] In general, when there are approximately equal volume fractions of the two phases, eutectics of binary alloys exhibit a lamellar structure. On the other hand, if one phase is present in a small volume fraction, this phase tends to be fibrous. As a rule of thumb, the eutectic microstructure obtained will tend to be fibrous when the volume fraction of the minor phase is less than 0.25, otherwise it will tend to be lamellar.[38] If both phases in the eutectic are non-faceted, the eutectic will exhibit a regular morphology. In this case, the microstructure is made up of either lamellae or fibers having a high degree of regularity and periodicity. On the other hand, if one phase is faceted, the eutectic morphology is often irregular. Even though the volume fraction of silicon in the aluminium-silicon binary is less than 0.252, the typical aluminium-silicon eutectic is closer to a lamellar structure than to a fibrous one. This is usually attributed to the strong anisotropy of growth of silicon and to the relatively low interfacial energy between silicon and aluminium.[38]

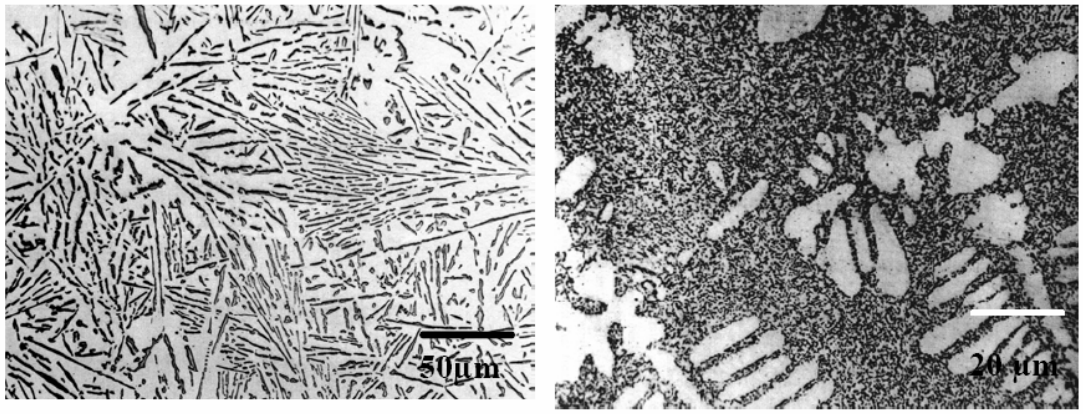

Fig. 4. Al-12.5wt% Si alloy (*left*) slowly cooled and (*right*) chill Cast.[37]

Gwyer and Phillips[39] determined the composition and temperature of the eutectic reaction in the Al-Si binary system to be 11.7%Si and 577°C respectively. Though the eutectic temperature is in accord with the currently accepted value, the eutectic composition was later changed to 12.2 ± 0.1 atom %Si.[40-42] The initial error in establishing the eutectic point is due to the fact that the temperature of formation of the primary constituents (aluminium and silicon), as well as the temperature of the Al-Si eutectic plateau are cooling rate dependent. Primary silicon undercools more than primary aluminium hence the eutectic structure forms at 10-12°C below the eutectic temperature without appreciable recalescence.[41,42] Consequently, at higher cooling rates, the system behaves as though the eutectic point is shifted to higher silicon contents and the eutectic temperature is depressed. Figure 4 illustrates this apparent shift in the eutectic point. Figure 4a, which depicts the microstructure of a eutectic aluminium-silicon alloy that is slowly cooled, shows no primary aluminium; on the other hand, Figure 4b, which depicts the microstructure of the same alloy cooled at a relatively faster rate, shows primary aluminium dendrites. Depression of the eutectic temperature with increased cooling rate may be explained on the basis of the coupled region effect.[43]

1.5.1.2. Unmodified and modified alloy

When the alloys are made simply by melting aluminium and silicon together, i.e., by the addition of solid silicon to liquid aluminium, so-called "normal" alloys result. When the alloys are made by direct electrolytic reduction, or when the normal alloys are treated after simple melting with an alkali fluoride or with sodium or potassium, so-called "modified" alloys result, and that in the case of the normal alloys, the silicon occurs as relatively large plates and needles, while in the modified ones the silicon is in a state of high dispersion. The preparation of both normal and modified alloys has been the subject of a number of patents.

The microstructure of an unmodified Al–Si eutectic is shown in Figure 4a. The silicon particles in an unmodified alloy seem to be disconnected when viewed at low magnification without deep etching. Consequently, it was initially believed that each of the coarse silicon particles is an isolated crystal. Later, Gurtler[41,42,44] observed that radial silicon particles grew across the primary aluminium dendrites as shown in Figure 5 and concluded that such an occurrence cannot be possible unless the silicon

particles extended in three dimensions. Crosley and Mondolfo[45] suggested that the needle-like silicon particles observed in unmodified alloys must be flakes or sheets.

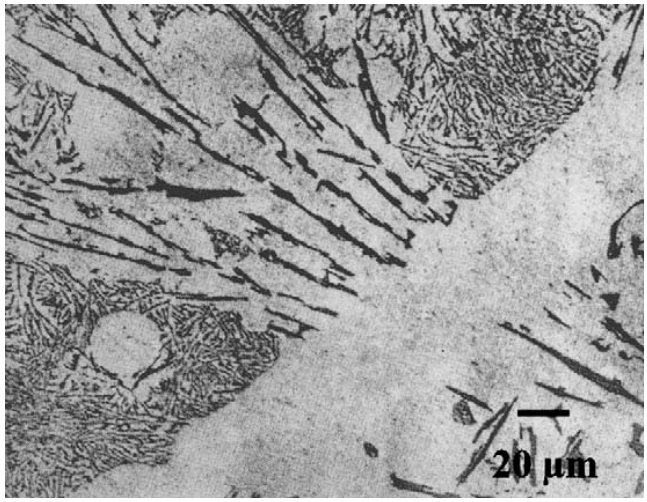

Fig. 5. Eutectic silicon particles around a primary aluminium dendrite.[45]

Recently, it was confirmed that silicon in unmodified Al-Si eutectic has the plate-like shape as shown in Figure 6.[41]

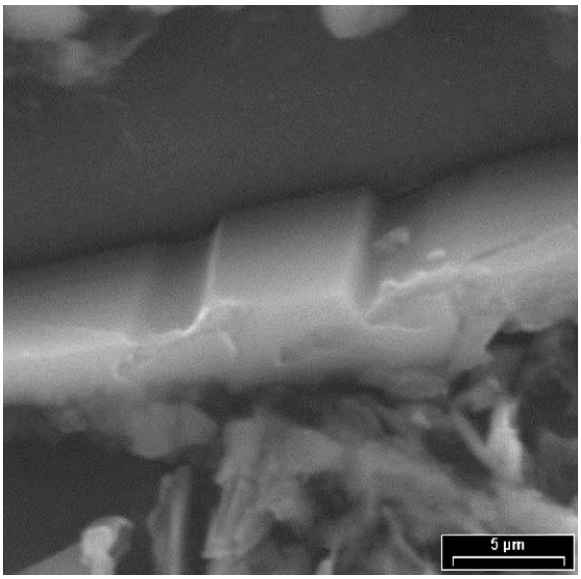

Fig. 6. SEM micrograph showing the flake morphology of silicon in an unmodified aluminium silicon eutectic alloy.[41]

At relatively fast cooling rates, such as in chill casting, the Al-Si eutectic is much finer and the silicon assumes fibrous morphology as shown in Figure 7.[46]

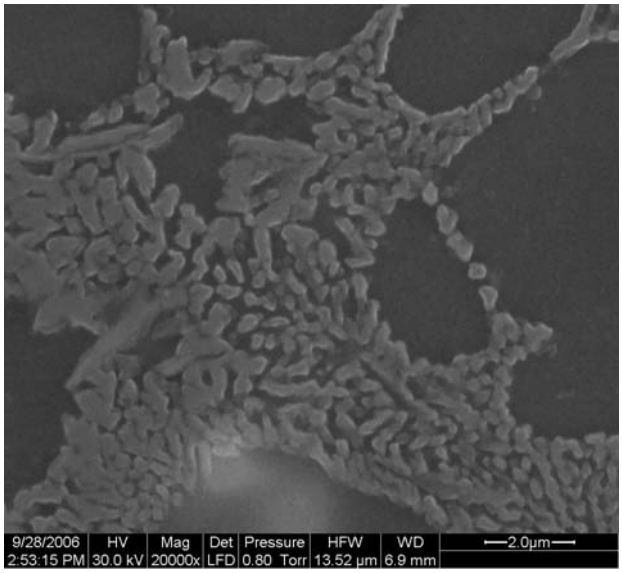

Fig. 7. Silicon crystals in the eutectic region of die cast AlSi7Mg alloy. SEM micrograph in lightly etched condition.[46]

Figure 8 shows the microstructure of a chemically modified alloy.[41] The silicon particles appear as isolated spherical crystals when observed at low magnification as shown in Figure 8a. In reality, Figure 8b reveals the fibrous morphology of silicon particles in deep etched conditions. These changes are accompanied by a considerable improvement in the mechanical properties of the alloy. Modification increases hot tear resistance and alloy feeding characteristics, decreasing shrinkage porosity.
The higher the silicon level in an alloy, the more modifying elements is needed to change the structure. The faster the freezing rate, the lower the amount of modifier required[47] (Article 1, pp.41-56).

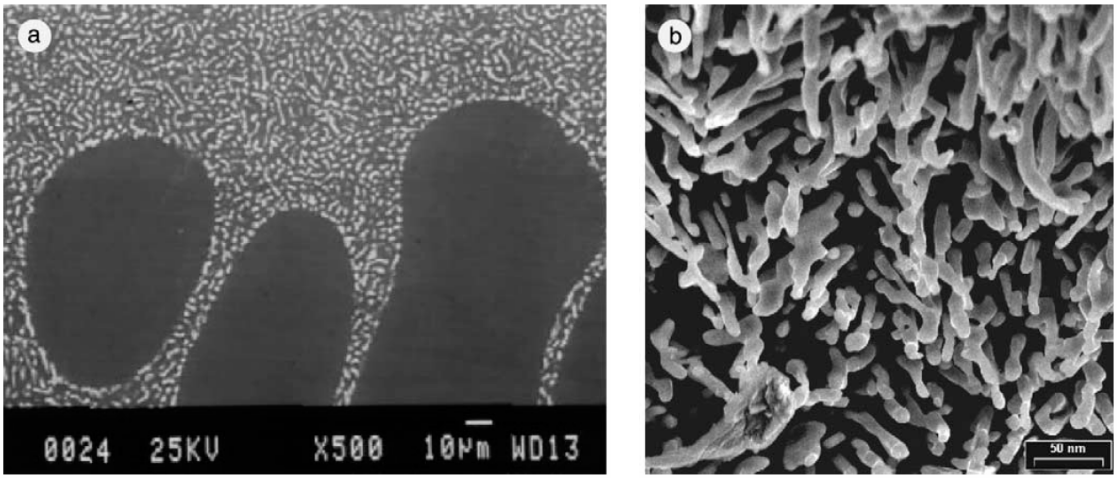

(a) (b)

Fig. 8. Microstructure of a Sr modified Al–Si alloy (a) at low magnification, and (b) at higher magnification and deeply etched.[41]

The first hypoeutectic modifiers were based on sodium and they are still widely used today although "fade", the gradual loss of sodium with time, can be lead to control problems. Sodium has a very large undercooling effect so that it is particularly useful in slowly cooled casting processes such as sand casting. because of its reactivity, sodium is vacuum packed in aluminium containers for convenient addition. Sodium-based fluxes may also be used.[48-50]
Strontium has a modifier has the advantage over sodium that is less reactive and can be added in the form of master alloys so that precise control over additions is possible and fade only occurs over a period of several hours but it is less effective in heavy section castings.[48]
The range of chemical modified microstructures is divided into 6 classes to assess the modification level (Figure 9).[24]

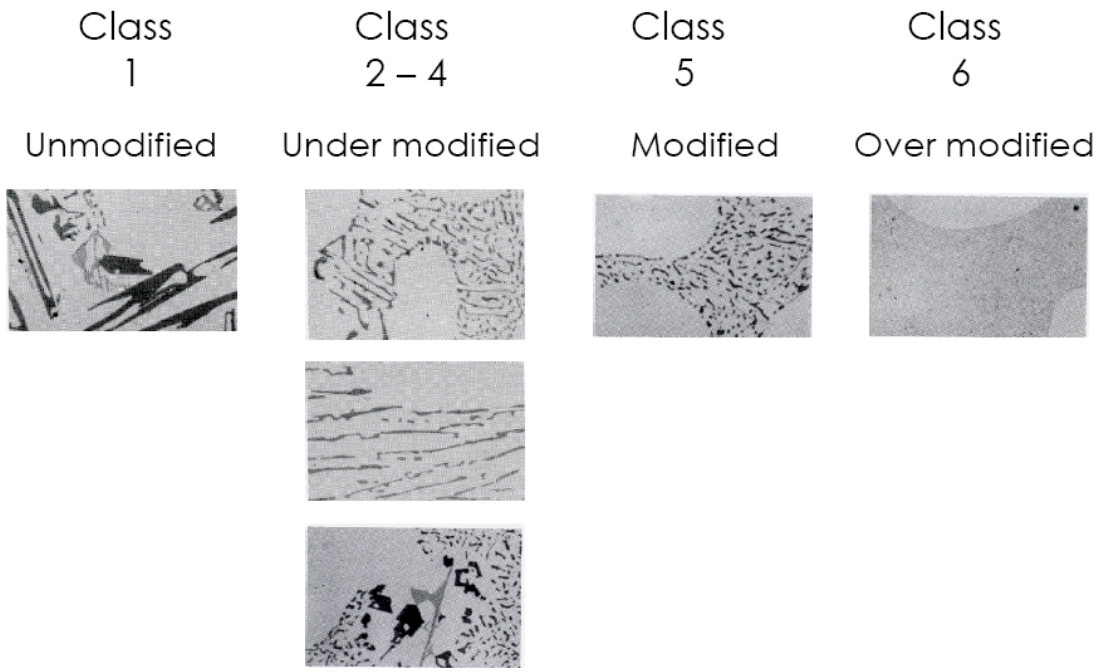

Fig. 9. Classification of chemical modified microstructures to assess the modification level.[24]

1.6. The pouring of aluminium alloy melts

The success of pouring operation depends partly upon certain *qualities* of the metal itself, for example its composition and temperature, the content of oxides and inclusions, which influence flow, and partly upon properties and design of the mould, including the nature of the moulding material and the gating technique used to introduce the metal into the mould cavity.[7,9,15,16,31,51-59] The flow properties of the liquid metal is here considered[60] (Article 2, pp.57-72).

1.6.1. Fluidity of liquid metals

Although other terms such as *castability* have been used to describe certain aspects of flow behaviour, the term *fluidity* is most widely recognised. In the broad sense it can be defined as that quality of the liquid metal which enables it flow through mould passages and to fill all the interstices of the mould, providing sharp outlines

and faithful reproduction of design details.[7,14,31] It follows that inadequate fluidity may be a factor in short run castings or in poor definition of surface features. It can at once be appreciated that fluidity is not a single physical property in the same sense as density or viscosity, but a complex characteristic related to behaviour under specific conditions within a foundry mould.

In considering the factors influencing flow, viscosity might be expected to predominate. When liquid is flowing in an enclosed passage, its viscosity will determine the extent to which the drag imposed by the passage wall is transmitted to the bulk of the liquid: it will therefore influence the rate of flow, which is found to bear a simple reciprocal relation to the viscosity. More directly related to the capacity of a liquid to flow under its own pressure head is the kinematic viscosity, that is the absolute viscosity divided by the density.[15]

Further consideration indicates that these properties will not be decisive in determining the relative mould filling capacities of metals under foundry conditions. One of the fundamental characteristics of the liquid state is the ability of any liquid to conform in time to shape of its container. This would occur rapidly in the case of liquid metal held at constant temperature since viscosities of liquid metals are very low.[61] Under casting conditions failure to fill the mould cavity results not from high viscosity but from premature solidification.[7,56] Thermal conditions and mode of solidification are thus the critical factors with respect to cessation of flow. The concept of fluidity takes these aspects into account.

1.6.1.1. The measurement of fluidity

Since fluidity cannot be assessed from individual physical properties, empirical tests have been devised to measure the overall characteristic. These are based on conditions analogous to the casting of metals in the foundry and measure fluidity as the total distance covered by molten metal in standardised systems of enclosed channels before cessation of flow.[7,56] A further parameter in such tests is the flow time of fluid "life".[15]

Early uses of a straight flow channel , with its disadvantages of excessive length and sensitivity to angle, were discontinued in favour a the spiral test, of which numerous variations have been used. A typical spiral fluidity test is illustrated in Figure 10.[31,62] Variations in the spiral test have been mainly concerned with the problem of obtaining truly standard conditions of flow.[54,63] This problem has been approached through various designs of reservoir system to regulate the pressure head, and constant speed pouring devices to ensure a uniform rate of metal delivery to the system. Since fluidity measurements are also sensitive to small changes in thermal properties and surface characteristics of the mould, graphite and metal moulds have been used by some investigators in attempts to minimise variation in these factors.

The closest approach to complete standardisation is achieved in the vacuum fluidity test.[31,62] Using this apparatus, shown in Figure 11, the metal flows through a smooth glass or metal tube under suction induced by a partial vacuum; the pressure head is thus accurately known and the human factor in pouring eliminated.[31,54]

These later refinements of technique approach the ideal of excluding mould variables and measuring fluidity as a property of the metal alone. Using these and other techniques the major factors in fluidity have been established.

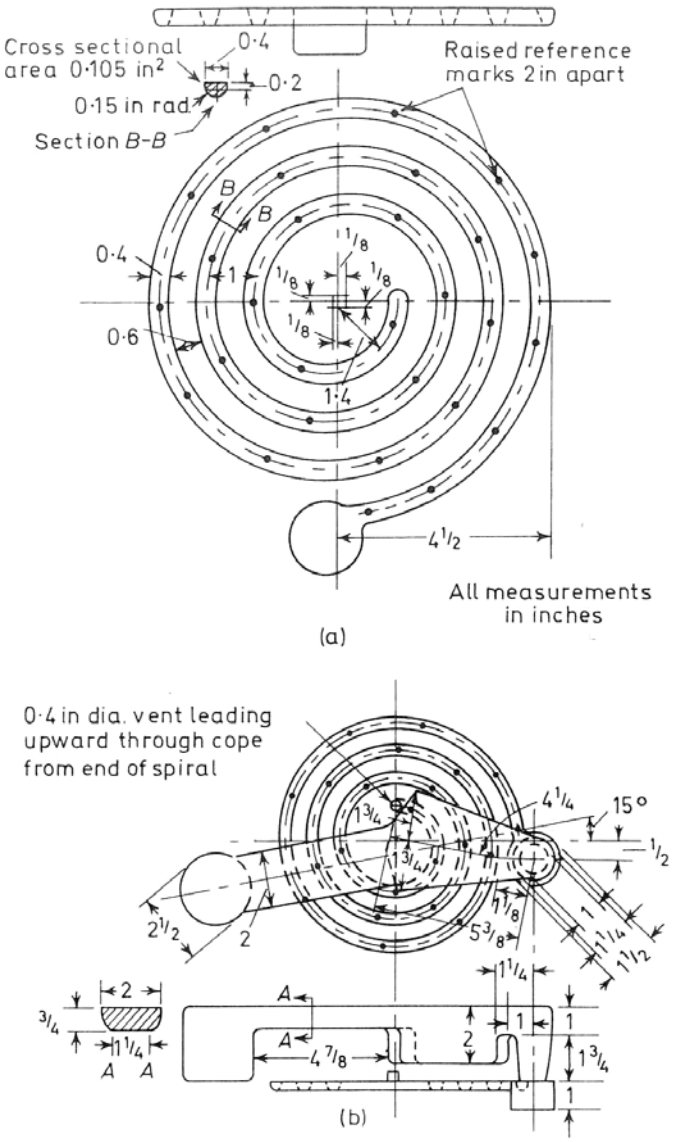

Fig. 10. Spiral fluidity test casting. (a) Standard fluidity spiral, (b) arrangement of down-gate and pouring basin for standard fluidity spiral.[31]

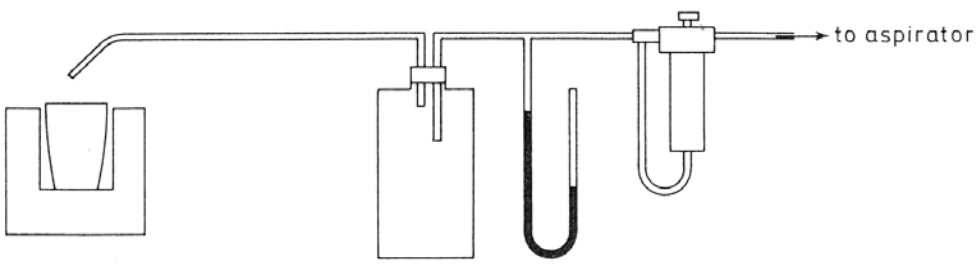

Fig. 11. Vacuum fluidity test apparatus.[31]

1.7. Production techniques

The purpose in this paragraph is to examine briefly the main permanent mould processes used in Aluminium Foundry, such as *gravity*, *low-pressure* and *high-pressure* die castings. This to give the reader sufficient background in the interpretation of the results in the appended articles.

1.7.1. Gravity die casting

The gravity die casting process is notable for the very large output of castings in aluminium alloys, for which the process is predominant as a mass production technique. The process is suitable for fluid alloys owing to the high freezing rates obtained in metal moulds.[14-16,23,31,64]

Dies for gravity casting are often of comparatively simple construction. A typical two die part is split along a vertical joint line passing through the die cavity, the running, feeding and venting system being disposed in the same plane. Internal cavities may be produced by using separate metal cores, which can in many cases be directly retracted from the casting; in other cases collapsible core construction is required to enable loose core pieces to be withdrawn sideways from undercut sections. Cavities are frequently produced with the aid of shell, sand of plaster cores, permitting greater flexibility of design. Dies are provided with various arrangements of pin locators, clamping devices and ejection systems for casting removal.

To facilitate assembly and mutual location the die halves may be hinged. Modern practise is also characterised by increasing die mechanisation similar to that used in pressure die casting, with provision of advanced equipment for automatic opening and closing, locking, and actuation of core movement and ejection systems. A production cycle of less than 1 minute is feasible with these systems, according of course the casting dimensions.[64]

The dies, of high quality cast iron or in special cases tool steel, are cleaned and sand blasted (Figure 12).

Fig. 12. The mould segments are cleaned and sand blasted.[64]

The dies are preheated and coated with insulating refractory dressings before use (Figure 13).

Fig. 13. Refractory coating is applied to the dies before use.[64]

During the production cycle the die is brought to an equilibrium operating temperature, usually between 300 and 400°C, by maintaining a regular time cycle for casting and ejection.[15,16,23,64] The cycle can be shortened and production increased by provision of cooling fins, by forced air cooling or by incorporation of water cooling systems in the die blocks. For gravity semi-permanent mould technology, sand cores are placed before pouring (Figure 14a). For good casting quality, great care is required in pouring to avoid turbulence and dross formation (Figure 14b).[7] Tilt pouring can be used for steady mould filling.[16,64] The die cooling system can be used to developed the required temperature gradients in the casting to obtain a directional solidification.

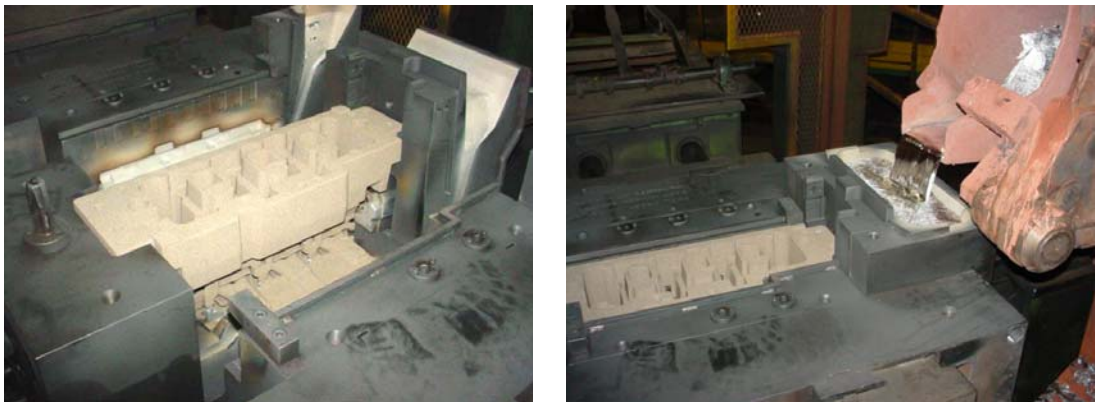

(a) (b)

Fig. 14. (a) Mould with sand cores placed, ready to close and move to pouring station; (b) mould being poured by automatic device.[64]

Dies must be designed to allow easy removal of the finished casting. Manually operated dies are often designed to allow a hand-held lever to be used to free the casting from the cavity without damage to a critical area of the casting. Automatic machines usually have a dedicated unloader to extract the casting from mould (Figure 15a) and to partially remove the sand core (Figure 15b).

(a) (b)

Fig. 15. (a) End of solidification - extraction of casting from mould; (b) partial sand core removal.[64]

Dies lives are typically around 30000-50000 shots.[16,64] Dies are increasingly being designed with the aid of computer programs which simulate the filling and solidification processes (Figure 16).[65,66] Their use can save weeks and trial and error, significantly reducing the time and cost of bringing a new casting into production[67] (Article 3, pp.73-83).

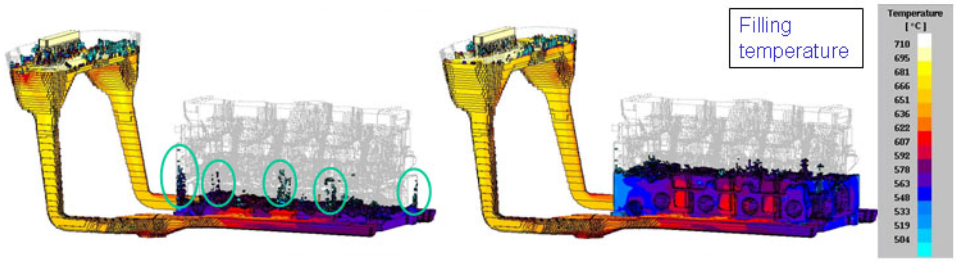

(a)

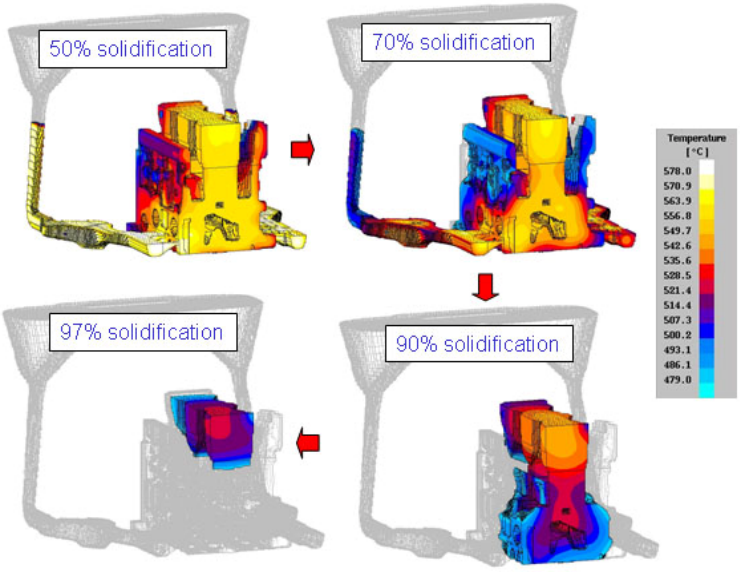

(b)

Fig. 16. (a) Evolution of filling in a semi-permanent mould casting process; (b) evolution of solidification.[68]

Examples of gravity permanent and semi-permanent mould castings are shown in Figure 17.[64]

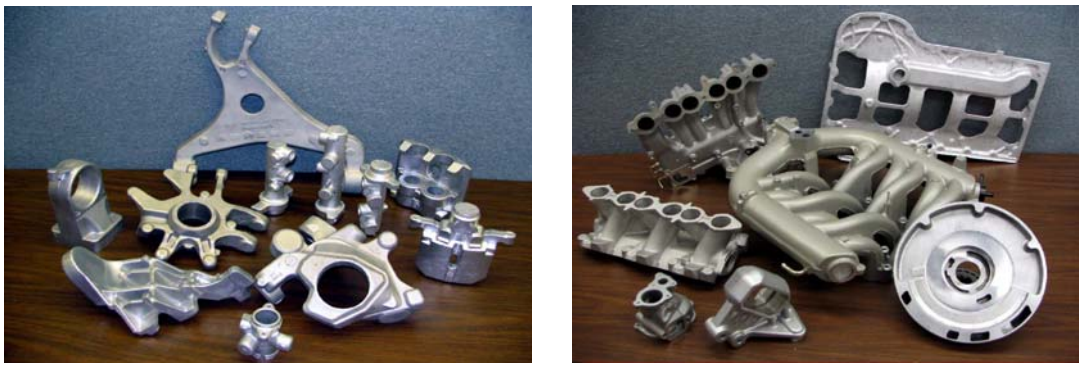

(a) (b)

Fig. 17. Cases of (a) permanent and (b) semi-permanent mould castings.[64]

1.7.2. Low-pressure die casting

A metal die is mounted above a sealed furnace containing molten metal. A refractory-lined tube, called a riser tube or stalk, extends from the bottom of the die into the molten metal. When air or inert gases are introduced into the furnace under low pressure (15-100 kPa), the molten metal rises up the tube to enter the die cavity with low turbulence, the air in the die escaping through vents and the parting lines of the die.[15,16,23,31,64] A typical Pressure vs. Time curve used is displayed in Figure 18.[69]

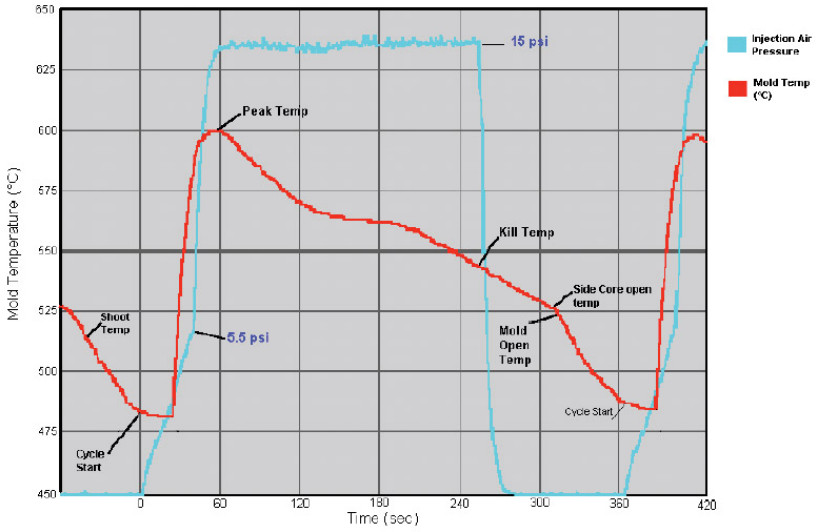

Fig. 18. Injection profile from an EN AB-42000 aluminium alloy low-pressure die casting.[69]

When the metal has solidified, the air pressure is released allowing the still-molten metal in the riser tube to fall back into the furnace. After a further cooling time the die is opened and the casting extracted. The design of a typical low-pressure die casting machine is shown in Figure 19.

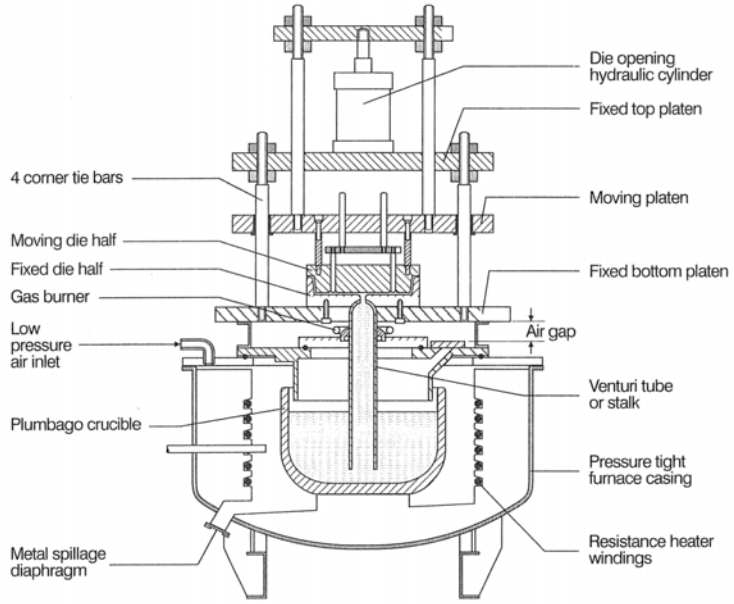

Fig. 19. Low-pressure die casting machine construction.[23]

After correct process optimisation, low-pressure die casting is capable of making high quality castings with the possibility of further heat treatments[70] (Article 4, pp.85-105). With correct die design, directional freezing of the casting is achieved so eliminating the need for risers, the casting being filled and fed from the bottom. Because there is usually only one ingate and no feeders, casting yield is exceptionally high, generally over 90% (Figure 20).[64,69] Good dimensional accuracy and surface finish are possible and complex castings can be made using sand cores.

(a)

Fig. 20. Typical gravity (*left*) and low-pressure (*right*) die casting yields.[64]

(b)

Fig. 21. Cases produced in Aluminium alloy by low-pressure die casting.[64]

Large aluminium castings up to 150 kg can be made but can only be justified in special cases because of high die costs.[23] The process is particularly suitable to the production of symmetrical castings, such as automotive wheels, or castings of high

quality, such as critical aerospace castings, electric motor housing, suspension brackets etc. (Figure 21).

1.7.3. High-pressure die casting

In conventional high-pressure die casting the metal is injected into the die at high velocity and solidified under externally applied pressure. These conditions give a unique capacity for the production of intricate components at relatively low cost; thin-walled components are possible and little or no machining is needed on the cast, since holes, grooves and recesses can be finish cast. The process thus is of great engineering importance.[16,19,23,64,66]

Aluminium alloys are cast in cold-chamber die casting machines. The die is made of tool steel usually of two cavities into which the molten metal is forced. The die halves are closed and locked together hydraulically to withstand the high injection pressure. Molten metal is introduced through a ladle into the shoot sleeve, then a steel plunger forces the liquid metal into the die cavity under a pressure of up to 100 MPa (Figure 22).

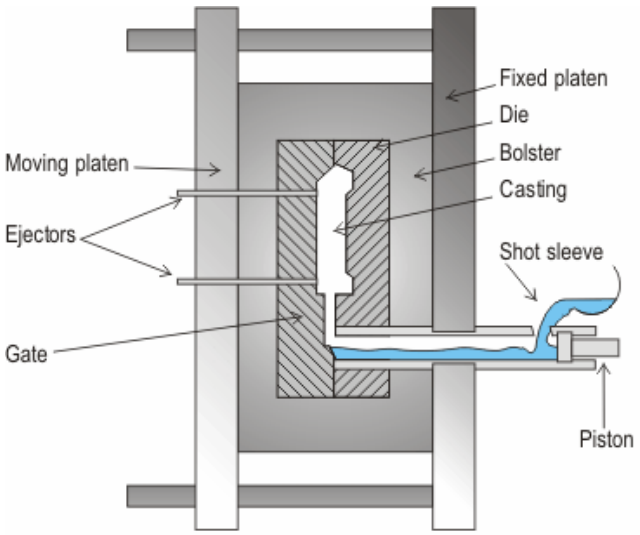

Fig. 22. A schematic view of high-pressure die casting.[66]

Die filling times are very short, castings with wall thickness of 3-4 mm are filled in less than 0.1 seconds. The metal solidifies rapidly because of the good thermal contact with the water-cooled die and the die set is opened to eject the finished casting together with its sprue, the process is then repeated. Cycle times depend on the size and section thickness of the component, being typically 40 shots per hour for a component of 5 kg.[66]

Machines are described by their locking force, which determines the cross-sectional area of the casting which can be made, which is in turn related to the overall size and weight of casting. Machines can have locking forces from 100 to over 4000 tonnes.

Dies are expensive but can have life of more than 100000 shots.[23] The process is therefore most suitable for intensive production. One disadvantage of the process is that almost inevitably air and oxides are trapped in the die with the liquid metal, so that the casting contains gas porosity and oxide inclusions[71-75] (Article 5, pp.107-

120). The presence of internal gas prevents subsequent heat treatment: the residual gas expands and distorts the casting, diminishing the surface casting quality (*blistering*), as shown in Figure 23 [46] (Article 6, pp.121-140).

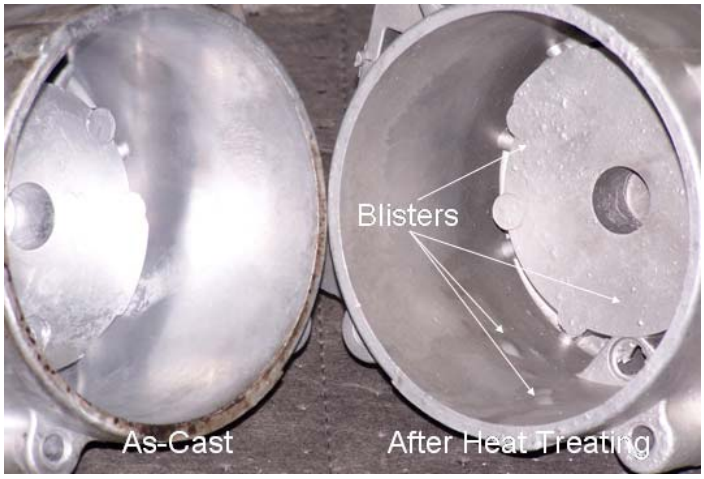

Fig. 23. Blistering of die castings.[68]

The presence of defects also places a limit on the mechanical properties obtained by castings.[5-7,19] For this reason, the process has mainly been used for castings which do not require the highest strength. Another disadvantage is that sand cores cannot be used, since the high pressure liquid metal would destroy the core. Coring is thus limited to straight inserts.
One of the main features of recent research has been the development of special machines and processes which improve the hydraulic integrity and mechanical properties of high-pressure die cast components.

There are three stages in the process of die casting illustrated in Figure 24:

1. Injection in the shot sleeve – the slow shot phase (1-7 s);
2. The die filling phase (0.01-0.3 s);
3. Pressurisation during freezing (400-1200 bar for 5-20 s).

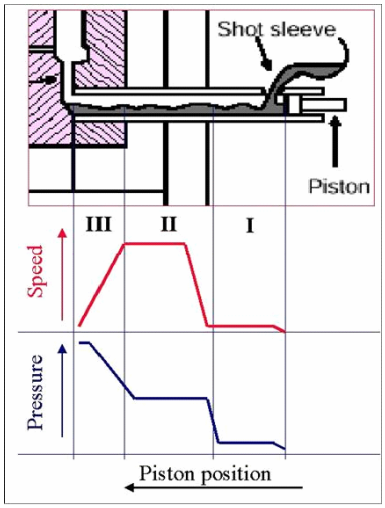

Fig. 24. Schematic view of typical injection-control stages during high-pressure die casting.[66]

Significant discrepancies between the measured and the programmed injection values can give indications of the quality of the casting. With die filling times as short as 0.1 seconds, metal flow speeds are very high (around 50 m/s gate speeds), the metal stream sprays in the die cavity trapping air within the casting.
It is a common conception that an optimal movement of the plunger is a prerequisite to obtain high quality die castings. Formerly, the plunger movement was instantaneously brought to die filling speed when the shot sleeve pouring was completed. This typically resulted in the entrapment of air, and it was therefore necessary to improve the plunger movement in the slow shot phase. The application of maximum pressure is delayed until freezing has started, pressure is then intensified to maintain as high a pressure as possible on the remaining liquid metal without causing the formation of flash.
Modern die casting machines are equipped with interactive control systems to stabilise the production conditions. Die temperature can be controlled by thermocouples set into the die which control the temperature distribution; temperature can be also controlled by pumping oil through channels in the die so that combined heating and cooling can be achieved. This enables the die set to be preheated before casting starts so reducing the amount of start-up scrap.
Once the proper temperature is reached, the casting must be extracted as soon as possible. This stage, in die casting processes, requires opening of the moving part of the die, the action of ejection pins, and the robotic handling of the product.
High-pressure die casting allows the achievement of castings with a good surface quality, sometimes not requiring further machining. From the metallurgical point of view, the high pressure applied during solidification gives a good feeding effect. Very complex geometries can be achieved (Figure 25), with excellent tolerances (0.02-0.05 mm) and very thin wall thickness (up to 1 mm).[66]

Fig. 25. Cases produced in aluminium alloy by high-pressure die casting.[68]

Many developments have been made to overcome the basic problems of low integrity of the high pressure die castings due to air entrapment:[19]
- Vacuum die casting;

- Pore-free die casting;
- Indirect squeeze casting;
- Semi-solid metalcasting.

1.8. Heat treating

Heat treating processes for aluminium alloys are precision processes. They must be carried out in furnaces properly designed and built to provide the thermal conditions required, and adequately equipped with control instruments to insure the desired continuity and uniformity of temperature-time cycles. To insure the final desired characteristics, process details must be established and controlled carefully for each type of product. The general types of heat treatments applied to aluminium and its alloys are:[15,31]

- *Preheating* or *homogenisation*, to reduce chemical segregation of cast structures and to improve their workability;
- *Annealing*, to soften strain-hardened and heat treated alloy structures, to relieve stress, and to stabilise properties and dimensions;
- *Solution heat treatments*, to effect solid solution of alloying constituents and improve mechanical properties;
- *Precipitation heat treatments*, to provide hardening by precipitation of constituents from solid solution.

The fundamental aspects of heat treating processes for strain-hardenable aluminium alloys are not covered in this review due to the enormous amount of literature.
The solution heat treatment of cast aluminium alloys is briefly treated here, to give the reader sufficient background in the interpretation of the results in the appended articles[46] (Article 6, pp.121-140).

1.8.1. Solution Heat Treatment

Solution heat treatment improves mechanical properties by developing the maximum practical concentration of the hardening constituents in solid solution. This requires heating the product to a temperature close to eutectic temperature, holding there long enough to effect the desired solution, and then quenching fast enough to retain the desired solid solution.[16]

1.8.1.1. Temperature requirements

Temperature controls should be set so that the maximum temperature the metal can attain at the hottest location in the load is at or close to the nominal recommended temperature plus 5°C. Proper settings must be established carefully, to insure against this maximum temperature being exceed, even momentarily. This is particularly critical for Cu-rich alloys, for which the initial eutectic melting temperature is only few degrees higher than the recommended maximum solution temperature. It should be recognised that in changing a furnace from one operating range to another, a period of time is required to permit it to reach equilibrium conditions and normal temperature distribution at the new setting. If a furnace is loaded too soon after the temperature is changed, the metal temperature may not be uniform, even through indicating instruments may show satisfactory readings.

1.8.1.2. Time requirements

Recommended soaking times for wrought and cast aluminium alloys are given by International Standards. In salt bath furnaces, soaking time begins when the load is immersed, if there is enough molten salt so that the load does not cause the bath temperature to drop more than 5°C below the specified nominal temperature. If the temperature drops below this minimum, the soaking period should be counted from the time all portions of the bath have recovered to the specified nominal temperature minus 5°C.

In an atmosphere furnace, it is preferable to use one or more load thermocouples to establish when the load attains the desired temperature and when to start the solution-treatment time cycle. Without load couples, the time the load reaches temperature must be estimated, taking into account the lag of the metal temperature behind the furnace-atmosphere temperature as the metal is heated. In a single-zone furnace, the time cycle begins when the furnace control indicates recovery to the set temperature. In a large furnace with multiple control instruments, the cycle begins when the last instruments indicates recovery to the setting for the zone it controls. To prevent excessive diffusion in some products, furnaces must be capable of recovery to temperature in not more than 35 minutes for thickness of 2.60 mm and less, and more than 1 hour for thicker products.

When a reliable load thermocouple arrangement is employed, soaking time may be measured from the time the last metal-temperature indicator reaches the specified nominal temperature minus 5°C. With load thermocouples indicating actual metal temperature, the minimum soaking times employed may be reduced to those listed for salt bath furnaces. This is particularly advantageous in limiting time to a minimum for some products.

Different aluminium alloys can be solution heat treated together if the same heat treating temperature is satisfactory. When products of different thickness are treated together, soaking time is controlled according to the requirement for the thicker section.

Soaking periods longer than the minimum requirements have no harmful.[76] Generally aluminium casting alloys require soaking times much longer than those employed for wrought alloys, because microcostituents are coarser and require substantially longer time at temperature to effect the necessary degree of solid solution.

Repeated solution heat treatments are permissible where the temper desired can be achieved. Obviously, material to be retreated must not have been damaged by “high-temperature oxidation” or eutectic melting from preceding heat treatments.

The results of bad practice leading to eutectic melting or “high-temperature oxidation” sometimes are readily apparent to an experienced heat treating technician. If sufficiently severe, eutectic melting produces myriads of closely spaced, small rounded blisters and susceptibility of cracking on quenching. “High-temperature oxidation” in gross degrees causes a finer type of general surface roughening, patterned in very small blisters aligned in the working direction. Unfortunately, less but still important degrees of these conditions can be detected only by examining specimens metallographically. The effects of a small degree of eutectic melting on the mechanical properties are greater than those of a slight degree of “high-temperature oxidation”. Both phenomena can cause embrittlement; elongation values are first affected, and then the tensile strength, as the conditions become more severe.

2. OBJECTIVES AND SURVEY OF THE ARTICLES

The aim of Article 1 was to study the combined effect of modification and solidification rate on Al-Si cast alloys. Generally in these alloys, silicon forms brittle plate-like particles, which reduce mechanical properties in cast structures. Thus, the modification stage is a key-task to control microstructure and affect the casting quality. Traditional thermal analysis is a useful tool to determine modification level of the alloy, then to control the modification treatment. In the present paper, the solidification process of Al7SiMgTi, Al9SiMgTi and Al11SiMgTi alloys, modified by sodium and by strontium, was followed by means of thermal analysis and subsequent metallographic examination of the solid samples. Different cooling conditions in thermal analysis experiments were set up and the combined effects of modification and solidification conditions on eutectic temperature and silicon morphology were presented. Considering the thermal analysis results previously obtained, gravity cast wheels, where several solidification conditions are present, were finally analysed.

The aim of Article 2 was to investigate the fluidity of four different high-pressure die cast (HPDC) Al-Si alloys at different pouring temperatures. A vacuum fluidity test apparatus was used to measure fluidity. One alloy was then contaminated with 50% scrap addition, increasing the amount of oxide inclusions. The fluidity of the contaminated melt was then measured and compared with the fluidity of the clean melt.

The aim of Article 3 was to study the porosity level and the local solidification conditions on a reference gravity step-bar casting. Porosity level and local solidification time are generally acknowledged to affect both dynamic and static properties of cast aluminium alloys intended for structural applications. To analyse these effects, an investigation was carried out examining permanent mould cast A319 and A356 aluminium alloys. Step-bar castings were poured at different temperatures. The porosity level and the secondary dendrite arm spacing were examined using image analysis of randomly selected fields. In every casting, porosity level and SDAS increased with section thickness. The numerical simulation results showed a good correlation to experimental data.

The aim of Article 4 was to study the impact behaviour on KV sub-size Charpy samples drawn from A356 aluminium alloy 17-inch wheels, produced by a low-pressure die casting process. The wheels showed different geometry and thermal treatment. In this paper, the effects of microstructure and defects on the impact properties were studied. Numerical simulations were performed to study the filling and solidification behaviour of the alloy of the wheels analysed, in order to predict the final microstructure and shrinkage formation.

The aim of Article 5 was to study the effect of casting defects on mechanical properties for a high-pressure die cast aluminium alloy. A series of U-shaped components were cast using a fully controlled cold chamber high-pressure die casting machine with different process parameters. Defects existed in gas and shrinkage pores as well as oxide inclusions. An X-ray equipment was used for a preliminary quality control. Tensile bars were extracted from different locations in the castings in order to map the distribution of the mechanical properties.

The aim of Article 6 was to study the influence of solution heat treatment time and temperature on the microstructure and mechanical properties, and mode of fracture of a high-pressure die cast AlSi7Mg0.3 alloy. Metallographic and image analysis techniques were used to quantitatively examine the microstructural changes occurring during solution heat treatment.

3. CONCLUSIONS

The following conclusions can be draw from this doctoral thesis work:

1. The modification level of Al-Si cast alloys can be well estimated by means of eutectic depression measurement, i.e. the difference between the eutectic temperatures before and after a modification treatment. In Al7SiMgTi alloy, modification level improves by increasing the strontium amount and the optimum is reached in a range of 100-200 ppm. Similar results are not obtained in Al9SiMgTi and Al11SiMgTi alloys, which show partially modified microstructure in spite higher strontium content. Sodium modification results in a low growth temperature and no recalescence effect indicating good modification. By increasing the solidification rate, the eutectic depression of Al9SiMgTi and Al11SiMgTi alloys increase and the modification level improve. While Al7SiMgTi alloy shows a well modified microstructure without any increment of solidification rate, higher cooling rate seems to be essential for hypoeutectic alloys with high silicon content. The consequences are important for real shaped castings, as shown for gravity cast wheels, where different solidification conditions are present, due to different heat transfer rates.

2. The fluidity length of Al-Si cast alloys close to eutectic composition present a different flow behaviour if compared to hypoeutectic alloys, showing a different sensitivity to pouring temperatures. Addition of scraps in molten metal increases the amount of oxides and reduces the fluidity of the melt.

3. The porosity amount, evaluated in step-mould gravity castings of A319 and A356 alloys, increase with increasing section thickness. At the same pouring temperature, the percentage porosity for every thickness is higher in the core of castings. As the pouring temperature increases, the percentage porosity also increases. The percentage porosity of the A319 step castings is always higher than the A356 ones in both the sections analysed The measurements of the secondary dendrite arms spacing (SDAS) demonstrate the close relationship between SDAS and the section thickness.

4. Impact strength tests performed, on Charpy V-notch specimens drawn from different A356 17-inch wheels, produced by low pressure die casting, show interesting correlations between impact strength values and microstructure; a finer microstructure always corresponds to higher impact strength. Impact energy values are lower in as cast wheels than in the T6 heat treated wheels. The resistance to crack propagation is in the range of 60-75% of the total absorbed energy and the highest values are shown by as cast wheels. A direct correlation between the resistance to crack propagation and SDAS is found. The crack crosses the interdendritic eutectic region where a significant fraction of cracked eutectic silicon and intermetallic particles is found. Casting defects become critical when concentrated around the V-notch where they reduce the load bearing area of Charpy specimens. Therefore, the presence of defects is critical on impact properties and can overcome the effect of the microstructure.

5. A quality mapping approach can be used in high-pressure die castings to demonstrate how the amount and type of defects, and the mechanical properties

are distributed in a casting by changing the process parameters. Significant variations of the defect distribution and amount are found in castings produced with different process parameters or under the same conditions, indicating the stochastic nature of defects in die castings. The amount of defects influences considerably the plastic properties of the material but not the elastic characteristics.

6. It has been revealed that conventional high pressure die cast aluminium alloys, may be successfully heat treated at elevated temperature without encountering problems with surface blistering. This solution involves reducing solution treatment temperature and time. A solution treatment of 15 min at 475°C, or even more at 525°C, causes spheroidisation, coarsening and an increase in inter-particle distance of the eutectic silicon particles leading to substantially changes on the microstructure and mechanical properties.

7. Commercial casting simulation software can be a useful tool for predicting the final *quality* of aluminium alloy castings.

4. REFERENCES

1. R. H. Bacon: 'The car: engine and structure'; 1968, London, Macmillan & Cleaver.
2. W. H. Crouse and D. L. Anglin: 'Automotive engines'; 1995, New York, Glencoe/McGraw-Hill.
3. S. Viswanathan, A.J. Duncan, A.S. Sabau, Q. Han, W.D. Porter and B.W. Riemer: AFS Trans., 1998, **106**, 411-417.
4. C. Garzia and E. Mollona: 'Aluminium for the transportation industry in Europe: Innovation and competitive advantages a system dynamics approach', 1-47; 2002, EGEA, Bocconi University Press.
5. C. H. Cáceres and B. I. Selling: Mater. Sci. Eng. A, 1996, **220**, 109-116.
6. X. Dai, X. Yang, J. Campbell and J. Wood: Mater. Sci. Technol., 2004, **20**, 505-513.
7. J. Campbell: 'Castings', 2nd edn; 2003, Oxford, Elsevier Butterworth-Heinemann.
8. B. Zhang, S.L. Cockcroft, D.M. Maijer, J.D. Zhu and A.B. Phillion: JOM, 2005, **57**, 36-43.
9. X. Dai, X. Yang, J. Campbell and J. Wood: Mater. Sci. Eng. A, 2003, **354**, 315-325.
10. D. Dispinar and J. Campbell: Int. J. Cast Metals Res., 2006, **19**, 5-17.
11. J. Espinoza-Cuadra, G. Garcìa-Garcìa and H. Mancha-Molinar: Materials and Design, 2007, 28, 1038-1044.
12. Foseco: Foseco Foundry Practise, 1995, **226,** 14-17.
13. N.R. Green and J. Campbell: Mater. Sci. Eng. A, 1993, **173**, 261-266.
14. R.A. Flinn: 'Fundamentals of metal casting', 1st edn; 1963, Addison-Wesley Publishing Company, Massachusetts.
15. E.V. Blackmun: Casting. In: Kent, R., Van Horn, Aluminum vol. III – Fabrication and Finishing, 3rd edn, 43-80; 1968, American Society for Metals, Metals Park, OH.
16. E.L. Rooy: Nonferrous casting alloys – Aluminum and aluminum alloys. In: American Society of Metals (ASM), Casting - ASM Handbook vol. 15, 9th edn, 743-770; 1992, ASM International, Materials Park, OH.
17. UNI EN 1706:1999: Aluminium and aluminium alloys - Castings - Chemical composition and mechanical properties.
18. A. Kearney, Kearney & Company, E.L. Rooy: Aluminum Company of America, “Aluminum foundry product”, Introduction to Aluminum and Aluminum Alloy”, Properties and Selection: Non ferrous alloys and Special purpose Materials vol. 2, 123-151; 1993, ASM Metals Handbook.
19. A.C. Street: 'The Die Casting Book', 2nd edn; 1986, Portcullis Press.

20. B. Faresin: MS Thesis, University of Padova, Department of Management and Engineering, 2006.
21. S.P.F.C. Jaspers and J.H. Dautzenberg: J. Mater. Process. Technol., 2002, **121**, 123-135.
22. J. E. Gruzleski and B. M. Closset: 'The treatment of liquid aluminium-silicon alloys'; 1990, IL, USA, The American Foundrymen's Society.
23. R. Brown: 'Foseco non-Ferrous foundryman's handbook', 11th edn; 1999, Butterworth-Heinemann, Oxford.
24. M.M. Makhlouf: Proc. 8th Int. Summer School on 'Casting and Solidification of Aluminium- and Magnesium Alloys', Trondheim, NO, August 2006.
25. M. Divandari and J. Campbell: Int. J. Cast Metals Res., 2004, **17**, 182-187.
26. X. Yang, X. Huang, X. Dai, J. Campbell and J. Tatler: Int. J. Cast Metals Res., 2004, **17**, 321-331.
27. M. Divandari and J. Campbell: Int. J. Cast Metals Res., 2005, **18**, 187-192.
28. D.E.J. Talbot: Int. Metall. Rev., 1975, **20**, 166-184.
29. J.P. Anson and J. E. Gruzleski: AFS Trans., 1999, **99-26**, 135-142.
30. L. Andreoni, M. Case and G. Pomesano: 'Quaderni della colata a pressione delle leghe di alluminio'; 1995, Brescia, Edimet.
31. P.R. Beeley: 'Foundry Technology', 1st edn; 1972, London, Butterworth & Co.
32. J. Wannasin, D. Schwam and J. F. Wallace: J. Mater. Process. Technol., 2007, **191**, 242-246.
33. D. Doutre, B. Gariépy, J. P. Martin and G. Dubé: Light Met., Proc. 114th Annual Meeting of the Metallurgical Society of AIME, Warrendale, Pennsylvania,1985, 1179-1195.
34. M.A. Easton and D.H. StJohn: Acta Mater., 2001, **49**, 1867-1878.
35. L. Bäckerud and M. Johnsson: Light Met., 1996, 679-685.
36. J.L. Murray and A.J. McAlister: Bull. Alloy Phase Diagrams, 1984, **5**, 74-84.
37. A. Hellawell: Prog. Mater. Sci., 1970, **15**, 1-78.
38. W. Kurz and D.J. Fisher: 'Fundamentals of Solidification', 4th edn; 1998, Trans. Tech. Publications.
39. A.G.C. Gwyer and H.W.L. Phillips: J. Inst. Metals., 1926, **36**, 283.
40. H.W. Kerr, J.A. Bell, and W.C. Winegard: J. Aust. Inst. Met., 1965, **10**, 64-69.
41. H.V. Guthy: MS Thesis, Worcester Polytechnic Institute, 2001.
42. M.M. Makhlouf and H.V. Guthy: J. Light Met., 2001, **1**, 199-218.
43. L.M. Hogan: The Journal of the Australian Institute of Metals, 1964, **9**, 228-239.
44. G. Gurtler: Z. Metallkunde, 1953, **44**, 503.
45. P.B. Crosley and L.F. Mondolfo: Mod. Castings, 1966, **46**, 89-100.
46. G. Timelli, O. Lohne, L. Arnberg and H.I. Laukli: Submitted for publication in Metallurgical and Materials Transactions A, 2007.

47. A. Manente, G. Timelli and F. Bonollo: Submitted for publication in Journal of Materials Science, 2007.

48. L. Bäckerud, G. Chai and J. Tamminen: 'Solidification Characteristics of Aluminum Alloys vol. 2 – Foundry Alloys'; 1990, American Foundrymen's Society, Inc., IL, USA.

49. A. Manente, P. Ferro and E. Della Rovere: Metall. Ital., 2003, **6**, 27-35.

50. F. Piasentini, F. Bonollo and A. Tiziani: Metal. Sci. Tech., 2003, **23**, 11-20.

51. M. Di Sabatino, L. Arnberg, S. Brusethaug and D. Apelian: Int. J. Cast Metals Res., 2006, **19**, 94-97.

52. H. Kaufmann, W. Fragner and P. J. Uggowitzer: Int. J. Cast Metals Res., 2005, **18**, 273-278.

53. M. Di Sabatino, S. Shankar, D. Apelian and L. Arnberg: Proc. Int. Conf. on 'Shape Casting: The John Campbell Symposium', M. Tiryakioglu, P.N. Crepeau (Eds.), San Francisco, USA, February 13-17, 2005, TMS, 2005, 193-202.

54. M. Di Sabatino, F. Syvertsen, L. Arnberg and A. Nordmark: Int. J. Cast Metals Res., 2005, **18**, 59-62.

55. Young-Dong Kwon and Zin-Hyoung Lee: Mater. Sci. Eng. A, 2003, **360**, 372-376.

56. M. C. Flemings: 'Solidification processing'; 1974, London, McGraw-Hill.

57. M. Di Sabatino, L. Arnberg and F. Bonollo: Metal. Sci. Tech., 2005, **23**, 3-10.

58. M. Di Sabatino and L. Arnberg: Int. J. Cast Metals Res., 2005, **18**, 181-186.

59. M. Di Sabatino, L. Arnberg, S. Rørvik and A. Prestmo: Mater. Sci. Eng. A, 2005, **413-414**, 272-276.

60. G. Timelli and F. Bonollo: Submitted for publication in International Journal of Cast Metals Research, 2007.

61. D. Wang and R. A. Overfelt: Int. J. Thermophys., 2002, **23**, 1063-1076.

62. M. Di Sabatino and L. Arnberg: Metal. Sci. Tech., 2004, **22**, 9-15.

63. M. Di Sabatino, L. Arnberg, S. Brusethaug and D. Apelian: Int. J. Cast Metals Res., 2006, **19**, 94-97.

64. J.L. Jorstad: Proc. 8th Int. Summer School on 'Casting and Solidification of Aluminium- and Magnesium Alloys', Trondheim, NO, August 2006.

65. A. Schroth and D. Schemme: Casting Plant and Technology, 2003, **19**, 8-18.

66. F. Bonollo and S. Odorizzi (Editors): 'Numerical Simulation of Foundry processes', 1st edn; 2001, Padova, SGE, Italy.

67. F. Bonollo, G. Timelli, N. Gramegna and B. Molinas: Proceeding of 3rd International Conference High Tech Die Casting, Vicenza, Italy, September 21-22, 2006.

68. IDEAL project (Integrated Development Routes for Optimised Cast Aluminium Components – Contract n. GRD2-2001-50042), supported by European Union inside Growth Programme.

69. J.R. Van Wert: Proc. Int. Summer School on ' Manufacturing High Integrity Aluminum and Magnesium Castings', Worcester, USA, July 2003.
70. N. Tomanin, MS Thesis, University of Padova, Department of Management and Engineering, 2005.
71. G. Timelli and F. Bonollo: Proceeding of 3rd International Conference High Tech Die Casting, Vicenza, Italy, September 21-22, 2006. Also submitted for publication in Metallurgical Science and Technology, 2007.
72. M. Sadocco: MS Thesis, University of Padova, Department of Management and Engineering, 2006.
73. A. Urbani: MS Thesis, University of Padova, Department of Management and Engineering, 2006.
74. O. Panozzo: MS Thesis, University of Padova, Department of Management and Engineering, 2007.
75. F. Groppo: MS Thesis, University of Padova, Department of Management and Engineering, 2007.

PART 2

ARTICLES

ARTICLE 1

THE EFFECTS OF MODIFICATION AND SOLIDIFICATION RATE ON ALUMINIUM-SILICON CAST ALLOYS

A. Manente*, G. Timelli**, F. Bonollo**

* Alluminio Veneto – S.A.V. S.p.A.
I-35010 Trebaseleghe (PD)
ITALY

** Department of Management and Engineering – DTG
University of Padova
I-36100 Vicenza
ITALY

Submitted for publication in: Journal of Materials Science, 2007

ABSTRACT
Al-Si castings alloys are essential in the automotive, aerospace and engineering sectors in order to cast complex shapes. The silicon forms brittle plate-like particles, which reduce mechanical properties in cast structures. Thus, the modification stage is a key-task to control microstructure and affect the casting quality. Traditional thermal analysis is a useful tool to determine modification level of the alloy, then to control the modification treatment. In the present paper, the solidification process of Al7SiMgTi, Al9SiMgTi and Al11SiMgTi alloys, modified by sodium and by strontium, is followed by means of thermal analysis and subsequent metallographic examination of the solid samples. Different cooling conditions in thermal analysis experiments are set up and the combined effects of modification and solidification conditions on eutectic temperature and silicon morphology are presented. Considering the thermal analysis results previously obtained, gravity cast wheels, where several solidification conditions are present, are finally analysed.

Keywords: Aluminium alloys; Casting; Solidification; Eutectic structure; Modification; Sodium; Strontium; Thermal analysis; Wheel.

1. INTRODUCTION

Due to their excellent castability and good compromise between mechanical properties and lightness, Al-Si alloys are the most important and widely used casting alloys [1]. Aluminium alloys with 5-20 wt.% silicon are in common use. The feature of these alloys is that they consist of a primary phase, aluminium or silicon, and an eutectic mixture of these two elements. Below the eutectic composition, close to 12 wt.% Si, aluminium precipitates from the liquid as the primary phase in the form of dendrites [2,3]. It is of interest not only to control the size of dendrites, but also to influence the two co-precipitating phases in the eutectic mixture [4]. In normal Al-Si alloys the eutectic silicon particles grow in a faceted manner, along certain crystallographic directions. Some twin planes, forming "re-entrant edges", seem to be effective in promoting growth [3-6]. In directional solidification experiments it can be shown that silicon particles grow as flakes ahead of the aluminium phase, nucleating from few sites [5,6]. This kind of eutectic structure doesn't guarantee good mechanical properties to the casting. It is well known how the addition of certain elements like sodium, calcium or strontium, completely changes the morphology of eutectic silicon crystals from coarse and plate-like to fine and fibrous structure. Other elements have been reported to have modifying properties, such as Sb, Ba, Y or Yb [4,7]. Investigations dealing with the mechanism of this structure modification have led to the assumption that sodium or strontium may "poison" the re-entrant edge growth step in the silicon crystals [3,8]. Atoms of the modifying element are absorbed on silicon surface and thereby disturb the growth step. This forces frequent twinning of the silicon crystals which results in enhanced branching. The modifying elements should have an affinity to silicon and preferably form chemical compounds with this element. This would facilitate adsorption on the surface of silicon. A certain size ratio of modifying atoms to silicon atoms of ~1.65 has been proposed as optimum to induce an high level of twinning [8]. Sodium and strontium are close to this ratio. Since sodium has a high vapour pressure and high affinity to oxygen, it readily burns off and its modification effect fades in short time [3,9,10]. In contrast with sodium, strontium remains active in the melt for much longer time. It is easily to add in proper amount via a master alloy, allowing an easy process control.

Due to the interaction between modifying elements and silicon crystals, eutectic nucleation and growth processes are altered. Generally, the solid fraction of starting point for eutectic reaction increases to higher values and a distinct decrease in the eutectic temperature is observed [4-10]. For this reason, the so-called "depression", i.e. the difference between the eutectic temperatures before and after a modification treatment, can be used to assess and control the modification level by means of traditional thermal analysis. The possibility of monitoring the solidification evolution, through the acquisition and analysis of cooling curves by means of traditional thermal analysis or the Fourier thermal analysis, have demonstrated their industrial importance, both in terms of process control and of microstructure understanding [10].

Recent works have shown the effect of alloying elements, such as Mg, Cu and Si, on eutectic depression and how this should be considered during the practical application of thermal analysis [11,12]. With an increasing Si content, a decrease in the depression values was observed while the microstructure remains almost unaffected. Increasing Cu content, higher depression values and a kind of overmodified eutectic microstructure were shown. A critical behaviour with respect to eutectic modification was revealed adding Mg. In an Al-Si alloy, Joenos *et al.*

observed decreasing eutectic depression values with an increasing Mg content and a deterioration of the resulting eutectic microstructure [12]. Thus, the determination of the eutectic reference temperature is needed. The safest way of getting hold of this temperature is through a thermal analysis of the non-modified melt. This approach is time-consuming and it extends the preparation time for the melt in the foundry. Sometimes this approach is even impossible since the metal is pre-modified with strontium or sodium. To overcome this problem, empirical equations were developed to take into account the influence of alloying elements on the eutectic temperature [13]. This requires not only the knowledge of the chemical composition, but also similar cooling conditions to those used to obtain the mentioned equations. From another point of view, the better the cooling conditions in thermal analysis is close to casting reality the better is the prediction of the expected modification in cast part.
In the present paper, the metallurgical and microstructural effects of the modification, by sodium and by strontium, of Al7SiMgTi, Al9SiMgTi and Al11SiMgTi alloys are reviewed by means of thermal analysis and subsequent metallographic examination of the solid samples. Different cooling conditions in thermal analysis experiments are set up and the combined influence of modification and solidification conditions on eutectic temperature and silicon morphology is presented. After a first test step based on a thermal analysis approach, this study turns to real complex-shaped castings like wheels, which are cast in gravity permanent mould technology.

2. MATERIALS AND EXPERIMENTS

A steel thermal analysis cup was used and a K-type thermocouple, calibrated before, was positioned in the centre of the melt. The output from the thermocouple was connected to a PC (via amplifier and an A/D converter) where the temperature/time data were recorded and later processed. Master alloys, in the form of 6 kg ingots, were melt in a resistance furnace and kept at a temperature of 750°C before pouring. The Sr modification was performed using a master alloy rod with 10 wt.% Sr. For sodium modification, pure sodium wrapped in aluminium foil was introduced into the melt. Since the cup temperature doesn't affect the measured eutectic temperature, no attention was paid to monitor the crucible temperature [11].
First of all, the solidification evolution of unmodified AlSi7, AlSi9 and AlSi11 alloys was monitored and an eutectic temperature determined (*Test I*). Due to the combined effect of different modifiers and solidification conditions, the study was then carried out in four parts.
The experiments dealing with Sr were done with Al7SiMgTi, Al9SiMgTi and Al11SiMgTi alloys at the same magnesium and titanium content. These experiments looked at the influence of increasing Sr amount on the thermal analysis' results and on the evolution of eutectic silicon crystals. The Al7SiMgTi alloy was studied with Sr addition of 58, 149 and 181 ppm; Al9SiMgTi alloy with 264, 489 and 565 ppm; Al11SiMgTi alloy with 226, 420 and 580 ppm. The experiments were named *Test II*, *III* and *IV* respectively.
With regard to sodium modification, experiments were carried out with the aforementioned aluminium alloys but, while the first two alloys were modified with 50 ppm Na, in the Al11SiMgTi alloy 65 ppm Na were added.
By means of a wide set of experimental arrangements, the cooling rate in thermal analysis tests was varied. Al9SiMgTi and Al11SiMgTi alloys were submitted to this investigation, where the Sr amount was kept constant at 390 ppm. At first the

modified melt was examined by means of standard thermal analysis. Three different systems with increasing cooling conditions were adopted to change the solidification history of the samples: a chill plate (150x150x20 mm) at the bottom of the cup (Figure 1a), a chill plate with pressurized air blown on the cup (Figure 1b) and a chill plate with pouring water (Figure 1c). In order to compare the previous results obtained with increasing amount of strontium, the experiments, with increasing cooling conditions, were respectively named *Test II*, *III* and *IV*. Another test was carried with Al9SiMgTi alloy, where, to work with higher cooling rates, the thermal analysis crucible was dipped into a water bath at room temperature (*Test V*).

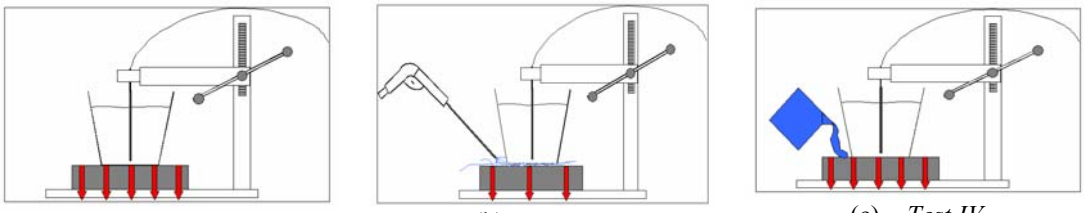

(a) – *Test II* (b) – *Test III* (c) – *Test IV*

Fig. 1. Systems used to change the cooling conditions during thermal analysis tests.

To take into account the effect of alloying elements on the eutectic temperature of unmodified alloys an empirical equation was used [13]:

$$T_{eutectic} = 577-(12.5/\%Si)\cdot[4.43\cdot(\%Mg)+1.43\cdot(\%Fe)+1.93\cdot(\%Cu)+1.7\cdot(\%Zn)+3\cdot(\%Mn)+4\cdot(\%Ni)] \quad (1)$$

The eutectic depression, ΔT(°C), was established as the difference between the calculated and measured eutectic temperature, before and after modification respectively.
Additionally, metallographic examinations were carried out to correlate the results of thermal analysis with the corresponding microstructures.
Finally, to verify the results obtained with a thermal analysis approach, automotive wheels were cast and analysed. Wheels were cast with Al7SiMgTi and Al11SiMgTi alloys in gravity permanent mould technology, at the same pouring temperature (750°C) and with the same mould and production cycle. While the Al7SiMgTi alloy was modified with 200 ppm Sr or with 50 ppm Na, in the Al11SiMgTi alloy 400 ppm Sr or 50 ppm Na were added respectively. On account of the geometry and wall thickness ratios, the solidification rate varies in different areas of the wheel. Therefore, to evaluate the combined effects of local solidification conditions and modification treatment on eutectic silicon morphology, the front flange and the hub area were studied by means of metallographic examinations and the results compared with those obtained from thermal analysis (Figure 2). The hub is a massive, thick region, while the front flange is a thin zone, characterized by higher solidification rate.

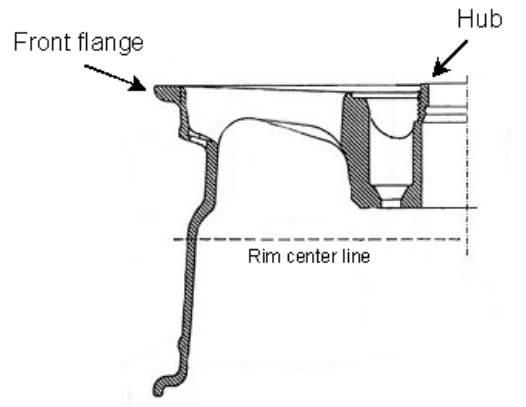

Fig. 2. Wheel cross section with the zones analysed.

3. RESULTS AND DISCUSSION

3.1. Analysis of non-modified AlSi7, AlSi9 and AlSi11 alloys – Test I

As expected, the experiments with non-modified AlSi7, AlSi9 and AlSi11 alloys showed that the influence of silicon on the eutectic temperature in binary Al-Si alloys is almost negligible. For the investigated silicon range, i.e. from 7 to 11 wt.%, the eutectic temperature was measured around 576°C. This can be considered a good result, compared to 577°C from Al-Si phase diagram, if the measurement error of the thermocouples is taken into account. Figure 3 shows typical solidification curves T(t) of the unmodified alloys where it is possible to observe how the different Si content has no influence on the eutectic temperature but on the eutectic solidification time, due to the different eutectic amount. Thus, the eutectic stage appeared as a plateau, without any depression of nucleation and growth temperature or recalescence prior to growth. On the contrary, the solidification of α-Al phase was strongly influenced by the silicon content.

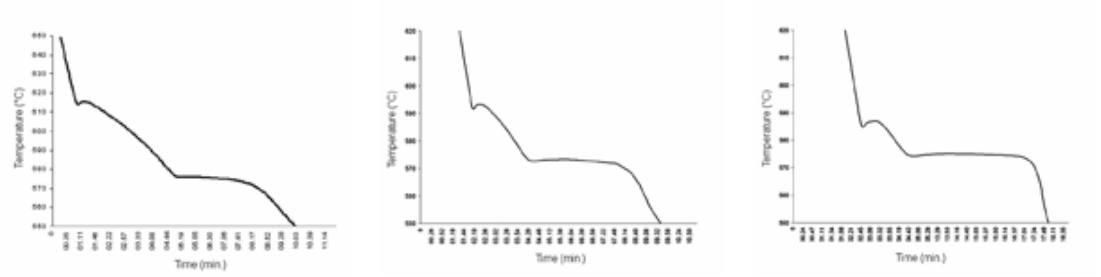

(a) (b) (c)

Fig. 3. Solidification curves T(t) of unmodified (a) AlSi7, (b) AlSi9 and (c) AlSi11 alloys.

The eutectic temperature, calculated with eq. (1), had a gap of ~0.6°C with the measured one. Thus, the empirical equation has been determined at similar cooling rates compared to the conditions in the present work, warranting the reliability of data.

The micrographs showed that the unmodified samples contain silicon in the form of large plates with sharp sides and ends (Figure 4). In AlSi11 alloy primary silicon

crystals were also observed. The metallographic examinations confirmed how the eutectic fraction increased with increasing silicon content, thus explaining the extended eutectic solidification time.

(a) (b) (c)

Fig. 4. Microstructure of thermal analysis samples of (a) AlSi7, (b) AlSi9 and (c) AlSi11 alloys.

3.2. Strontium modification

3.2.1. Al7SiMgTi alloy

Strontium additions resulted in a deep change of cooling curves in the vicinity of the eutectic reactions, as shown in figure 5a where a representative AlSi7 solidification curve is also drawn. An increasing depression of the eutectic nucleation and growth temperatures was observed with increasing Sr amount. The analysis revealed an eutectic temperature of about 570, 567 and 565°C and a depression of about 6, 9 and 10°C with 58, 149 and 181 ppm Sr respectively (Figure 5b). Up to a level of 150 ppm Sr it corresponded a sharp rise of eutectic depression (~9°C), while, increasing of other 30 ppm the content of Sr, an increment of only 1°C was revealed. Therefore, strontium seems to be close to a saturation level in Al7SiMgTi alloy and this is detectable through thermal analysis.

An undercooling of 2-3°C and a deep recalescence function, during which the liberation of latent heat surmounts the heat extraction from the system, was monitored.

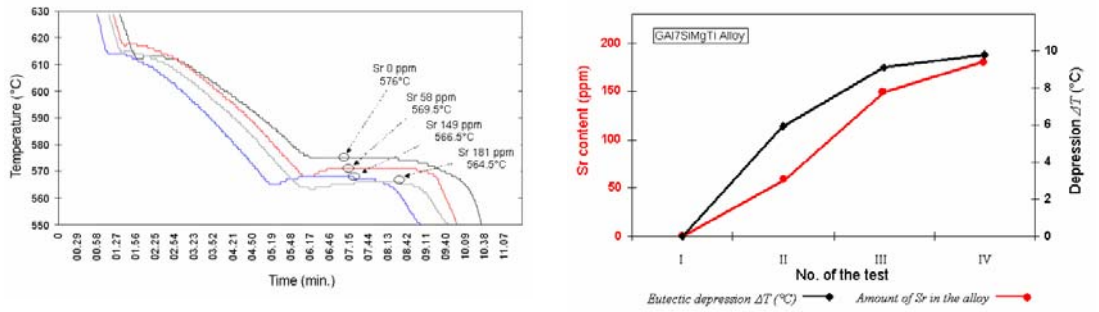

(a) (b)

Fig. 5. (a) Cooling curves and (b) variation of eutectic depression with different Sr amount in Al7SiMgTi alloy.

A comparison of micrographs shows how the determined depression values correspond with the real modification behaviour (Figure 6). While in the microstructure of the 50 ppm Sr modified alloy some coarse lamellar eutectic islands are present, the other samples contain silicon in the form of fine fibrous particles. No distinct difference can be evidenced in the modification level of the 150 and 180 ppm Sr modified specimens. Backerud *et al.* reported how the optimum strontium level for Al7SiMgTi alloy is in the range of 100-200 ppm, even if low additions however fade rapidly [3].

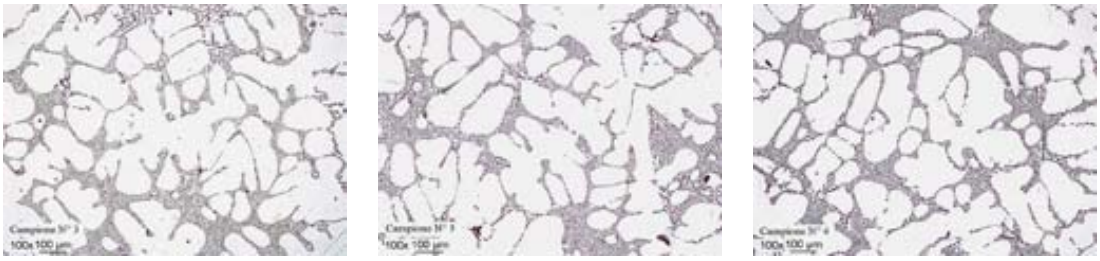

(a) (b) (c)

Fig. 6. Microstructure of thermal analysis samples of Al7SiMgTi alloy with (a) 58, (b) 149 and (c) 181 ppm Sr.

3.2.2. Al9SiMgTi alloy

The strontium level in this alloy was kept higher than in the Al7SiMgTi alloy due to the higher silicon content. The eutectic depression was 6.5, 7.1 and 6.8°C with 264, 489 and 565 ppm Sr respectively. As observed in the Al7SiMgTi alloy, the eutectic depression had the greatest increment at first strontium addition and then it tended to become stable or actually decrease at highest strontium level. An undercooling of 2-3°C and a deep recalescence effect was monitored.

The microstructural investigations revealed a not well modified microstructure. Despite the high strontium amount, eutectic islands of unmodified silicon were present (Figure 7).

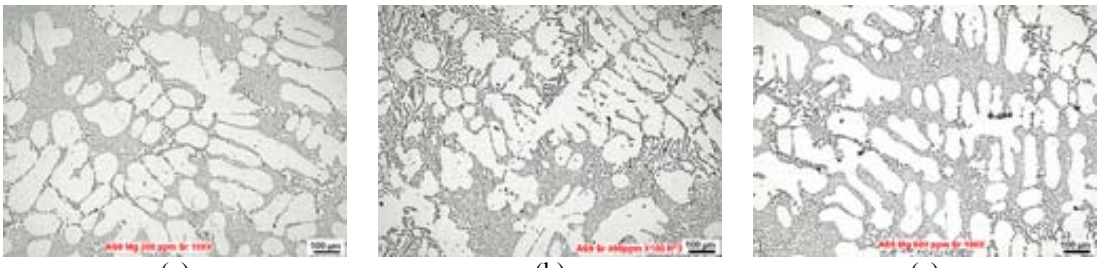

(a) (b) (c)

Fig. 7. Microstructure of thermal analysis samples of Al9SiMgTi alloy with (a) 264, (b) 489 and (c) 565 ppm Sr.

Samples with 489 ppm Sr showed appearance of particles of Al_4SrSi_2 type, which do not contribute to the modifying effect (Figure 8) [3,14]. These intermetallics were located in the zones where the eutectic silicon was weakly modified. This is because the Al_4SrSi_2 particles reduce the amount of strontium in solution and thereby its

effect. Increasing the percentage of strontium led to higher fraction of Al_4SrSi_2 particles.

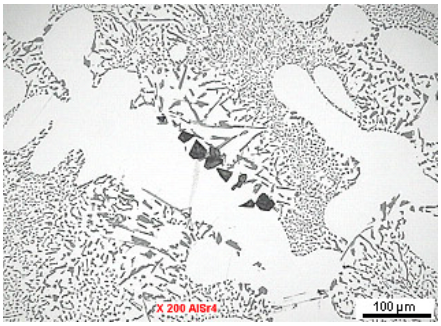

Fig. 8. Samples showing particles of Al_4SrSi_2 type.

3.2.3. Al11SiMgTi alloy

As in the previous alloy, the strontium amount was kept in the range of 230-580 ppm. The eutectic depression was calculated as 4.1, 3.1 and 3.4°C with 226, 420 and 580 ppm Sr respectively. The eutectic depression is lower if compared to the previous alloys. The highest depression value was at first strontium addition, then a decreasing trend was observed. An undercooling of 2-3°C and a deep recalescence effect was recorded.

(a) – *Test II* (b) – *Test III* (c) – *Test IV*

Fig. 9. Microstructure of thermal analysis samples of Al11SiMgTi alloy with (a) 226, (b) 420 and (c) 580 ppm Sr.

The microstructural investigations revealed a not well modified microstructure, due to the presence of unmodified eutectic islands (Figure 9). At a level of 420 ppm Sr, particles of the Al_4SrSi_2 type appeared and were located in the zones where the eutectic silicon was weakly modified. Increasing the percentage of strontium to 520 ppm, the fraction of Al_4SrSi_2 intermetallics increased.

Figure 10 summarizes the results obtained from thermal analysis tests of Al7SiMgTi, Al9SiMgTi and Al11SiMgTi alloys. The eutectic depression decreases considerably increasing the silicon content in the alloy. While a mean value of 9 and 7°C can be observed for Al7SiMgTi and Al9SiMgTi alloys respectively, a value of ~4°C was detected for Al11SiMgTi alloy despite the increasing amount of strontium. The eutectic depression tends to decrease with the highest strontium addition in Al9SiMgTi and Al11SiMgTi alloys and the presence of Al_4SrSi_2 particles seems to

indicate a supersaturation of strontium, which would make useless the effect of lower strontium contents. A common feature for the alloys analysed is the highest relative depression value at low strontium level, which tends to fade with higher amount.

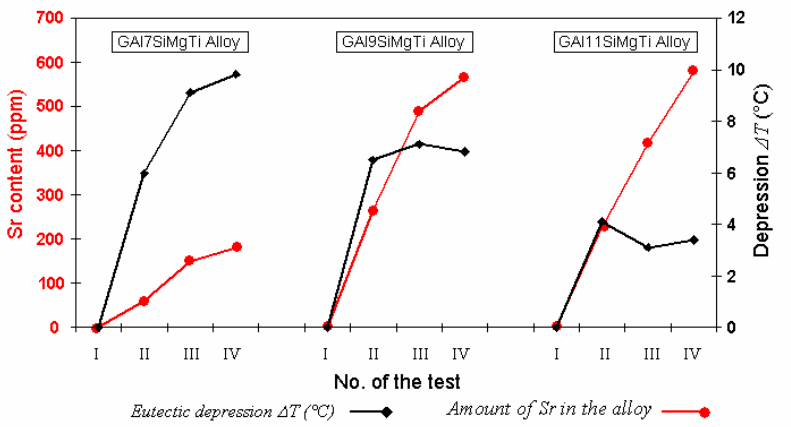

Fig. 10. Variation of eutectic depression with different Sr amount at slow solidification conditions.

3.3. Sodium modification

In this study, eutectic depression of Na modified Al7SiMgTi, Al9SiMgTi and Al11SiMgTi alloys was 7.5, 7.3 and 7.8°C respectively. While in the first alloys the sodium content was 50 ppm, in Al11SiMgTi was increased to a level of 65 ppm due to the high silicon content. In spite the silicon content was so different and the sodium amount so close, the eutectic temperature showed a similar stable decrease. The low growth temperature and practically no recalescence effect indicate good modification, which is also shown in the corresponding micrographs (Figure 11).

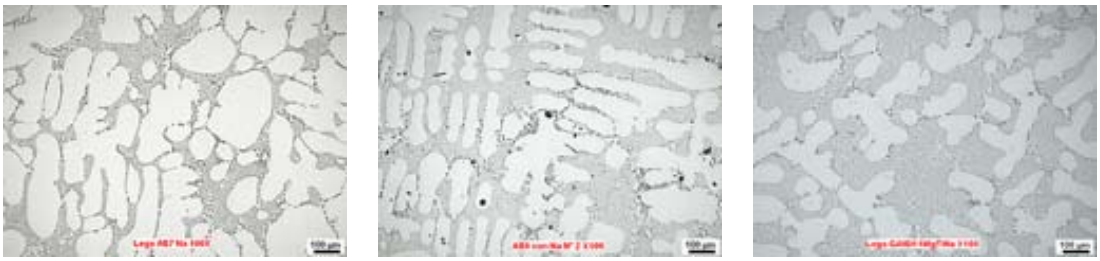

(a) (b) (c)

Fig. 11. Microstructure of thermal analysis samples of (a) Al7SiMgTi 50 ppm Na, (b) Al9SiMgTi 50 ppm Na and (c) Al11SiMgTi 65 ppm Na alloys.

In conditions of slow solidification, it can be asserted that the alloys analysed, modified with strontium, behave in unstable way if compared to materials modified with sodium. Therefore, for Al-Si alloys with high silicon content it would be better using Na modification, which guarantees a remarkable eutectic depression and a good silicon change.

3.4. Effect of solidification rate and strontium modification

3.4.1. Al9SiMgTi alloy

It was clearly seen that, due to the higher cooling conditions, the eutectic reaction took place at a higher undercooling, which resulted in a lower indicated eutectic temperature. It is known that rapid solidification, in the growth rate range of 400 to 1000 µm/s (quench modification), changes the shape of eutectic silicon which appears identical to chemical modified eutectic Si [14]. The addition of 390 ppm Sr and slow solidification conditions showed a depression of only 5.7°C and, as it is possible to see in figure 12a, the result was a microstructure where only 70/80% were modified. Using the thermal analysis devices aforementioned, an eutectic depression of 10, 10, 9.1 and 10.2°C was observed during *Tests II*, *III*, *IV* and *V* respectively and a well modified structure resulted (Figure 12b).

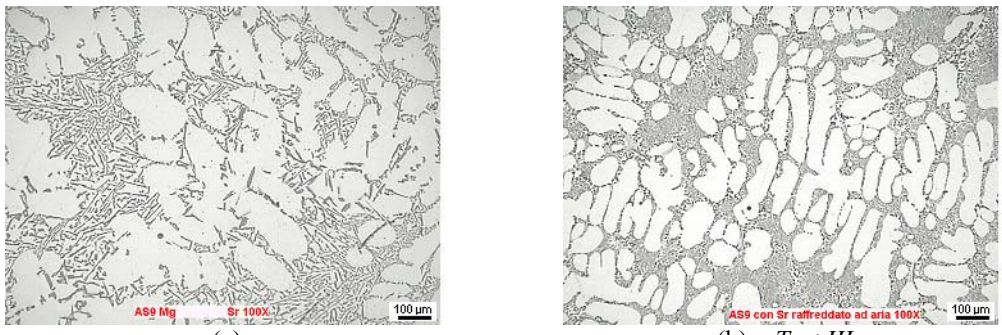

(a) (b) – *Test III*

Fig. 12. Microstructure of thermal analysis samples of Al9SiMgTi alloy with 390 ppm Sr at (a) slow and (b) fast (Test III) solidification rate.

3.4.2. Al11SiMgTi alloy

The Al11SiMgTi alloy, modified with 390 ppm Sr and slowly solidified, showed an eutectic depression of only 3.5°C, but, increasing the solidification rate, values of 6, 6 and 7°C with *Tests II*, *III*, and *IV* respectively were reached.

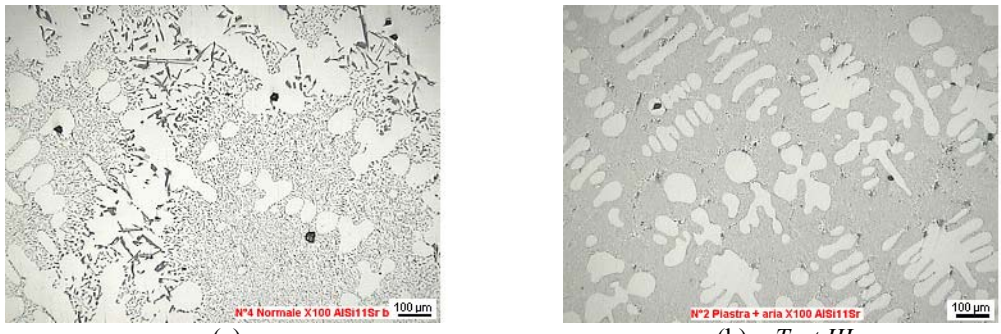

(a) (b) – *Test III*

Fig. 13. Microstructure of thermal analysis samples of Al11SiMgTi alloy with 390 ppm Sr at (a) slow and (b) fast (Test III) solidification rate.

The microstructural investigations corresponded well with the real modification level. While eutectic silicon particles in modified alloy, solidified at slow cooling

rate, appeared acicular, in samples obtained at higher solidification rates were fibrous (Figure 13).

Figure 14 summarizes the results of eutectic depression obtained from thermal analysis of Al7SiMgTi, Al9SiMgTi and Al11SiMgTi alloys, changing the strontium amount or the solidification conditions. While in Al7SiMgTi alloy a good modification level was already observed with strontium in a range of 100-200 ppm even at slow cooling conditions, the Al9SiMgTi and Al11SiMgTi alloys didn't respond to continuous strontium addition at the same solidification rates. It was observed that for these two alloys, increasing the cooling rate of thermal analysis system, the eutectic depression increased to higher level, reaching mean values of about 10 and 6°C respectively, i.e. an improvement of 43% and 50%. The eutectic depression caused by strontium modification grows if high cooling rates prevail. Thus, while for Al7SiMgTi alloy it is not required an increment of solidification rates, this seems essential for hypoeutectic alloys with high silicon content in order to reach a good modification level. The consequences are important thinking to real shape castings, where several solidification conditions are present, due to different heat transfer rates. Controlling the heat transfer, it is possible to obtain, to a large degree, an homogeneous microstructure and an improvement in the final quality of castings. In particular, the optimisation of cooling channels in permanent mold casting is very influential as they typically account for 90% or more of heat extraction [15].

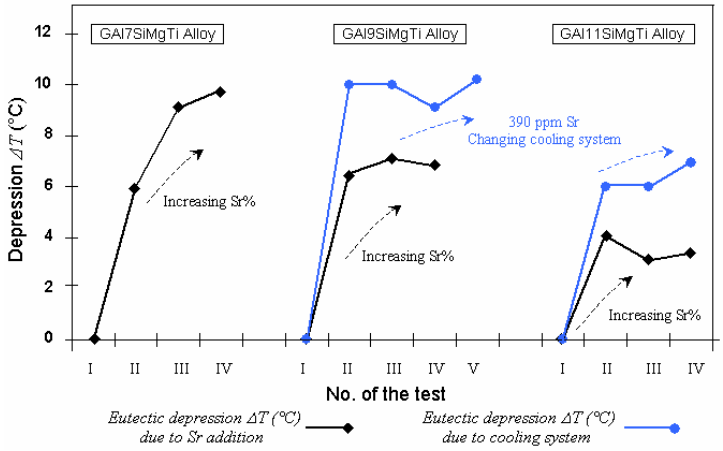

Fig. 14. Variation of eutectic depression with different Sr amount at slow solidification rate and with constant Sr addition (390 ppm) at higher cooling rates.

Microstructural characterization has been completed with the measurements of the secondary dendrite arms spacing (SDAS) of α-Al phase, generally correlated to the solidification speed. Results from these measurements together with eutectic temperatures from thermal analysis are shown in figure 15 for Al9SiMgTi and Al11SiMgTi alloys. As expected, with traditional thermal analysis system, i.e. at slow cooling rate, SDAS showed the highest values, around 70 µm, while changing the cooling device, i.e. increasing the cooling conditions from *Test II* until *Test V*, SDAS decreased up to 25 µm. The same trend was partially observed on the eutectic temperature. The latter was highest in unmodified alloys at slow solidification rate,

as previously said, while it decreased to a stable temperature, 564 and 568°C for Al9SiMgTi and Al11SiMgTi alloys respectively, independently from changing the thermal analysis system.

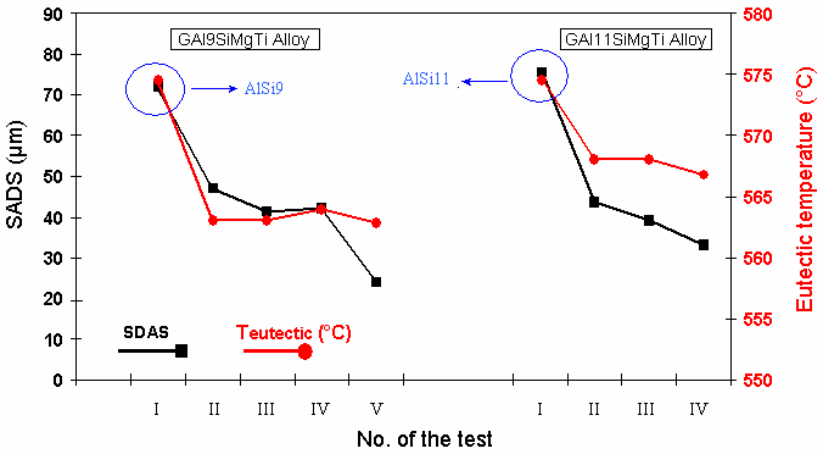

Fig. 15. A comparison between SDAS and eutectic temperature of Al9SiMgTi and Al11SiMgTi alloys in the different tests.

3.5. Effect of solidification rate and modification on gravity cast wheels

3.5.1. Al7SiMgTi alloy

The wheels, cast with Al7SiMgTi alloy and modified with strontium or sodium, revealed a well modified microstructure in the hub and in the front flange region. SDAS values were higher in the in the hub (~43 µm) than in the front flange area (~25 µm), demonstrating the close proportional relationship between SDAS and section thickness. In spite the different solidification conditions and modification type, the eutectic silicon appeared in the form of fine fibrous particles (Figures 16 and 17). The analysis carried out on real complex-shaped casting confirms what previously observed with thermal analysis, where, even at slow solidification rate, an eutectic depression of 10 and 7.5°C for strontium and sodium modification were measured respectively. The Al7SiMgTi alloy shows a good modification level with sodium or strontium addition independently of cooling conditions.

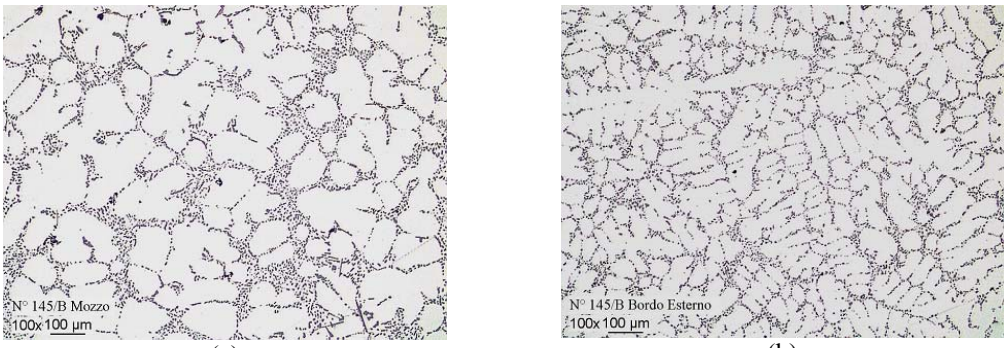

(a) (b)

Fig. 16. Microstructure in (a) the hub and (b) in the front flange region of wheels cast with Al7SiMgTi alloy and modified with 200 ppm Sr.

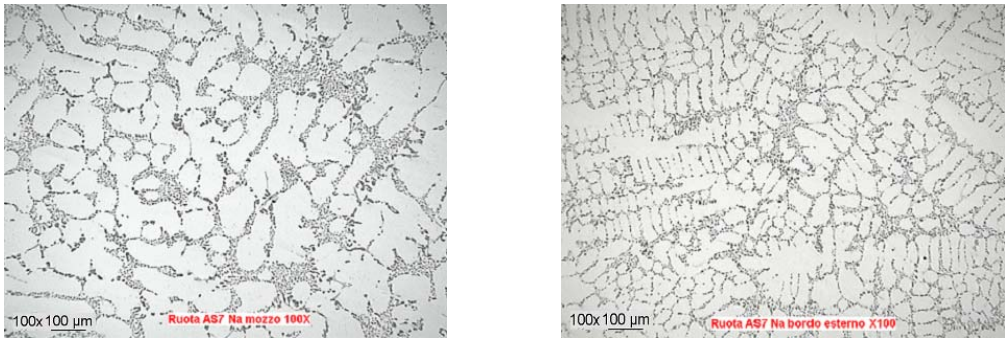

(a) (b)

Fig. 17. Microstructure in (a) the hub and (b) in the front flange region of wheels cast with Al7SiMgTi alloy and modified with 50 ppm Na.

3.5.2. Al11SiMgTi alloy

Figure 18 shows the microstructure in the hub and in the front flange region of the wheels cast with Al11SiMgTi alloy and modified with 400 ppm Sr. While several unmodified eutectic islands are present in the hub (Figure 18a), where the solidification is slow, the strontium amount combined with higher cooling rate modified the silicon particles from large flakes to fine fibers in the front flange area (Figure 18b). As previously observed with thermal analysis tests, the eutectic depression can increase by more than 4°C by increasing the solidification rate, with the same strontium amount.

The wheels modified with 50 ppm Na revealed a fine fibrous eutectic structure with few unmodified eutectic islands in the hub region (Figure 19). However, this confirms the thermal analysis results, where an eutectic depression of 7.8°C was measured with 65 ppm Na at slow solidification conditions.

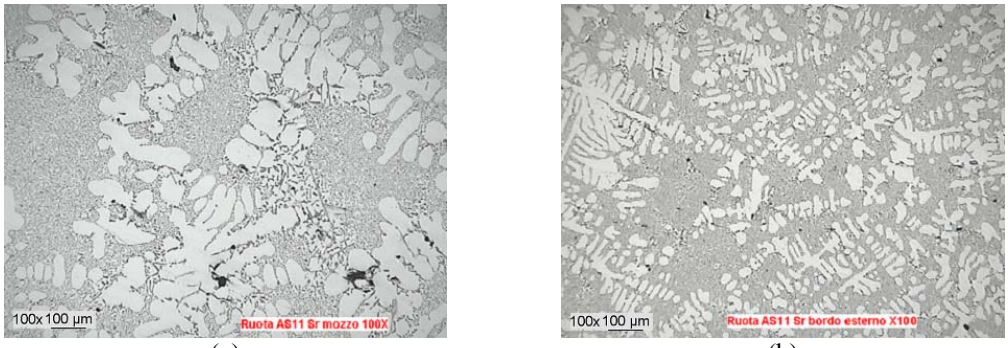

(a) (b)

Fig. 18. Microstructure in (a) the hub and (b) in the front flange region of wheels cast with Al11SiMgTi alloy and modified with 400 ppm Sr.

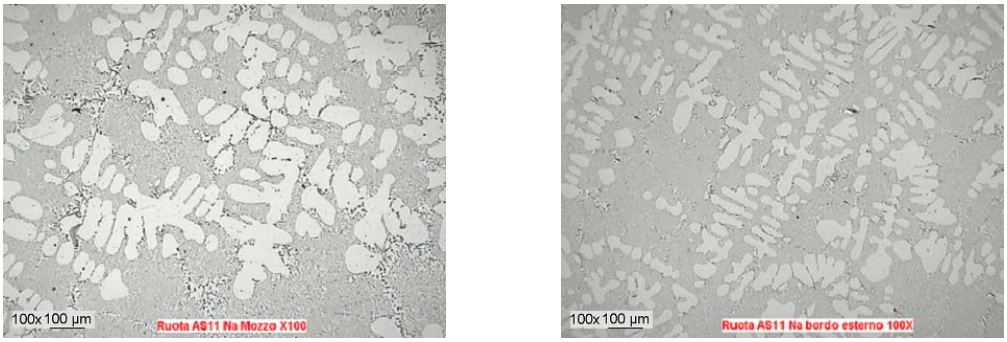

(a) (b)

Fig. 19. Microstructure in (a) the hub and (b) in the front flange region of wheels cast with Al11SiMgTi alloy and modified with 50 ppm Na.

4. CONCLUSIONS

Eutectic depression, i.e. the difference between the eutectic temperatures before and after a modification treatment, was used to assess the modification level of Al7SiMgTi, Al9SiMgTi and Al11SiMgTi alloys, modified by sodium and by strontium. Thermal analysis and subsequent metallographic examination of the solid samples were carried out. The results showed that, in Al7SiMgTi alloy, modification level improved by increasing the strontium amount and the optimum was reached in a range of 100-200 ppm. Similar results were not obtained in Al9SiMgTi and Al11SiMgTi alloys, which showed partially modified microstructure in spite higher strontium content. Sodium modification resulted in a low growth temperature and no recalescence effect indicating good modification, which were also shown in the corresponding micrographs.

From another point of view, the better the cooling conditions in thermal analysis is close to casting reality the better is the prediction of the expected modification in cast part. Therefore, in order to study the combined effect of solidification rate and strontium modification, getting close to casting reality, the cooling rate in thermal analysis tests was varied by means of a wide set of experimental arrangements. After a first test step based on a thermal analysis approach, this study turned to gravity cast wheels, where several solidification conditions are present. The eutectic depression of Al9SiMgTi and Al11SiMgTi alloys increased by increasing the cooling rate and the modification level improved as confirmed by metallographic inspection. While Al7SiMgTi alloy showed a well modified microstructure without any increment of solidification rate, this seems essential for hypoeutectic alloys with high silicon content in order to obtain similar results. The consequences are important for real shaped castings where different solidification conditions are present, due to different heat transfer rates. Controlling the heat transfer, it is possible to obtain, to a large degree, an homogeneous microstructure and an improvement in the final quality of castings.

ACKNOLEDGMENTS

The authors would like to acknowledge Mr. Manuele Rossetto for help with casting, Mr. Silvano Rossetto for the scientific support, as well as Mr. Valerio Rossetto and Società Alluminio Veneto S.A.V. S.p.A. for the financial support.

REFERENCES

1. W.H. CROUSE, D. L. ANGLIN, “Automotive engines”, 1995, McGraw-Hill (Ed.).
2. W. KURZ and D.J. FISHER, Fundamentals of solidification. Trans. Tech. Publications, Switzerland (1998).
3. L. BACKERUD, G. CHAI and J. TAMMINEN, Solidification Characteristics of Aluminum Alloys-Vol.2: Foundry Alloys. American Foundrymen's Society, Inc., IL, USA (1990).
4. J.E. GRUZLESKI, B.M. CLOSSET, The treatment of liquid Aluminum-Silicon alloys, (1990), The American Foundrymen’s society Inc, IL, USA (1990).
5. S. SHANKAR, Y.W. RIDDLE, M.M. MAKHLOUF, Metall. Mat. Trans. 35A, 9 (2004), pp.3038-3043.
6. A.K. DAHLE, K. NOGITA, S.D. McDONALD, C. DINNIS, L. LU, Mater. Sci. Eng. A413–414, (2005), pp.243–248.
7. A. KNUUTINEN, K. NOGITA, S.D. McDONALD, A.K. DAHLE, J. Light Met. 1, (2001), pp.229-240.
8. SHU-ZU LU, A. HELLAWELL, Met. Trans. 18A, (1987), pp.1721-1733.
9. A. MANENTE, P. FERRO, E. DELLA ROVERE, Metall. Ital. 6, (2003), pp.27-35.
10. F. PIASENTINI, F. BONOLLO, A. TIZIANI, Metal. Sci. Tech. 23, 2 (2003), pp.11-20.
11. L. HEUSLER, W. SCHNEIDER, J. Light Met. 2, (2002), pp.17-26.
12. A. JOENOES, E. GRUZLESKI, Cast Metals 4, 2 (1991), pp.62-71.
13. D. APELIAN, G.K. SIGWORTH, K.R. WHALER, AFS Transactions, (1984), pp.297-307.
14. M.M. MAKHLOUF, 8th International Summer School, Trondheim, Norway, August 21-25, (2006).
15. K. DAVEY, S. HINDUJA, L.D. CLARK, Proc. Instn. Mech. Engrs., Vol. 216 Part B: J Engineering Manufacture, (2002), pp.1589-1609.

ARTICLE 2

ON THE FLUIDITY OF ALUMINIUM ALLOY DIECASTINGS

G. Timelli*, F. Bonollo*

* Department of Management and Engineering – DTG
University of Padova
I-36100 Vicenza
ITALY

Submitted for publication in: International Journal of Cast Metals Research, 2007

ABSTRACT
The aim of the present work was to investigate the fluidity of four different high pressure die cast (HPDC) Al-Si alloys at different pouring temperatures. A vacuum fluidity test apparatus has been used to measure fluidity. The analysed alloys showed a different flow sensitivity to casting temperature. Further, it is showed that among the considered alloying elements, magnesium and silicon affected the fluidity of the melt. One alloy was then contaminated with 50% scrap addition, increasing the amount of oxide inclusions. The fluidity of the contaminated melt has then been measured and compared with the fluidity of the clean melt. The results show that the fluidity of the alloy with scrap addition is lower than that of the clean melt. Further the fluidity linearly increases at raising temperatures within the range between 580°C and 680°C until it reaches a plateau at the highest pouring temperatures.

Keywords: Aluminium alloys; Fluidity; High-pressure-die-casting (HPDC); Oxide inclusions; Vacuum fluidity test.

1. INTRODUCTION

Weight reduction has long been a key issue for vehicle manufacturers in the quest to find more and more solutions to the requirements of the fuel economy and the need to reduce the emission of pollutants.[1] In terms of application rates, aluminium and its alloys have an advantage over other light materials. The large demand of aluminium alloys has been identified in a number of key factors such as reduced aluminium prices, the recyclability, the development of improved alloys, the increased understanding of design criteria and life prediction for stressed aluminium components and an excellent compromise between mechanical performances and lightness.[2] A great contribution to the use of aluminium alloys comes from improvements in casting processes which allow to increase the production, lower the cycle time, and realize complex-shaped castings with thin wall thickness. As high pressure die casting (HPDC) reflects these advantages, different automotive components are made with this technique.[1,2]

Another important aspect for aluminium foundries is the recycling possibility of scraps from different manufacturing stages. On recycling aluminium scraps, great care shall be taken to avoid oxide inclusions, which have a dramatic effect not only on mechanical properties but also on the material castability.[3,4] A possible remedy could consist to pour the melt at higher temperatures, but this would increase the hydrogen solubility in the liquid.[5,6] A closer look at the alloys for HPDC is hence needed to explain the onset of casting problems in order to be able to avoid them and assure a high casting quality.

In the different casting processes the knowledge of fluidity of aluminium alloys plays a key role to obtain the highest process efficiency. It determines the application field of aluminium alloys for the different casting processes. The relationship between fluidity and filling of the die is clear and it is becomes even more critical for thin-walled castings.

Aim of the present study is to investigate the fluidity of some commercial aluminium alloys for high pressure die casting and to analyse how fluidity can be affected by recycling aluminium scraps.

2. THEORETICAL ASPECTS

2.1. Definition of fluidity

In terms of casting alloys, the fluidity is defined as the maximum distance to which the liquid metal will flow before it is stopped by solidification.[7] Thus, fluidity is simply a length measured, for instance, in millimetres. Generally fluidity can be defined as that property of the liquid metal enabling it to flow through the mould passages and to fill all the interstices of the mould, providing sharp outlines and accurate reproduction of design details.[7-9] Other terms such as castability have been used to describe this flow behaviour, even if the term fluidity is most widely recognised. Fluidity is not exactly a single physical property, as the density or the viscosity are, but a complex characteristic related to the alloy's behaviour under specific conditions within a foundry mould.[8,9] One of the fundamental characteristics of the liquid state is the ability of any liquid to conform in time to the shape of its container. This would occur rapidly in the case of liquid metal since viscosities of liquid metals are low, for instance below 1.15 mPa s for an A356 alloy.[8,10] Failure to fill the mould cavity results not from high viscosity but from premature solidification. Thermal conditions and solidification mode are the critical factors

affecting the cessation of flow. The concept of fluidity also takes these aspects into account.[7-9]
The use of the foundry term fluidity should not be confused with its use in physical chemistry, where fluidity is defined as the reciprocal of viscosity.[7] The foundry term fluidity , according to the work by Bastien *et al.*,[11] is independent of the viscosity of the liquid.

2.2. Fluidity tests

Since fluidity is an empirical measure of a processing characteristic, the foundryman measures this property in one of the several types of fluidity tests. Two common types are the sand-mould fluidity spiral and the vacuum fluidity test. In the sand-mould fluidity spiral test, the melt is poured into a spiral shaped channel with a small cross-sectional area. In the vacuum fluidity test, the melt is sucked into a glass or metal tube under a recorded reduced pressure. The vacuum fluidity test offers two advantages: it allows direct observation of the metal flow in the glass tube, and it is somewhat simpler than pouring a sand-cast spiral.[9] A disadvantage is that the thermal gradient and the nucleation conditions obtained by using a glass or metal mould wall are different from the typical values for sand moulds.[9]
Several studies were carried out to investigate the fluidity of aluminium alloys and the factors affecting it. However, available results are sometimes contradictory or scarcely comparable, since the researchers have often applied different variants of the fluidity test, so those tests conditions are not always consistent.[7,12]
Niyama *et al.*,[13] have studied the relationship between fluidity and various casting parameters in an A356 and Al-Si binary alloy with a vacuum fluidity apparatus. They showed how the fluidity of these alloys increases linearly not only with the temperature, but also with mould diameter and suction pressure used in the test. An increment in fluidity values was also observed when mould coating and inert gas were used. Campbell[7] demonstrated that different types of fluidity tests in the same mould materials can give consistent and equivalent results, provided that the surface tension and the casting modulus (i.e., the ratio between volume and cooling area of the casting) are taken into account.

2.3. Variables influencing fluidity

One factor affecting the fluidity of Aluminium alloys is the chemical composition. The silicon content in Al-Si binary alloys, for instance, is responsible for the increment of fluidity as a result of the latent heat of solidification of Silicon, which is one among the highest in nature and about 5 times greater than that of Al.[13] The fluidity in Al-Si system does not reach the peak at the equilibrium eutectic around 11 wt.% Si, but at a Silicon content of about 15 wt.%.[7,13-16] In general, fluctuations in alloy composition according to international alloy standards can significantly influence the fluidity of casting alloys, introducing repeatability errors into the casting process.[17] Especially in the A356 alloy it seems that Mg is the only element that greatly affects the fluidity: increasing the Mg content decreases the fluidity of the melt. Di Sabatino *et al.*[18] reported that the Fe content, instead, does not exert any effect on fluidity up to a maximum level of 0.23 wt.%. However other authors,[19,20] who underlined how the Fe-bearing phases formed in the alloys obstruct the interdendritic flow channels during the last stage of solidification, revealed a deleterious effect of iron on the fluidity of molten metal. Kaufmann *et al.*[17] noted that

there seems to be a conflicting behaviour generated by the addition of alloying elements: on the one side, they may have a positive effect on the fluidity of the alloy by increasing the total heat content, retarding therefore the solidification time; on the other side, they may affect negatively the fluidity due to an increase in viscosity generated by the intermetallics formed upon solidification. Chirkov *et al.*[21] mapped the fluidity of Al-Cu-Mg alloys analysing the simultaneous effect of Cu and Mg.

Other two factors influencing the fluidity are the casting temperature and the heat of fusion. Although the literature reports on results obtained by different testing procedures, the available data on the effect of temperature and heat of fusion on fluidity confirm that melt superheat affects fluidity.[7-9,12,18,22-24] A linear correlation was found to exist between fluidity and superheat temperature.[7-9,12,17,22-25] This can be interpreted as a fundamental effect of solidification controlling the duration of flow, since the superheat determines the quantity of heat to be dissipated prior to the onset of solidification.[8,24]

The mathematical model proposed by Flemings[24] provides the following simplified equation to determine the flow length L_f:

$$L_f = \frac{A\rho v(f_s^{cr}H + c\Delta T)}{hS(T - T_0)}\left(1 + \frac{B}{2}\right) \qquad (1)$$

where:
A is the mould cross sectional area;
ρ is the liquid density;
v is the flow velocity;
f_s^{cr} is the critical solid fraction for flow stoppage;
H is the latent heat of solidification;
c is the specific heat of metal;
ΔT is the melt superheat;
h is the heat transfer coefficient between mould and metal;
S is the circumference of the mould channel;
T is the liquid temperature;
T_0 is the room temperature;
B is a constant depending on the heat transfer coefficient and on the resistance to heat flow (metal-mould interface).

The model is based on the assumptions that:
(i) solid particles form during the flow in the fluidity channel and travel downstream with the liquid;
(ii) the flow stops when the solid fraction at the flow tip reaches a certain value (critical solid fraction, f_s^{cr});
(iii) the flow velocity remains constant until the flow stops.[24]

Equation (1) illustrates many of the important variables influencing the foundryman's fluidity. For instance, it can be noted that fluidity increases approximately linearly with increasing latent heat of solidification, melt superheat and velocity of flow.

Different works were carried out on the effect of grain refinement on fluidity of cast aluminium alloys; however, in this case the published results seem not to agree.

Dahle *et al.*[16] found a complex variation in fluidity with successive addition of AlTi5B1 grain refinement in Al–7 wt.%Si–Mg and Al–11 wt.%Si–Mg alloys

adopting a sand mould spiral test. The fluidity behaviour of the analysed alloys was explained with the relation between the added amount of grain refinement and the fraction solid at dendrite coherency existing in long freezing range alloys. On the other side, no statistically significant conclusions were instead observed by Di Sabatino *et al.*[26] in Al–7 wt.%Si–Mg alloy using a similar test apparatus. Finally, Kwon *et al.*[23] reported that the fluidity is improved with the addition of grain refinement especially at low pouring temperatures in an Al–4.5 wt.%Cu–0.6 wt.%Mn system.

The effect of oxide inclusions, the fraction of which was increased by adding contaminated alloy scraps, and hydrogen content was also investigated by Di Sabatino *et al.*[26,27] and Kwon *et al.*[23] for a commercial A356 alloy. The hydrogen content did not significantly affect the fluidity of A356 alloy even if, as expected, the porosity increased. The presence of oxide inclusions, instead, decreased the fluidity especially at low pouring temperatures, but the percentage of added scraps did not influence fluidity for the same content of inclusions and oxide in the melt.[27]

More recently, the fluidity of aluminium alloys was studied under high pressure die casting conditions.[28] It was revealed that the fluidity length increases with decreasing solidus temperature of an alloy at a given superheat. This is an opposite behaviour to former observations reporting that fluidity increases with increasing solidification interval under gravity casting conditions.

3. EXPERIMENTS

3.1. Fluidity test apparatus and experimental procedure

Fig. 1 shows a schematic view of the vertical vacuum fluidity test apparatus. An electric-resistance furnace with a graphite crucible was used to melt the alloys.

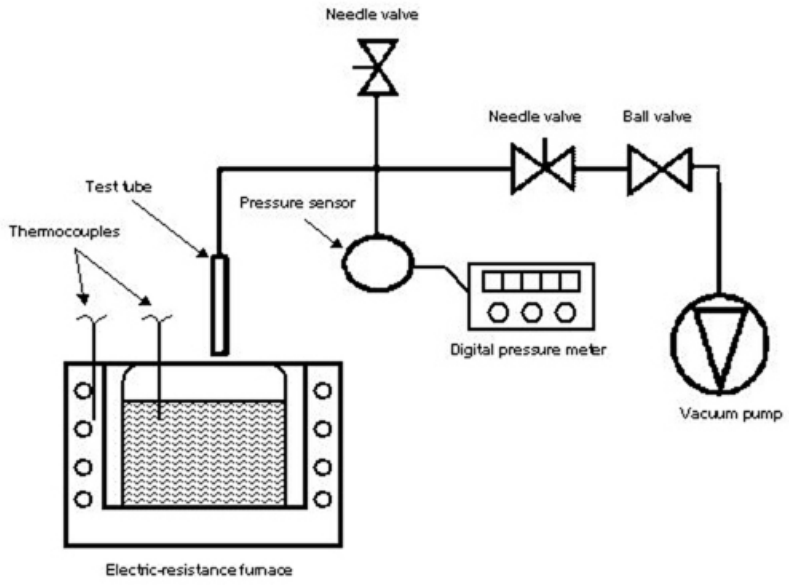

Fig. 1. Vertical vacuum fluidity test apparatus.

In order to control the temperature of the melt two K-type (Chromel-Alumel) thermocouples, connected to a data acquisition and control system, were inserted in the furnace wall and inside the molten metal, respectively. Once the set temperature was reached and stabilized, the dross skin on the top of the melt was manually removed with a rake before starting the fluidity test. As the injection temperature of HPDC Al-Si and Al-Si-Cu alloys normally extends from a minimum of 620°C to a maximum of 700°C,[29] the tests were carried out in the temperature range of 580-760°C with a step of 13°C. The melting method was the same for all the experiments to exclude any influence of the melting process on final fluidity results.[7,8,30-32]
The test tubes were made out of AISI 304 stainless steel; tube dimensions (length, inner diameter, wall thickness) were 500 mm x 9 mm x 1 mm. The tube was neither pre-heated before the fluidity test, nor coated with insulation material; each tube was replaced after testing. During the test the tube was dipped for 20 mm into the melt and after ~5 seconds a depression of 100 mbar was generated within the tube by connecting the free end of the tube to a vacuum pump. The atmospheric pressure (typical foundry condition) was continuously monitored and kept constant during the whole testing duration. The pressure sensor, the needle and ball valves were adopted to control the pressure inside the system and the pressure value was displayed on the digital pressure meter.
In the present work, the fluidity of the alloys was calculated as the maximum upstream length reached by the flowing metal in the tube from the melt surface level in the basin.

3.2. HPDC alloys

Four commercial Al-Si alloys were used in this work. The chemical composition of each alloy, listed in Table 1, was examined on samples taken from the melt by using an atomic emission spectrometer. Copper, magnesium, manganese, silicon and zinc are intentionally added to the commercial aluminium alloys to increase their strength. Zinc has the greatest solubility in aluminium, while most of other alloying elements form second phase microstructural intermetallics. Iron is always present in commercial aluminium alloys as undesired trace element. The presence of iron is in fact detrimental and efforts are made to keep its level as low as possible. However, in high pressure die cast alloys, iron is intentionally added to avoid die soldering. The contents of the secondary alloying elements in the alloys adopted in this work are common for the typical high pressure die cast alloys.

Table 1: Chemical composition of the four alloys used in the present work (wt.%).

Alloy No.	Al	Si	Fe	Cu	Mn	Mg	Zn	Ti	Sn	Pb	Na
Alloy #1	Bal.	11.59	0.87	1.663	0.179	0.093	0.999	0.041	0.034	0.158	0.0002
Alloy #2	Bal.	11.36	0.77	1.79	0.166	0.171	1.163	0.04	0.036	0.112	0.0003
Alloy #3	Bal.	9.62	0.82	1.98	0.152	0.206	0.475	0.035	0.024	0.049	0.0001
Alloy #4	Bal.	8.75	0.85	2.2	0.2	0.15	1.146	-	-	-	-

3.3. Effect of oxide inclusions on the fluidity

The melt was prepared adopting the alloy #1 with 50% scrap addition. Table 2 shows the chemical composition. The scrap addition originated from HPDC foundry returns

in form of refused castings, gating and runner systems and overflows of the same Al-Si alloy. The fluidity of the clean melt was compared with that of the contaminated one. As the amount and the dimensions of oxides in the melt can be influenced by the melting process, it can be stressed here that the melting method was the same for all the experiments to exclude any influence on final fluidity results.[7,8,30-32]

Table 2: Chemical composition of commercial and scrap-contaminated alloys (wt.%).

Alloy No.	Al	Si	Fe	Cu	Mn	Mg	Zn	Ti	Sn	Pb	Na
Alloy #1	Bal.	11.59	0.87	1.663	0.179	0.093	0.999	0.041	0.034	0.158	0.0002
Alloy #1 + 50%	Bal.	11,8	0,82	1,835	0,193	0,076	0,99	0,044	0,035	0,106	-

Samples were taken from the tip of the test tubes, sectioned along the axis (Fig. 2) and prepared for microstructural investigation. Optical microscopy was performed for microstructural analysis and to qualitatively assess dimensions and amount of oxides.

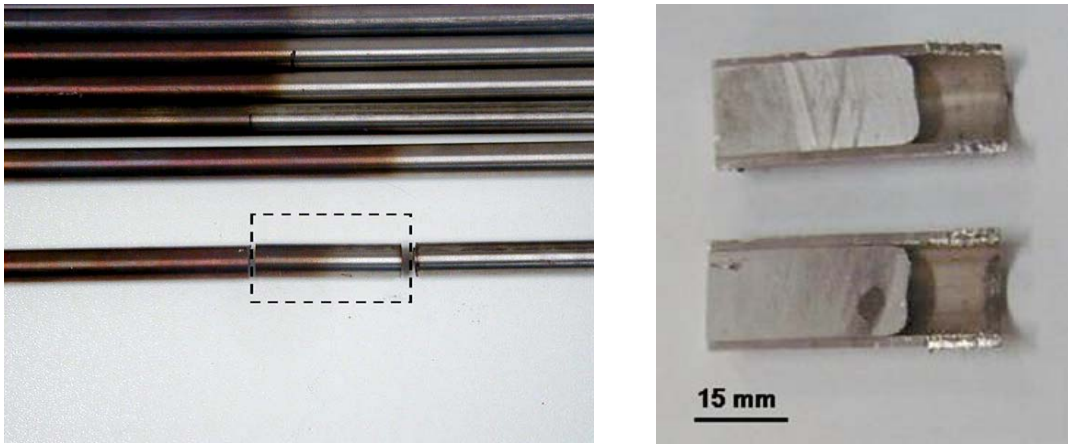

(a) (b)

Fig. 2. a) Location on the test tube of the samples used for microscopy and b) cut of the specimen along the axis.

3.4. Statistics

Within the pouring temperature range, the mean flow length $\bar{L}_f$ appears to be a linear function of pouring temperature T_p, which can be described using the following equation:

$$\bar{L}_f = A \cdot T_p + B \qquad (2)$$

Values of A and B were calculated using the least-squares regression method to give the best fit between the function and the experimental data.[33,34] The quality of the least-squares fitting to the original data was measured using the coefficient of determination, R^2:

$$R^2 = 1 - \frac{\sum_{i=1}^{n}\left(f(x_i) - g(x_i)\right)^2}{\sum_{i=1}^{n}\left(f(x_i) - \overline{f}(x_i)\right)^2} \qquad (3)$$

where x_i is the discrete variable, $g(x_i)$ is the corresponding calculated value using the regression function, $f(x_i)$ is the corresponding experimentally measured value, $\overline{f}(x_i)$ is the mean value of experimental data and n is the total number of experimental points.[33,34] When $R^2 = 1$, the fit is perfect.

The reproducibility σ of the fluidity test was calculated with five test series, that is four test series were performed on different cast alloys, while the last test series concerned the alloy #1 contaminated with 50% scrap addition. Each test series consisted of at least 14 fluidity measurements. The relative reproducibility[22,23,33,34] in percentage value was calculated for each test series of n fluidity measurements L_{if} as

$$\sigma(\%) = \sqrt{\frac{\sum_i \left(\left(L_{if} - \overline{L}_f\right)/\overline{L}_f\right)^2}{n-1}} \cdot 100 \qquad (4)$$

A statistical analysis of the results was also carried out to evaluate the influence of the different elements on the fluidity of each alloy. The Pearson's correlation coefficient (r) was evaluated among the different amount of elements and the fluidity of the alloys estimated at a pouring temperature of 645°C, which corresponds to the pouring temperature normally used in foundry for these alloys.[29] Pearson's correlation (sometimes known as the Pearson product-moment correlation) reflects the degree of linear relationship between two variables.[33,34] The formula for the Pearson's correlation may be expressed in many forms. A commonly used formula is:[33,34]

$$r = \frac{\sum xy - \frac{\sum x \sum y}{n}}{\sqrt{\left(\sum x^2 - \frac{\left(\sum x\right)^2}{n}\right)\left(\sum y^2 - \frac{\left(\sum y\right)^2}{n}\right)}} \qquad (5)$$

where x and y are the two variables and n is the number of experimental data. The Pearson's correlation coefficient ranges from +1 to -1. A correlation of +1 or -1 means that there is a perfect positive or negative linear relationship between variables, respectively, whereas a correlation equal to 0 means there is no linear relationship between the two variables.[33,34] The statistical significance of Pearson's correlation was estimated by means of the p-level value (also known as Pearson's index).[33,34] More technically, the p-level represents the probability of error that is involved in accepting our observed result as valid or as "representative of the population". The higher the p-level the less it is probable that the observed relation between two variables in the single sample is a reliable indicator of the relation between the respective variables in the population. In the present work, a significant correlation was considered only when the p-level was less than 0.05, i.e. there is a

5% probability that the relation between the variables found in the sample is fortuitous.

4. EXPERIMENTAL RESULTS AND DISCUSSION

4.1. Fluidity of HPDC aluminium alloys

Fig. 3 shows the results obtained from the fluidity measurements using the vacuum fluidity test. The effect of pouring temperature on the fluidity of the different HPDC aluminium alloys appears evidently. The fluidity of the alloys #1 and #2, having a similar composition, is close at lower temperatures, but when the pouring temperature rises from 600°C to 760°C the two alloys show a different behaviour. While the fluidity of alloy #1 increases from 210 mm to 330 mm (around 60%), for alloy #2 the increment is only from 230 mm to 318 mm (around 35%). The same considerations can be applied to alloys #3 and #4, whose composition mainly differs in the amount of Silicon. In the temperature range from 600°C to 760°C the fluidity increment for alloy #3 is around 67%, while the flow value for alloy #4 increases from 180 mm to 290 mm (around 60%). These values evidence that the fluidity of the alloys #1 and #2 is higher than that of the other two alloys.

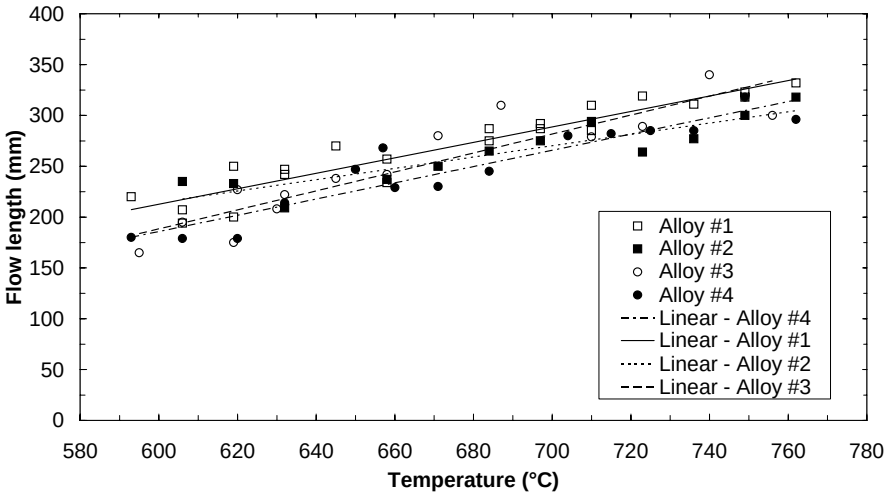

Fig. 3. Flow length versus pouring temperature of each alloy (linear fits are also shown).

This can be explained according two different factors: the different heat content and solidification behaviour of the alloys.[17,28,35] For instance, Kaufmann *et al.*[17] reported for an AlSi9Cu3 aluminium alloy (A380) at the upper (AlSi11Cu3.5) and the lower (AlSi8Cu2) limit of tolerated composition that the heat content at 700°C due to superheat was about 40% higher for the alloy at the upper compositional limit, and that this alloy showed a higher total heat content of about 14% compared with the alloy at the lower compositional limit. Another important aspect is the solidification behaviour of the analysed alloys. While alloys #1 and #2 are very similar to an eutectic alloy without distinct primary dendrites, in the alloys #3 and #4 primary α-Al dendrites form at the liquidus temperature. Tang *et al.*[35] suggested that, while in eutectic solidification the formation of eutectic "matrix" and intermetallics takes

place simultaneously without segregation of intermetallics in the remaining liquid, in hypoeutectic alloys dendrites form and reject solute, which enriches the liquid with intermetallics reducing the fluidity by blocking the interdendritic flow channels.
The fluidity results were fitted linearly by least-squares method. The values of slopes, A, and of the intercepts, B, as given by equation (2), are shown in Table 3. The square correlation coefficient, R^2, is also listed in Table 3.

Table 3: Statistics of the fluidity test.

Data	Alloy #1	Alloy #2	Alloy #3	Alloy #4	Alloy #1 + 50%
Slope (mm °C^{-1})	0.761	0.557	0.932	0.799	0.614
Intercept (mm)	-243.7	-119.6	-370.8	-293.6	-178.8
R^2	0.89	0.81	0.83	0.88	0.70
Reproducibility σ (%)	5.9	5.5	8.6	6.7	9.8

It is possible to observe how the slope of the curves is different for each alloy, decreasing with the amount of silicon content. As reported elsewhere, the variation in pouring temperature is responsible for the most pronounced change in fluidity of the melt.[7-9,12,17,18,22-25] However, increasing the casting temperature will also increase the solubility of Hydrogen in the melt. As a result, more Hydrogen will be liberated during cooling, generating higher gas porosity in the casting.[5] The solubility of Hydrogen in liquid aluminium at 1000°C is over 40 ml kg^{-1}.[7] If there was any hydrogen content available in the melting environment, the gas content in the melt would not increase, independently from the temperature. In practice, since some source of hydrogen is always present in the environment, pouring is preferentially not performed at very high temperatures in order to achieve a good control of the gas porosity level. Therefore HPDC foundries cast the melt at the minimum possible pouring temperature, especially if the gating system is good.[7,29] Fig. 3 shows also the different flow sensitivity of each alloy to the casting temperature.
Table 3 reports the reproducibility σ of each test series, as well. The vacuum fluidity test apparatus has an average reproducibility of 7.3%, which is fairly good considering the several factors influencing the fluidity.
The Pearson's analysis revealed a strict correlation between the amount of Silicon and Magnesium and the fluidity of the alloys at the pouring temperature of 645°C (Table 4). While Silicon has a positive effect on fluidity due to the latent heat of solidification (r ~ 0.97), increasing the Magnesium content from 0.093wt.% to 0.206wt.% leads to a decrease of the flow length of molten metal (r ~ -0.99), as shown in Fig. 4. In the present work Pearson's correlation didn't reveal any reliable correlation about the influence of Iron and Zinc content on flow length; in fact, the p-level for Iron and Zinc is ~0.98 and ~0.57, respectively. On the opposite side, Di Sabatino *et al.*,[19] Mbuya *et al.*[20] and Gowri *et al.*[36] reported that increasing the amount of Iron and Zinc decreases the fluidity of molten metal. Considering the effect of Copper and Manganese on fluidity, it seems that the addition of Manganese has a positive linear influence (r ~ 0.90) on the fluidity at 645°C, while Copper causes a decrease in the flow length (r ~ -0.88). However, the statistical analysis revealed p-level values higher than 0.05 (respectively ~0.10 and ~0.12 for Mn and Cu) to guarantee the reliability of the above mentioned relationships. Sheshradri *et al.*[37] studied the effect of alloying elements on fluidity of pure aluminium and found

that, among the elements which decrease the casting fluidity, Ti, Fe and Zr exert a moderate effect, while Cr, Mn and Cu have a minor effect.

Table 4: Results from Pearson's correlation.

Correlation type	Pearson correlation coefficient (r)	p-level
Silicon (Si) vs. $Fluidity_{645°C}$	0.973	0.027
Iron (Fe) vs. $Fluidity_{645°C}$	-0.017	0.983
Copper (Cu) vs. $Fluidity_{645°C}$	-0.881	0.119
Manganese (Mn) vs. $Fluidity_{645°C}$	0.897	0.103
Magnesium (Mg) vs. $Fluidity_{645°C}$	-0.987	0.013
Zinc (Zn) vs. $Fluidity_{645°C}$	0.429	0.571

In general, the chemical composition of the alloys affects their solidification range, i.e. the interval between liquidus and solidus temperature.[17] The solidification range plays an important role on castability because it influences both casting properties and defects. The solidification range strongly influences the mode of solidification, as shown by Flemings,[24] and it has been shown that the mode of solidification significantly affects the fluidity of the melt.[7,24] In pure aluminium, dilute alloys and eutectics, the mode of solidification of the stream in a fluidity test appears to be by planar front solidification from the walls of the mould towards the centre. In the solute rich alloys with a wide solidification range, fluidity is limited by choking. The flow is choked by precipitation of equiaxed grains at the leading tip of the flowing stream and by the accumulation of solid crystallites.[7,24]

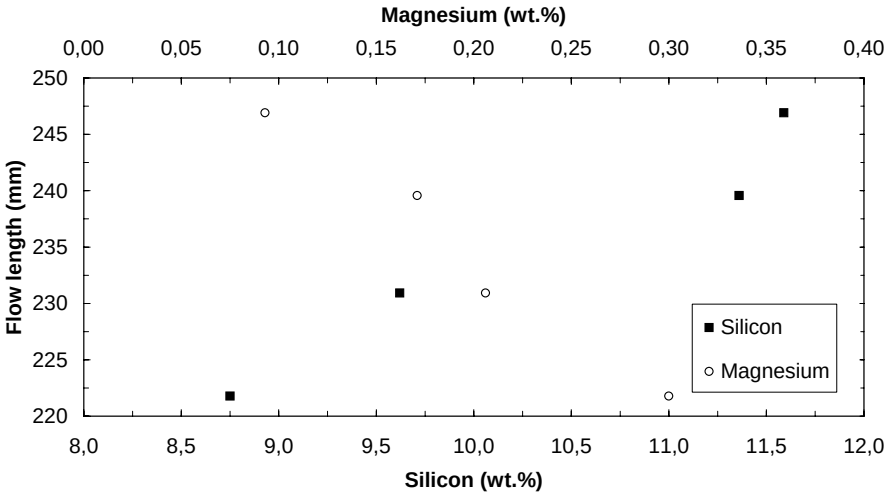

Fig. 4. Effect of alloying elements on fluidity of HPDC alloys.

4.2. Effect of scrap addition on fluidity

Fig. 5 shows the effect of scrap addition on the fluidity of alloy #1. In general, the fluidity of the alloy contaminated with scrap is lower than the normal melt. However, while the decrease in fluidity due to the scrap addition is around 8% at 600°C, it

reaches values of 3% and 20% at 660°C and 750°C pouring temperatures respectively.

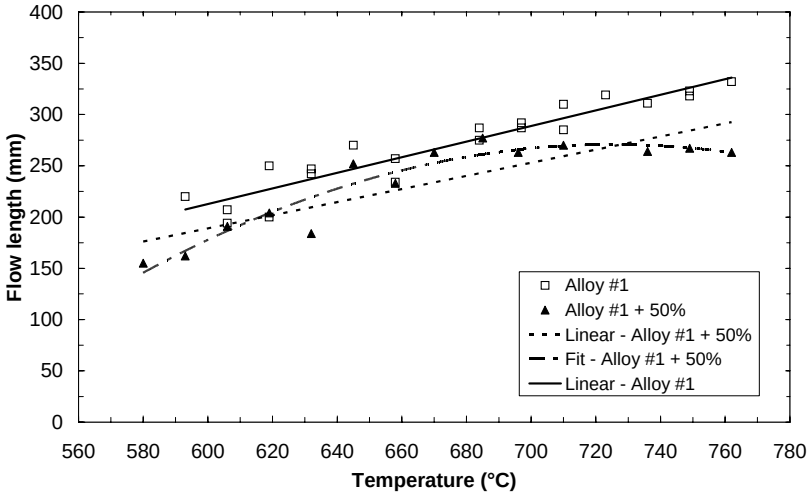

Fig. 5. Effect of scrap addition on fluidity of Alloy #1 (fits are also shown).

Between 580°C and 680°C the fluidity values linearly increase with the temperature reaching a stationary level at higher pouring temperatures. A fit curve was added to the diagram shown in Fig. 5 to evidence the trend of the contaminated alloy. A possible explanation of this behaviour could be the higher formation rate of oxides and inclusions at rising pouring temperatures. Also, this effect could occur because the melt is kept at high temperature for a long time, or because of the turbulence introduced during the test. In fact, as the inclusions can be lighter or heavier than the melt, if the melt is in a stationary condition they can either float at the surface or sink to the bottom of the crucible.[27] However, the turbulence originated by the induction field, which is greater at higher temperatures, can mingle the inclusions inside the crucible.

Even in this situation the flow data can be fitted linearly, as formerly done by Kwon *et al.*.[23] The resulting values of slope, A, intercept, B, and coefficient of determination, R^2, are given in Table 3. The slope value, in particular, shows how the contaminated alloy exhibits a lower sensitivity to the pouring temperature than the clean melt, but the low R^2 value suggests further investigations to explain this behaviour. The optical investigation of the samples taken from the tip of the test tubes revealed that alloy #1 didn't show oxides and other inclusions at all tested pouring temperatures, while the melt contaminated with the 50% scrap addition was more evidently affected by oxides. Thus, it can be concluded that adding scraps to the melt generates an increasing amount of oxides, reducing therefore the fluidity of the melt as this effect diminishes the critical solid fraction at the flow tip (i.e., the solid fraction value at which the flow stops).[7,24] The molten metal cleanliness was not quantitatively measured (using industry standard methods, e.g., LiMCA, PoDFA and K-Mold techniques,[5,30-32]), but a qualitative analysis of the dimensions and the amount of oxides in the contaminated melt was nonetheless performed by means of optical microscopy. Results showed that the oxide content significantly increased

with the pouring temperature. Fig. 6 shows optical micrographs of the samples taken from the tip of the test tubes at different pouring temperatures.

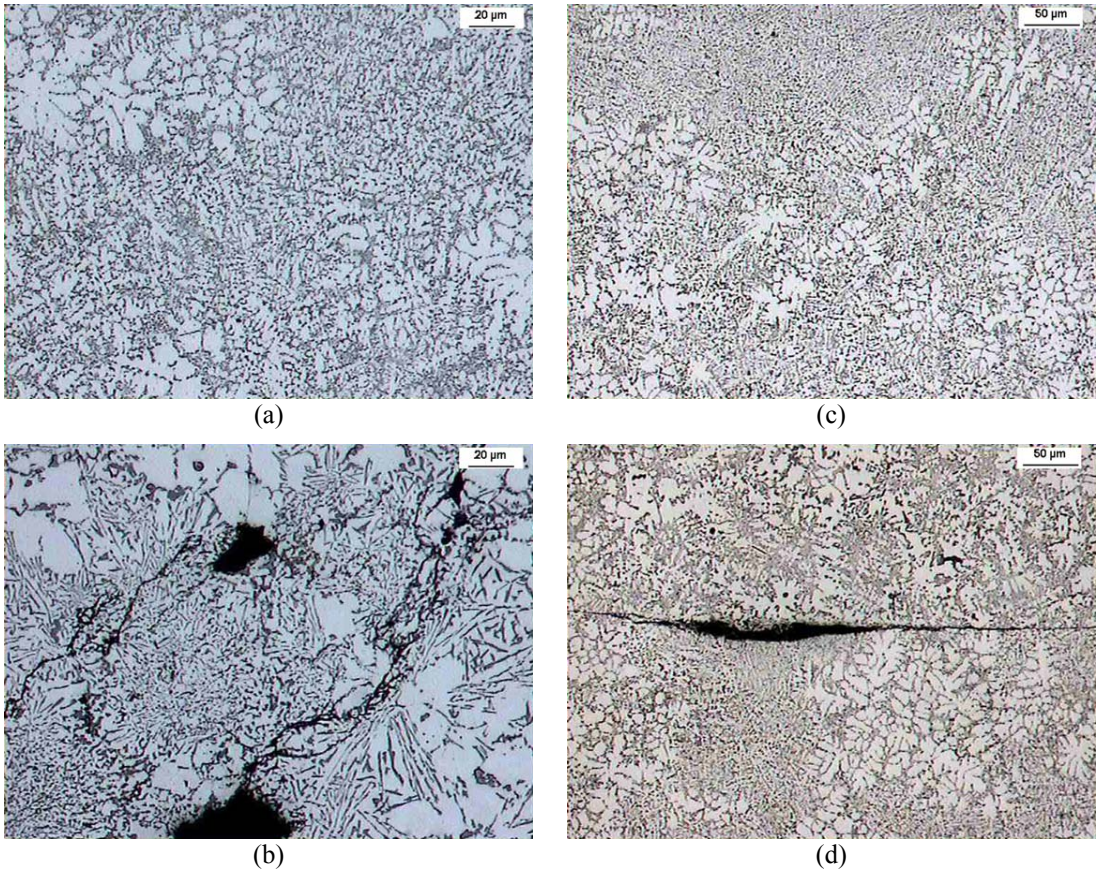

Fig. 6. Optical micrographs of the analysed samples: a) Alloy #1 at 600°C pouring temperature; b) Alloy #1 + 50% at 600°C pouring temperature; c) Alloy #1 at 750°C pouring temperature; d) Alloy #1 + 50% at 750°C pouring temperature.

5. CONCLUSIONS

(i) The fluidity length of four different high pressure die cast Al-Si alloys was investigated at different pouring temperatures. Alloys close to eutectic composition (alloy #1 and #2) presented a different flow behaviour compared to hypoeutectic (alloy #3 and #4) alloys, showing a different sensitivity to casting temperature. Within the chemical composition of the alloys analysed, magnesium and silicon affected the fluidity of the molten metal.

(ii) The influence of scrap addition was analysed on an Al-Si alloy commonly used for HPDC applications. The scrap addition came from HPDC foundry returns in the form of refused castings, gating and runner systems and overflows of the same alloy. Addition of scraps increased the amount of oxides, reducing the fluidity of the melt. The fluidity of the contaminated melt, which resulted lower than that of the clean melt, increased linearly between 580°C and 680°C and reached a stationary level at higher pouring temperatures. This behaviour was interpreted in terms of reduction of the critical solid fraction, which is affected by the amount of oxide inclusions in the flow channel. The amount of oxides, in

turn, is increased by a turbulent melt (due to induction field, greater at high temperatures), which can mingle the inclusions inside the crucible.

ACKNOWLEDGEMENTS

The Authors acknowledge the experimental contribution to this work given by dr. E. Faltracco, dr. A. Masi and dr. E. Carraro. Many thanks are also due to dr. E. Della Rovere and G. Mazzacavallo. Dr. D. Del Genovese is gratefully acknowledged for proofreading the manuscript. This work has been carried out under the Contract "Applicazione di Nuovi Materiali, Processi Innovativi e Tecniche di Calcolo Numerico in Fonderia", between MURST (Italian Ministry of University and Research) and Venezia Tecnologie SpA.

REFERENCES

1. R. H. Bacon: 'The car: engine and structure'; 1968, London, Macmillan & Cleaver.
2. W. H. Crouse and D. L. Anglin: 'Automotive engines'; 1995, New York, Glencoe/McGraw-Hill.
3. C. H. Cáceres and B. I. Selling: Mater. Sci. Eng. A, 1996, **220**, 109-116.
4. X. Dai, X. Yang, J. Campbell and J. Wood, Mater. Sci. Technol., 2004, **20**, 505-513.
5. J. E. Gruzleski and B. M. Closset: 'The treatment of liquid aluminium-silicon alloys'; 1990, IL, USA, The American Foundrymen's Society.
6. J. P. Anson and J. E. Gruzleski: AFS Transactions, 1999, **99-26**, 135-142.
7. J. Campbell: 'Castings', 2nd edn; 2003, Oxford, Elsevier Butterworth-Heinemann.
8. P. R. Beeley: 'Foundry Technology', 1st edn, 13-22; 1972, London, Butterworth & Co.
9. R. A. Flinn: 'Fundamentals of metal casting', 1st edn, 87-97; 1963, Massachusetts, Addison-Wesley Publishing Company.
10. D. Wang and R. A. Overfelt: Int. J. Thermophys., 2002, **23**, 1063-1076.
11. P. Bastien, J. C. Armbruster and P. Azou: AFS Trans., 1962, **70**, 400-409.
12. M. Di Sabatino, L. Arnberg, S. Brusethaug and D. Apelian: Int. J. Cast Metals Res., 2006, **19**, 94-97.
13. E. Niyama, K. Anzai, T. Funakubo and S. Hiratsuka: J. Mater. Process. Technol., 1997, **63**, 779-783.
14. J. Campbell and R. A. Harding: 'Talat Lecture 3207', 1-29; 1994, European Aluminium Association (EAA).
15. A. C. Street: 'Die Casting Book', second ed.; 1996, London, Portcullis Press.
16. A. K. Dahle, P. A. Tøndel, C. J. Paradies and L. Arnberg: Metall. Mat. Trans. A, 1996, **27**, 2305-2313.

17. H. Kaufmann, W. Fragner and P. J. Uggowitzer: Int. J. Cast Metals Res., 2005, **18**, 273-278.
18. M. Di Sabatino, S. Shankar, D. Apelian and L. Arnberg: Proc. Int. Conf. on 'Shape Casting: The John Campbell Symposium', M. Tiryakioglu, P.N. Crepeau (Eds.), San Francisco, USA, February 13-17, 2005, TMS, 2005, 193-202.
19. M. Di Sabatino and L. Arnberg: Metal. Sci. Tech., 2004, **22**, 9-15.
20. T. O. Mbuya, B. O. Odera and Ng'ang'a: Int. J. Cast Metals Res., 2003, **16**, 451-465.
21. E. F. Chirkov: Mater. Sci. Forum, 1996, **217-222**, 265-270.
22. M. Di Sabatino, F. Syvertsen, L. Arnberg and A. Nordmark: Int. J. Cast Metals Res., 2005, **18**, 59-62.
23. Young-Dong Kwon and Zin-Hyoung Lee: Mater. Sci. Eng. A, 2003, **360**, 372-376.
24. M. C. Flemings: 'Solidification processing'; 1974, London, McGraw-Hill.
25. M. Di Sabatino, L. Arnberg and F. Bonollo: Metal. Sci. Tech., 2005, **23**, 3-10.
26. M. Di Sabatino and L. Arnberg: Int. J. Cast Metals Res., 2005, **18**, 181-186.
27. M. Di Sabatino, L. Arnberg, S. Rørvik and A. Prestmo: Mater. Sci. Eng. A, 2005, **413-414**, 272-276.
28. Qingyou Han and Hanbing Xu: Scripta Mater., 2005, **53**, 7-10.
29. Luigi Andreoni, Mario Case and Giorgio Pomesano: 'Quaderni della colata a pressione delle leghe di alluminio'; 1995, Brescia, Edimet.
30. J. Wannasin, D. Schwam and J. F. Wallace: J. Mater. Process. Technol., 2007, **191**, 242-246.
31. D. Doutre, B. Gariépy, J. P. Martin and G. Dubé: Light Met., Proc. 114th Annual Meeting of the Metallurgical Society of AIME, Warrendale, Pennsylvania,1985, 1179-1195.
32. M. M. Makhlouf: Proc. 8th Int. Summer School on 'Casting and Solidification of Aluminium- and Magnesium Alloys', Trondheim, NO, August 2006.
33. G. L. Squires: 'Practical physics', 4th edn; 2001, Cambridge, Cambridge Univ. Press.
34. STATISTICA® v.7.0, User's Manual, StatSoft Inc., 1995, Tulsa, OK, USA.
35. S. K. Tang and T. Sritharan: Mater. Sci. Technol., 1998, **14**, 738-742.
36. S. Gowri and F. H. Samuel: Metall. Mat. Trans. A, 1994, **25**, 437-448.
37. M. R. Sheshradri and A. Ramachandran: AFS Trans., 1965, **73**, 292-304.

ARTICLE 3

PERMANENT MOLD CASTING OF ALUMINIUM ALLOYS: CORRELATION AMONG PROCESSING, MICROSTRUCTURE AND SIMULATION

F. Bonollo*, G. Timelli*, N. Gramegna**, B. Molinas***

* Department of Management and Engineering – DTG
University of Padova
I-36100 Vicenza
ITALY

** EnginSoft Trading S.p.A.
I-35129 Padova
ITALY

*** Venezia Tecnologie S.p.A.
I-30175 Porto Marghera (VE)
ITALY

Proceeding of 3rd International Conference High Tech Die Casting, Vicenza, Italy, September 21-22, 2006

ABSTRACT
Porosity level and local solidification time are generally acknowledged to affect both dynamic and static properties of cast aluminium alloys intended for structural applications. To analyse these effects, an investigation was carried out examining permanent mold cast A319 and A356 aluminium alloys. Step-bar castings were poured at different temperatures. The castings were sectioned and samples extracted from each step. The porosity level and the secondary dendrite arm spacing were examined using image analysis of randomly selected fields. Results were obtained for steps of thickness 5, 10, 15 and 20 mm. The riser was also sectioned where the thickness was about 35 mm. In every casting considered, porosity level and SDAS increased with section thickness. A computer simulation approach was also carried out to predict SDAS values. The simulation results showed a good correlation to experimental data.

Keywords: Cast aluminium alloys; A356; A319; Solidification; SDAS; Microstructure; Defects; Porosity; Simulation; Step casting.

1. INTRODUCTION

The automotive industry are increasingly using computer simulation to attain their design objectives, reducing hardware prototyping and improving the parts design and manufacturing processes [1-3]. One important automotive design aim is the overall weight reduction of the vehicle for better fuel economy and for reducing pollutants emission. Aluminium alloys have been substituted for cast iron because they are around one third of the specific weight of cast iron [4]. Shape aluminium casting is then an economically beneficial method of producing high performance components. Thus, while the benefits of replacing cast iron with aluminium alloys seems clear, a successful replacement requires the solution of different design problems, which increase with the complexity of component [1]. However, unlike forging or other thermomechanical processes, the properties of shape aluminium casting are almost entirely dependent upon the solidification conditions, which should be considered during the design chain [2]. For example, from a stress-engineering viewpoint, thickening up a section of a component will lead to increased load-bearing capacity at that location. During casting, a thicker region will solidify more slowly and, for aluminum alloys, a coarser microstructure will result in lower mechanical strength. Problems with feeding and shrinkage defects may also arise in thicker sections. Of course, a component design that worked well for cast iron may be entirely unsuitable for an aluminum alloy casting [1].

During the cooling of cast aluminium alloys the main body solidifies forming a dendritic structure. The dendrites consist of primary, secondary and sometimes tertiary dendrite arms [5-6]. Casting having a finer microstructure, i.e. a high solidification rate, shows better mechanical properties and this is associated with a low secondary dendrite arm spacing (SDAS) [6]. On industrial casting production it is more difficult to control the solidification rate, and therefore the SDAS value, due for example to the complexity and the different wall thickness of the real-shaped casting [7]. For this reason, testing plates are separately poured in sand or chill mould, in which the solidification rates needed to achieve various SDAS are controlled by varying the thickness and the material of the mould, or the sample size [6,8]. Thus, the factors that influence SDAS, the relationship between SDAS and mechanical properties of cast aluminium alloys and a correlation with real-shaped casting can be easily assessed.

The aim of this work is to correlate the microstructure with the solidification conditions of separately cast plates. The experiments consider a wide range of as cast thicknesses ranging from 5 to 20 mm. Castings in the form of a stepped bar were produced, sectioned and examined. SDAS and percentage porosity levels were also determined. Concurrent with this, SDAS has been assessed via simulation codes in an attempt to validate computer simulation approach. This path will help to reduce the cost of manufacture by enhancing right-first-time design with lower scrap and efficient use of material.

2. EXPERIMENTS

The geometry of the mould is shown in figure 1a. The whole dimension of the die was 310x250x115 mm and the thickness of the cope and drag was 45 mm and 75 mm respectively. The weight of the steel die was around 140 Kg. The castings used in this study were step castings. Front and side views of the step castings are shown in figure 1b. The casting, as it is possible to observe in figures 1 and 2, includes a wide range of as cast thicknesses ranging from 5 mm to 20mm. The steps casting

was then gated from the side of the thinnest step and the riser put at the top of the casting to ensure a good feeding. Such configuration allows obtaining a range of solidification rates and consequently different microstructures from the same casting. The weight of the whole aluminium alloy casting was 1.4 Kg or 1Kg, including or not the runner system.

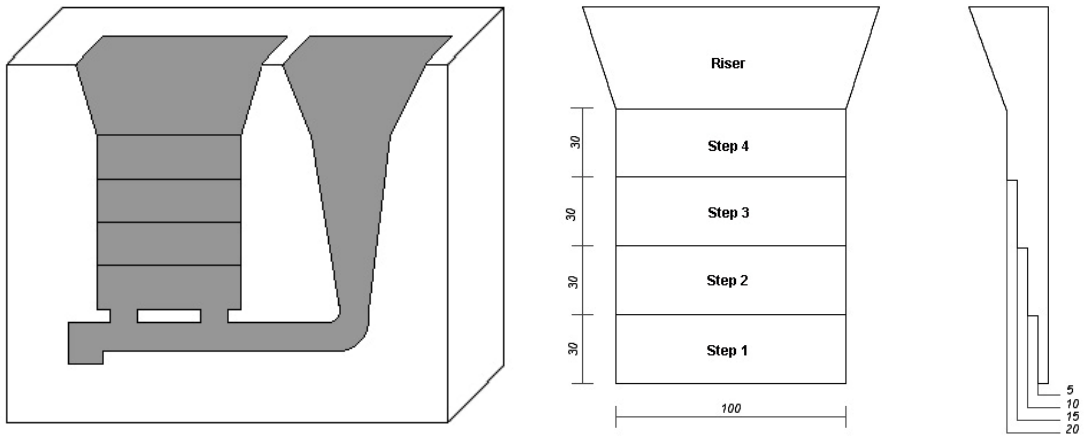

(a) (b)

Fig. 1. Schematic view of the die adopted (a); front and side views of the step castings (b). All the measures are in mm.

A semi-permanent layer of DYCOTE® F34 coating [9] was spray applied according the standard procedure on the wall of the die at the temperature of about 200°C. The functions of the die coating were here:

- control of the metal flow to ensure it reaches all parts of the mold;
- control of heat transfer;
- ensure that the castings were properly fed;
- easy release of the casting after complete solidification.

Before pouring the melt, the temperature of the mold was driven to about 250°C. Trough the use of a contact thermocouple, the temperature in different zones of the die was also monitored in order to evaluate the local temperature and assure a good reproducibility of the tests.

Step casting were poured from two commercial Al-Si alloys, A319 and A356 alloys, melted in a resistance furnace. The nominal composition of the alloys used in the present work is listened in Table 1 [10]. While the first alloy is normally used to cast cylinder heads, engine blocks or components where high mechanical properties are required, the second one is adopted to cast wheels, carters, gearboxes, where a good castability and weldability are necessary.

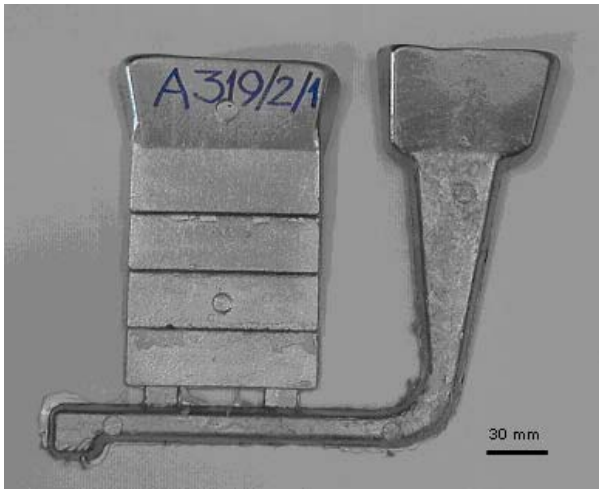

Fig. 2. The step casting used in the present work.

Different pouring temperatures were adopted in the present investigation to evaluate the impact on the microstructure and porosity level; while the A319 alloy was cast at 640°C and 720°C, the A356 alloy was cast at 720°C and 820°C.

Table 1: Chemical composition of the alloys used in the present work (wt.%) [10].

Alloy	Al	Cu	Fe	Mg	Mn	Ni	Si	Ti	Zn	Others
A319	Bal.	3-4	max 1	max 0.1	max 0.5	max 0.35	5.5-6.5	max 0.25	max 1	max 0.5
A356	Bal.	max 0.2	max 0.2	0.25-0.45	max 0.1	-	6.5-7.5	max 0.2	max 0.1	max 0.15

The castings were then sectioned and two samples were extracted from steps 1 through 4. Two specimens were also cut from the riser where the thickness was about 35 mm. Figure 3 shows how the step castings were sectioned and where the samples were extracted, from the middle and external zones of the castings. In this way it was possible to study the effect of the local temperature and the heat transfer on the solidification rate and, thus, on the microstructure. After the samples were cut, all the specimens were mounted in phenolic resin, ground and mechanically polished by standard preparation method.

Optical microscopy was adopted for microstructural analysis. The pictures were then analysed using a commercial image-analysis software package. The percentage porosity of each image was evaluated by counting the image pixels in each pore and dividing the sum of the pore area pixels by the total number of pixels in the image. The percentage porosities for the four images were then averaged to obtain the percentage porosity for the section. Both shrinkage and gas pores were found and considered in the percentage calculation. Average SDAS values were obtained using the linear intercept method. The linear intercept method involves measuring the distances (spacing) between secondary dendrite arms along a line normal to the dendrite arms. This procedure was repeated for a number of image frames and an average SDAS was calculated. Ten and four random images were acquired for SDAS and porosity analysis respectively.

Fig. 3. Side view of the step casting showing sectioning scheme.

3. CASTING SIMULATION

In order to validate computer simulation approach, a commercial finite difference based simulation package was used to obtain SDAS values from calculated solidification time. The CAD model was drawn and imported in simulation program where a mesh of 132000 elements for the casting was adopted (Figure 4a). To simulate the inlet boundary condition a flux profile, as shown in figure 4b was chosen, where the pouring time was measured during the experimental tests. For both the alloys the simulation analysis were carried out at the pouring temperature of 720°C. The heat transfer coefficient (HTC) was chosen among those present in the software database, taking into account affecting parameters like the type and thickness of coating, the alloy type and the pouring temperature. Virtual thermocouples were inserted in different zones of the die to monitor the temperature profiles and compare these values with those obtained through experimental approach.

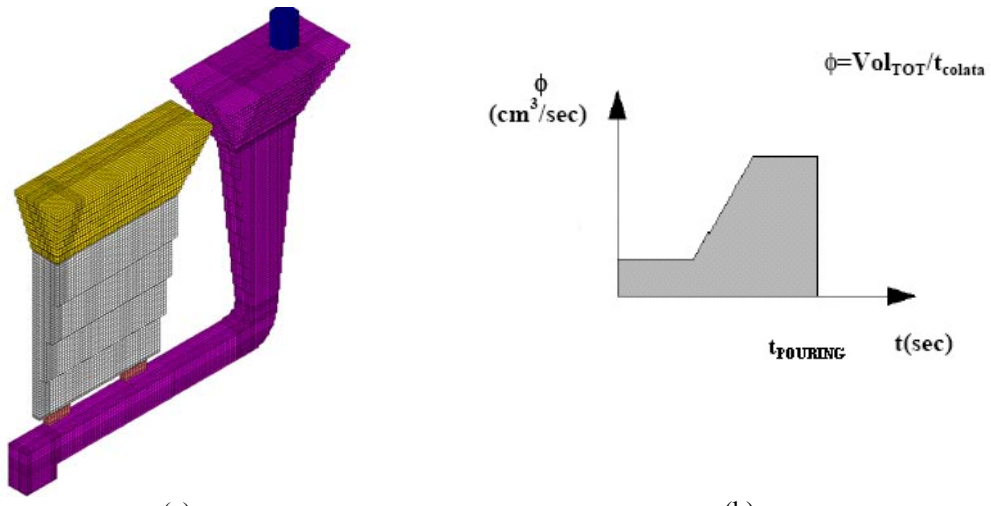

(a) (b)

Fig. 4. Mesh of the step casting analysed (a) with the inlet profile adopted (b).

With the use of computer simulation the solidification time was calculated in the different zones of the casting and the virtual SDAS values was obtained through the equation [11]:

$$SDAS = Kt_{sol}^{\ n} \qquad (1)$$

where t_{sol} is the calculated local solidification time and K and n constants related to the material. The constants adopted here were [12]:

- K=8.78 (A319) / 11.55 (A356);
- n=0.3 (A319) / 0.31 (A356).

The SDAS values so obtained were compared with experimental ones.

4. RESULTS AND DISCUSSION

4.1. A319 alloy

Figure 5 shows the percentage porosity versus the section thickness of the A319 step castings poured at the temperatures of 640°C and 720°C. In general, the trend for both the castings was similar: the amount of pores increased with the increasing of the step's thickness, i.e. with the increasing of the local solidification time. Considering the same pouring temperature, it is possible to observe how the percentage porosity for every section thickness was higher in the samples extracted from the inner section than the specimens from the external one (Figure 5). This behaviour can be related to the influence of heat transfer direction on the solidification rate and, thus, on the porosity formation. Considering the influence of the different pouring temperatures, figure 5 demonstrates that as the pouring temperature increased, the percentage porosity of the section also increases. While this gap was constant for the first three steps of the inner sections, the difference increased for the same specimens of the outer sections.

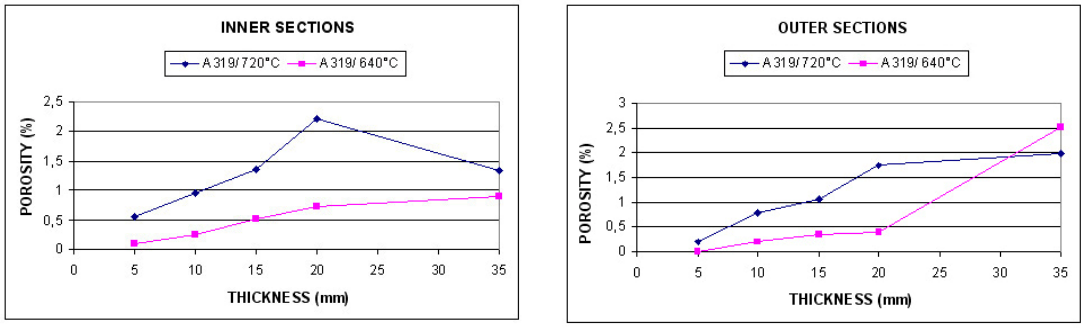

(a) (b)

Fig. 5. Relationship between percentage porosities and section thickness in A319 step castings poured at 640°C and 720°C – Inner (a) and outer (b) sections.

Figure 6 shows the data of SDAS analysis carried out in the samples extracted from inner and outer sections of step castings. The results demonstrate the close proportional relationship between SDAS and the section thickness: a slow solidification rate, characteristic of thick steps, drives to an increment of SDAS values, i.e. a coarsening microstructure. For every section thickness, the SDAS

values were higher in the samples extracted from the inner section than the specimens from the external one. Considering the influence of the different pouring temperatures, it seems to not affect SDAS.

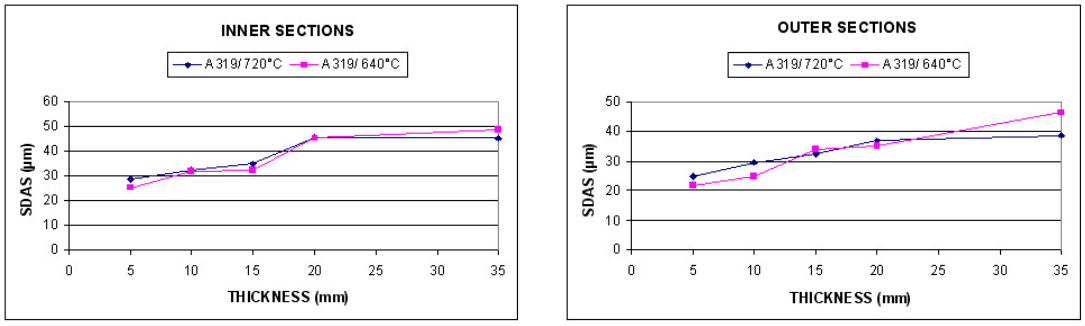

(a) (b)

Fig. 6. Relationship between SDAS and section thickness in A319 step castings poured at 640°C and 720°C – Inner (a) and outer (b) sections.

4.2. A356 alloy

The percentage porosity of A356 step castings poured at 720°C and 820°C was evaluated. Similar considerations previously done for the A319 step castings can be done:

- the amount of pores increased with the increasing of the step's thickness;
- considering the same pouring temperature, the percentage porosity for every thickness was higher in the samples extracted from the inner section than the specimens from the external one;
- as the pouring temperature increased, the percentage porosity of the section also increased.

Comparing the results of porosity analysis of both the alloys, it is interesting to observe how the percentage porosity of the A319 step castings is higher than the A356 ones in both the sections analysed; an example is shown in figure 7 where a comparison for samples cut from outer sections is taken.

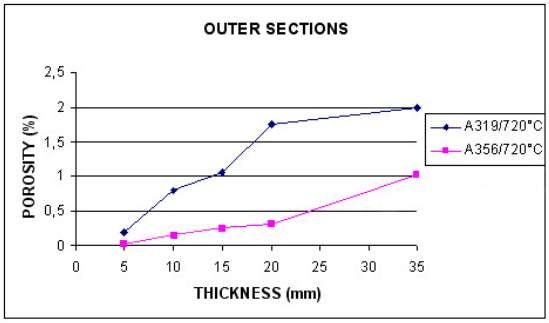

Fig. 7. Comparison between the percentage porosity of A319 and A356 step castings poured at 720°C – Outer sections.

This can be related to the amount of Cu in the A319 alloy. In fact, the Cu-free alloy A356 solidifies over a relatively narrow temperature range of about 60°C and contains nearly 50% of eutectic liquid. Thus, the feeding of the last eutectic liquid to solidify is relatively easy and the level of porosity is normally very low. In the case of alloy A319, Cu extends the solidification range to about 105°C and the fraction of binary eutectic is considerably less than in the Cu-free alloy, thus making the formation of shrinkage porosity much more likely [13]. From figure 7 it is also possible to observe how the sensitivity of the curves is different. This means that the amount of pores in the A319 alloy increases more rapidly decreasing the solidification rate than the A356 alloy.

Figure 8 shows the data of SDAS analysis carried out in the samples extracted from inner and outer sections of step castings. Similar considerations previously done for the A319 step castings can be done.

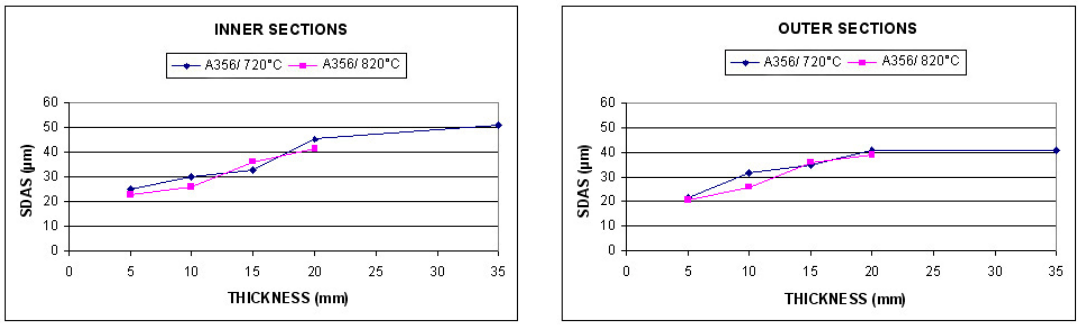

(a) (b)

Fig. 8. Relationship between SDAS and section thickness in A356 step castings poured at 720°C and 820°C – Inner (a) and outer (b) sections.

4.3. Computer simulation results

Figure 9 shows the comparison between the experimental and simulated SDAS values. As it is possible to observe the relationship is good, testifying the ability of the numerical simulation codes to predict the local solidification conditions and the characteristics of casting components.

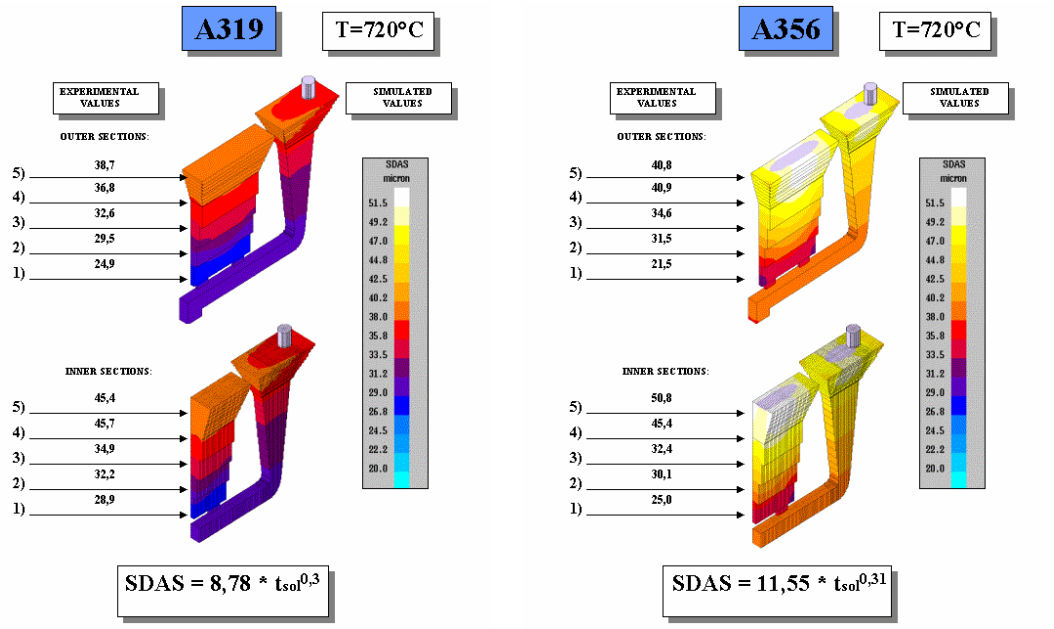

(a) (b)

Fig. 9. Comparison between simulated and measured SDAS in A319 (a) and A356 (b) step castings poured at 720°C. All the measures are in μm.

5. CONCLUSIONS

The porosity amount and the secondary dendrite arm spacing of A319 and A356 cast aluminium alloys were studied with step castings. Different pouring temperatures were used to analyse the influence on the percentage porosity. The overall trend observed was that the percentage porosity of both the alloys increased with increasing section thickness. At the same pouring temperature, the percentage porosity for every thickness was higher in the samples extracted from the inner section than the specimens from the external one. As the pouring temperature increased, the percentage porosity of the section also increased. Comparing the results of porosity analysis of both the alloys, the percentage porosity of the A319 step castings was higher than the A356 ones in both the sections analysed. This can be related to the amount of Cu in the A319 alloy, which changes the solidification range. The SDAS analysis demonstrated the close relationship between SDAS and the section thickness. Commercial simulation software was also adopted to calculate the local solidification time and a correlation with experimental SDAS values was carried out. This methodology showed a good correlation to experimental results.

ACKNOWLEDGMENTS

This work has been carried out under the Contract “Applicazione di Nuovi Materiali, Processi Innovativi e Tecniche di Calcolo Numerico in Fonderia”, between MURST (Italian Ministry of University and Research) and Venezia Tecnologie SpA. Many thanks are also due to Mr. M. Palù for his help in the experimental work as well as to Teksid SpA.

REFERENCES

1. S.G.R. BROWN, J.A. SPITTLE and J.D. JAMES, JOM-e: a web-only supplement to JOM, (January 2002).
2. P.D. LEE, A. CHIRAZI, R.C. ATWOOD and W. WANG, Mater. Sci. Eng. A365, (2004), pp.57-65.
3. R.C. ATWOOD and P.D. LEE, Acta Mater. 51, (2003), pp. 5447-5466.
4. S. VISWANATHAN, A.J. DUNCAN, A.S. SABAU, Q. HAN, W.D. PORTER, B.W. RIEMER, AFS Transactions 106, (1998), paper 98-103, pp.411-417.
5. V. RONTÓ and A. ROÓSZ, Int. J. Cast Metals Res. 13, (2001), pp.337-342.
6. B. ZHANG, M. GARRO and C. TAGLIANO, Metal. Sci. Tech. 21, (2003), pp.3-9.
7. F. BONOLLO, G. TIMELLI, G. MAZZACAVALLO, R. MOLINA, Proc. 30th Convegno Nazionale AIM, Vicenza (2004), AIM, Milano, paper 137.
8. S.T. McCLAIN, J.T. BERRY and B. DAWSEY, AFS Transactions 111, (2003), pp.147-158.
9. FOSECO, Dycote® Manual – Coatings for non-ferrous metal die-casting, pp.1-28.
10. American Society of Metals (ASM), Casting-Nonferrous casting alloys. ASM Handbook, vol.15, ASM International, Materials Park OH, (1991), pp.744.
11. W. KURZ and D.J. FISHER, Fundamentals of solidification. Trans. Tech. Publications, Switzerland (1998).
12. L. BACKERUD, G. CHAI and J. TAMMINEN, Solidification Characteristics of Aluminum Alloys-Vol.2: Foundry Alloys. American Foundrymen's Society, Inc., IL, USA (1990).
13. C.H. CÁCERES, M.B. DJURDJEVIC, T.J. STOCKWELL and J.H. SOKOLOWSKI, Scripta Mater. 40, (1999), pp.631-637.

ARTICLE 4

IMPACT BEHAVIOUR OF A356 ALLOY FOR LOW PRESSURE DIE CASTING AUTOMOTIVE WHEELS

M. Merlin*, G. Timelli**, F. Bonollo**, G.L. Garagnani*

* Department of Engineering – ENDIF
University of Ferrara
I-44100 Ferrara
ITALY

** Department of Management and Engineering – DTG
University of Padova
I-36100 Vicenza
ITALY

Submitted for publication in: Journal of Materials Processing Technology, 2007

ABSTRACT
Instrumented impact strength tests have been carried out on KV sub-size Charpy samples drawn from A356 aluminium alloy 17-inch wheels, produced by a low pressure die casting process. The wheels show different geometry and thermal treatment. In this paper, the effects of microstructure and defects on the impact properties are studied. The results indicate that the impact energy is lower in as cast wheel than in T6 heat treated wheels. A finer microstructure always corresponds to higher impact strength, while a direct correlation between the resistance to crack propagation values and SDAS exists. Casting defects, revealed by means of X-ray and density measurements techniques, become critical when concentrated around the V-notch, where they reduce the load bearing area of Charpy specimens. The fracture profile and surface of Charpy specimens have been investigated revealing how the crack crosses the interdendritic eutectic region where a significant fraction of cracked eutectic silicon and intermetallic particles is found.
Numerical simulations have been performed to study the filling and solidification behaviour of the alloy of the wheels analysed, in order to predict the final microstructure and shrinkage formation. A mean melt velocity value lower than 0.3 m/s is calculated for each type of wheel. The results show a good compromise between laminar filling and decreasing melt temperature. Solidification times, estimated by means of SDAS measurements and calculated with a numerical simulation approach, show a good correspondence. Critical areas, as concern hot spots and shrinkage porosities, are generally revealed in the zone of the wheels between the spoke and the rim, as well as in the rim area.

Keywords: Aluminium alloys; Impact strength; Castings defects; Microstructure; Numerical simulation.

1. INTRODUCTION

Lowering pollutant emission is a priority objective of international policies together with lowering energy consumption and increasing recycled materials; not only for its effect on the quality and environmental equilibrium, but because it has a strong impact in the competitiveness of companies in several sectors. In this context, only the introduction of technological innovation will be able to reconcile objectives of an environmental and energetic nature with those of a competitive type. Recently, the application of aluminium alloys in automotive sector can be one of these economically sustainable innovations, which enable a wider mix of objectives to be achieved. Due to their excellent castability and good compromise between mechanical properties and lightness, aluminium-silicon alloys are the most important and widely used casting alloys in order to cast components with complex shapes [1-3].

A consolidated example of aluminium alloy employment regards the production of wheels, which, together with an improved aesthetic appearance, guarantees an improvement of driving, like directed consequence of the inertia reduction of the wheels. These components are somewhat unique as they must meet, or exceed, a combination of requirements, from high quality surface finish, as wheels are one of the prominent cosmetic features of cars, to impact and fatigue performance, because wheels are critical safety components. Generally, the main process for casting aluminium alloy wheels is the low pressure die casting process, which guarantees to obtain a good compromise between high mechanical properties, high production, cost-effectiveness and design demand. Low pressure die casting allows to produce castings similar to those obtained by gravity casting, with good superficial aspect and thin thicknesses, but the advantage to have one central metal inlet and the absence of risers, that allows an optimal yield, around 85-95% [4].

Impact tests can give a measure of the capability of the material to resist to crash, providing an useful estimation of the ductility of an alloy under conditions of rapid loading [5]. The total absorbed energy of the sample subjected to impact test is the sum of the energy required for crack nucleation and the energy required for crack propagation and can therefore be used to describe the dynamic toughness of the material [5,6]. In the case of cast aluminium alloys the presence of a notch can decrease the impact values even further, by up 80%, when compared to un-notched specimens; even a shallow scratch of 0.1 mm reduces the energy absorption by 30% [7]. If a notch is present, the absorbed energy can be dependent on the notch geometry than on the microstructure [6].

Impact test is a useful methodology in evaluating the effects of process parameters and microstructure on dynamic fracture toughness of engineering materials. In the AlSi7Mg0.3 alloy with low iron level, the absorbed energy drops significantly by about 50% with increasing magnesium content from 0.32 wt.% to 0.65 wt.% [8]. Similar behaviour is observed increasing the iron content from 0.2 wt.% to 0.8 wt.%, at 0.32 wt.% Mg, due to an increased precipitation of β-Al_5FeSi platelets. The strontium modification, as well as an increase of solidification rate, improve the impact properties of sand and permanent mould castings, even if the effect is more pronounced at low magnesium and iron content [9].

The T6 heat treatment provides beneficial effects to cast aluminium components: it increases the yield strength, through the precipitation of a large number of fine β'-Mg_2Si particles, and improves the ductility, through spheroidisation of the eutectic silicon particles [5,7,10,11]. It is well known that the inter-particle spacing plays a dominant role in determining cracks' nucleation and propagation [12,13]. The

nucleation of the cracks usually starts with cracking of brittle particles. Once a large number of particles are cracked, cracks grow by linking microvoids formed by the cracking of these particles. With a smaller inter-particle spacing, the microvoids link and grow easily. Li *et al.* demonstrated that oxides, such as phosphorous oxides, which act as nucleation sites for Al_2Cu precipitates in A319-T6 alloy, can accelerate the cracking process reducing the impact properties [5].
While the benefit effect of T6 heat treatment is recognized, the additional cost and required time are substantial. Zhang *et al.* showed that shortening the total time of the T6 heat treatment cycle there exists a region where the impact energy decreases to a minimum before increasing [10]. The cause of this region seems due to a conflict between the negative effect of solution treatment on ductility and impact strength, associated with a rapid increase in the yield strength and the more slowly developing positive effect associated with the spheroidization and coarsening of silicon particles.
The aim of this study is to investigate the impact properties of KV sub-size Charpy specimens, drawn from A356 17-inch wheels with different geometry and temper, by means of instrumented Charpy impact testing including discussion of individual energy portions during fracture. Microstructural features, such as secondary dendrite arm spacing (SDAS) and eutectic silicon particles, have been correlated to impact properties: absorbed energy, maximum load, crack nucleation and propagation energy. Porosity is critical on mechanical properties of cast aluminium alloys, since it can overcome the effect of microstructure itself [14,15]. In order to evaluate the presence of porosity, density measurements and X-ray investigations have been carried out on KV samples. In addition to metallographic inspections, fractography has been presented to underline the effect of microconstituents on crack nucleation and propagation. Concurrent with experimental approach, the filling and solidification behaviour of the wheels analysed have been assessed via numerical simulation codes.

2. EXPERIMENTAL PROCEDURE

Instrumented impact tests have been performed on KV sub-size Charpy specimens drawn from different A356 17-inch wheels, named wheel-1, -2 and -3 respectively. While wheel-1 is a 7-spoke wheel in the as cast temper, wheels-2 and -3, which are 5-spoke wheels in the same T6 condition, differ on the geometry and thickness of the spokes. All the wheels were cast with a low pressure die casting process.

2.1. Alloy and casting parameters

The cast wheels were produced with A356 alloy, an hypoeutectic aluminium-silicon alloy, in the form of ingots, whose composition is indicated in table 1. The material was melted in an electric-induction furnace set up at 750±5°C. The melt was degassed with nitrogen and modified with Sr-containing master alloy. AlTi5B1 rod type grain refiner was also added to the molten metal. A Straube-Pfeiffer test was performed to evaluate the molten quality before casting [1,16].

Table 1: Chemical composition of A356 alloys studied in the present work (wt.%).

Alloy	Al	Si	Fe	Cu	Mn	Mg	Zn	Sn	Ni
A356	bal.	7.32	0.147	0.002	0.006	0.30	0.001	0.003	0.005

The die was made by an AISI H11 tool steel, and the die holder was made by a UNI 4010-75 FeG52 (C50) carbon steel. The temperature in the die, measured with thermocouples, was in the range of 450-520 ± 3°C.
The casting process is cyclic and begins with the pressurization of the furnace, which contains a reservoir of molten aluminium. The excess pressure in the holding furnace forces the molten aluminium to fill the die cavity. The casting cycle is divided in the following steps:

- filling the die cavity in 60±4 s up to a final pressure of 0.4±0.015 bar;
- overpressure of 2±0.03 bar, reached after 10±2 s from the end of the filling and applied for 210±5 s;
- discharging the pressure of the furnace in 5±1 s;
- after the complete solidification, the side dies are opened (5±1 s), the top die is raised vertically (10±1 s) and the casting is ejected (5±1 s).
- the die is closed and the cycle restarts.

Typical cycle time is about 6 minutes. During solidification, cooling rates are controlled by forcing air (2-3 bar) through internal channels in the top and bottom dies, at various times during casting cycle. On the side dies, cooling can be ensured by air jets, aimed at various sections of the exterior face. In spite of the different geometry, the wheels were cast with the same casting cycle.
The wheels-2 and -3 were solution treated in an air circulated furnace held at 535±5°C for 6h, quenched in a hot water bath, held at 80°C, and then artificially aged.

2.2. Impact testing

Impact tests were performed on Charpy samples drawn from the spoke and the rim region of the wheels (figure 1). Charpy specimens 5 x 10 x 55 mm and a V-notch of 2 mm depth with a root radius of 0.25 mm were made.

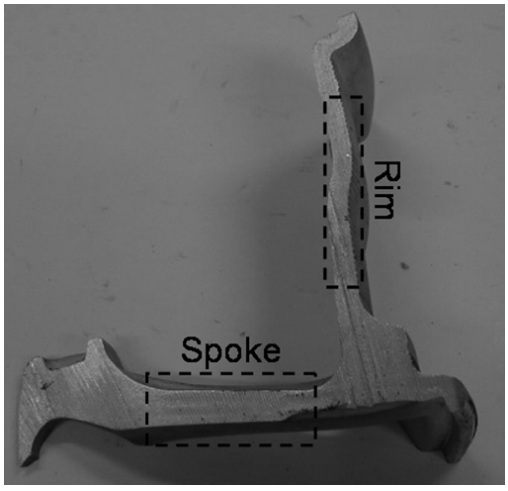

Fig. 1. Position of the spoke and the rim zone in the wheels analysed.

A Ceast instrumented Charpy pendulum, with an available energy of 50 J and an impact velocity of 3.46 m/s, was used. The pendulum impact machine, connected to a data acquisition system, is equipped with an auto-calibration system of the

hammer, in order to execute the appropriate adjustments due to pendulum frictions and air resistance. During impact testing the total impact energy (W_t), calculated as the integral of load-displacement curve, and the maximum load (F_m) were measured, as well as the energy at maximum load (W_m) and the crack propagation energy (W_p), i.e. the energy absorbed from the maximum load to the end of test, which is considered when the load comes to 2% of its peak. At the same time, the energy absorption was evaluated through the measurement of the pendulum's angle of rise (mechanical value, *CV*). W_t and *CV* describe the same phenomena in a different manner. The slight difference between W_t and *CV* was estimated equal to ~0.12 J.

2.3. Porosity measurement and X-ray investigation

In order to obtain a quantitative measure of percentage porosity on the same 5-spoke type wheel, samples taken from wheels-2 and -3 were analysed by means of density measurements. As previously said, these two wheels are 5-spoke wheels in the same T6 condition, differing on the geometry and thickness of the spokes. Every sample was weighted in air and water, and the density calculated according to Archimedes's principle:

$$\frac{W_a}{W_a - W_o}\rho_o = \rho \qquad (1)$$

where W_a and W_o are the sample's weights in air and water, ρ_o is the density of water at room temperature and ρ is the experimentally observed density. The percentage porosity was defined by the equation

$$\%Porosity = \frac{\rho_{nom} - \rho}{\rho_{nom}} \times 100 \qquad (2)$$

where ρ_{nom} is the density of fully dense material [16].

In order to localise the porosity distribution around the notch, impact test specimens were analysed with a micro focus X-ray equipment, which can magnify an image several times while still offering a better definition than a conventional X-ray tube. Every wheel was previously mapped throughout with a macro focus X-ray equipment for a preliminary analysis and comparison.

2.4. Image analysis and fractography

The microstructures of the as cast and the T6 heat treated impact test samples were observed using an optical microscope and quantitatively analysed by means of an image analyser. Average SDAS values were obtained using the linear intercept method. In each specimen, drawn from the hub, the spoke and the rim region of the wheels analysed, ten random areas were acquired over the entire sample surface for SDAS analysis. Several measurements were done, in order to obtain reliable mean values.

Important information, concerning fracture path and microstructure components involved in crack process, were obtained observing the fracture profile, on the prepared metallographic section, cut out perpendicularly to the fracture surface. An optical microscope was used for this investigation. Finally, the fracture surfaces of

the Charpy specimens after the impact test were observed and analysed by scanning electron microscopy (SEM) and by energy dispersive X-ray spectroscopy (EDS).

2.5. Casting simulation

The MAGMASOFT® software, with its module for low pressure die casting MAGMAlpdc, was used for numerically simulating the filling and solidification behaviour of analysed wheels. For every wheel, the CAD model was drawn and imported in the simulation software where a mesh of 15300000 control volumes for the whole system (die and casting) was adopted; a mesh of 670000 elements was generated for the die cavity. The physical constants and properties of the die and the alloy were chosen among those present in the software database, as well as the heat transfer coefficient (HTC), taking into account affecting parameters, like the type and thickness of coating, and the pouring temperature [17]. The process parameters, previously acquired from the casting process, were imported in the software, increasing the reliability of numerical simulation. Virtual thermocouples were inserted in the different zones of the die in order to control the temperature profiles and to compare these values with the real ones. Solidification time and feeding properties were assessed via numerical simulation codes, in order to predict the final microstructure and the shrinkage formation.

3. RESULTS AND DISCUSSION

3.1. Microstructural analysis

Impact strength tests can supply useful information on fracture mechanisms of the material under conditions of rapid loading and on the role played by the secondary phase particles and the defects like porosity, oxides and inclusions on crack trigger and propagation, and on fracture morphology.

The microstructure of the wheels analysed consists of a primary phase, α-Al solid solution, and an eutectic mixture of aluminium and silicon. α-Al precipitates from the liquid as the primary phase in the form of dendrites. Intermetallics compounds, such as Fe-rich intermetallics, were also observed.

The scale of microstructure in different zones of the wheels analysed was characterized by means of SDAS measurements and then correlated with impact properties. These data are described in Section 3.2.1.

In figure 2, typical microstructures of the wheels analysed are reported with reference to the different positions, in particular the hub (H), the spoke (S) and the rim (R) zones. While figure 2a shows the microstructure of as-cast wheel-1, in figure 2b the microstructure of T6 heat treated wheel-2 is presented.

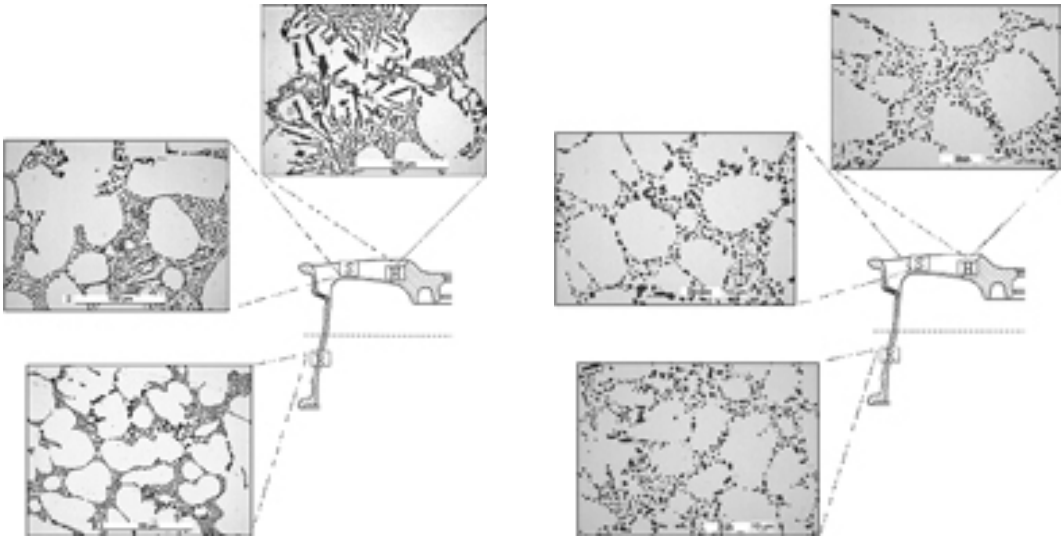

(a) (b)

Fig. 2. Microstructure of (a) wheel-1 and (b) wheel-2 with reference to the different positions analysed.

3.1.1. Microstructural defects and secondary phases

Microshrinkage were found in the spoke and in the rim region of each wheel, while no defects were observed in the hub zone. An example of microshrinkage porosity in the rim area is shown in figure 3.

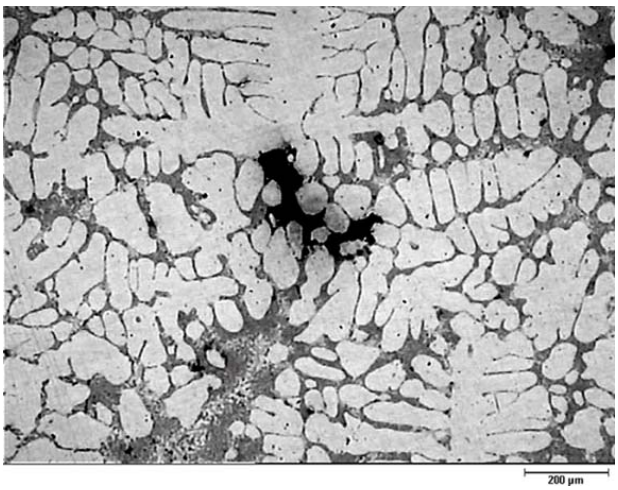

Fig. 3. Optical micrograph of a shrinkage porosity in the rim zone.

Secondary phase particles, such as Fe-rich intermetallics with typical needle shape, were observed in the samples analysed. In figure 4 and 5, the presence of secondary phases is evidenced in the specimens drawn from as cast wheel-1 and T6 heat treated wheel-3 [18,19]. The presence of Fe in the alloy involves a loss in ductility, shock resistance and machinability [20].

Concerning eutectic silicon, different size and morphology were observed in as cast wheel-1 than in the T6 heat treated wheels, as a consequence of the solution heat treatment. In both wheels-2 and -3, the eutectic silicon is present as well dispersed

globules (figure 5). In the as cast wheel, the eutectic silicon is in the form of fibrous particles due to Sr modification (figure 4). The different silicon morphology can affect the impact properties [7,9-11].

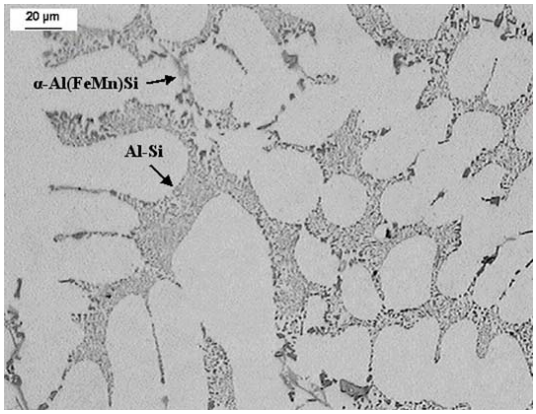

Fig. 4. Optical micrograph showing secondary phase particles in rim area of wheel-1. The eutectic silicon is in the form of fibrous particles in the interdendritic channels.

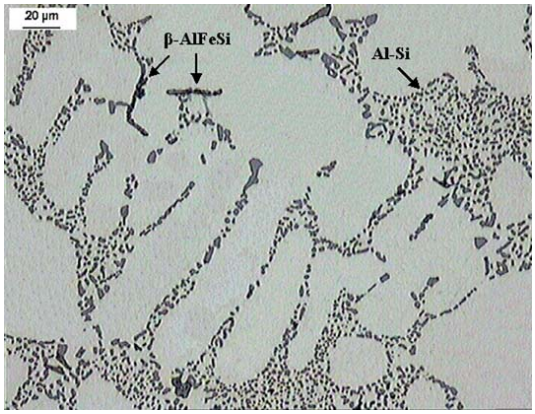

Fig. 5. Optical micrograph showing secondary phase particles in rim area of wheel-3. The distribution of eutectic silicon is homogeneous and globular.

3.2. Impact strength

Figure 6 shows the mean values of the total impact energy, with standard deviations, obtained on sub-size V-notch Charpy sample using the instrumented test method according to UNI EN ISO 14556:2003. The samples drawn from the spoke and the rim zone of as cast wheel-1 showed close impact energies, 1.53 and 1.55 J respectively, with low standard deviation (~0.10 J). In wheel-2, the impact energy increased from values of 2.24 J in the spoke to 2.55 J in the rim. In wheel-3 the trend and the increase were the same: the specimens drawn from the spoke region revealed lower impact values, 2.41 J against 2.75 J, even if the standard deviation was higher (~0.3 J). The T6 heat treatment influenced the impact properties, increasing the impact energy of the specimens by more than 60%, as evidenced in figure 6.

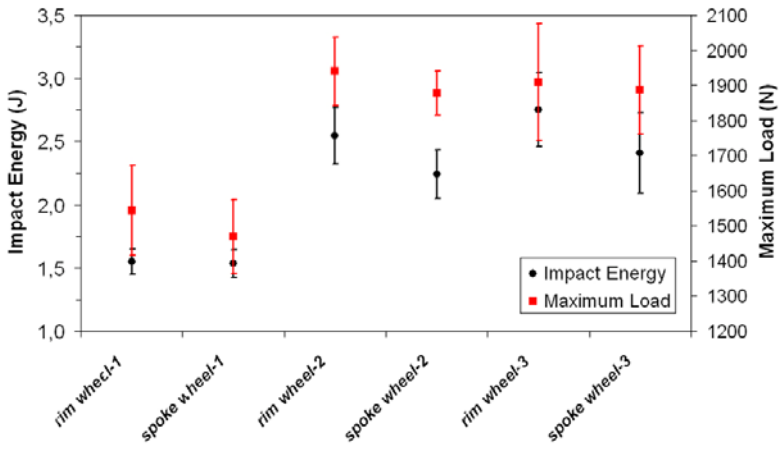

Fig. 6. Impact energy and maximum load measured in the different positions of the wheels. The standard deviations are shown as error bars.

The maximum load values as a function of the position of the specimens taken from the wheels is also shown in figure 6. Comparing the results of the heat treated with the as cast wheels, the T6 heat treatment increases the maximum load of about 26%. In wheel-1, the maximum load increases from 1470 N to 1544 N (about 5%), considering the spoke and the rim region, respectively. Similar trend was observed in wheels-2 and -3, where the maximum load was higher for the specimens drawn from the rim zone. While the value increases of about 3% in wheel-2, the increase is only 1.2% in wheel-3, where the standard deviation is however higher.
Figure 7 shows two load-time curves obtained from the instrumented impact tests. The curves refer to the samples obtained from the region of the spoke and the rim of wheels-1 and -3. The initial fluctuation of the curves is due to the inertial loading of the hammer as a result of the acceleration of the specimen from the remainder [5]. The shape of the load-time curves in figure 7a, similar to that obtained from T6 heat treated wheels (figure 7b), shows rather high values of nucleation and propagation energies. The load values are higher for the specimens drawn from the T6 heat treated wheels [5,6]. After the peak force, the slow load reduction indicates a controlled crack propagation.

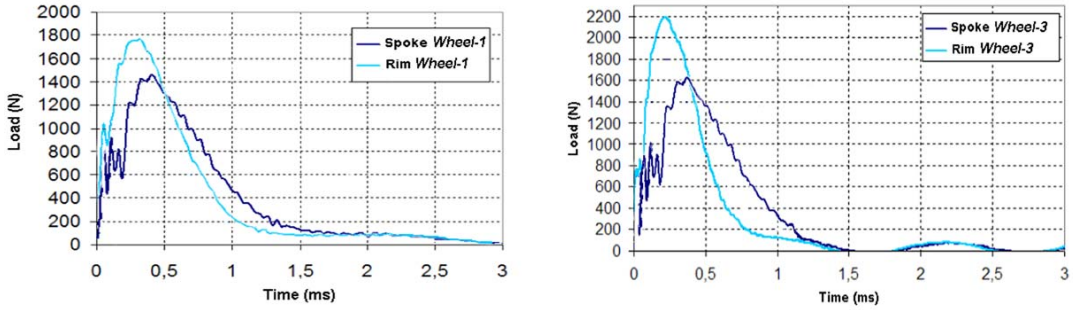

(a) (b)

Fig. 7. Load-time curves of samples obtained from spoke and rim area of (a) wheel-1 and (b) wheel-3.

From both figures 7a and 7b, it is possible to observe that the samples drawn from the spoke zone show lower F_m values, but higher time to fracture (T) and time at the peak load (T_m). The crack growth stability increases if the ratio between propagation energy and nucleation energy increases and the load reduction becomes slower [5,21,22].
Total absorbed energy was split into the two main complementary contributions, W_m and W_p, measured as previously described and reported as a percentage of the total impact energy. In figure 8 it is possible to observe that W_p values are in a range of 60-75% and the highest values are shown by the specimens drawn from as cast wheel-1, which shows thereby the lowest energies at maximum load. W_p values are generally higher in the region of spoke where the standard deviation is also higher.

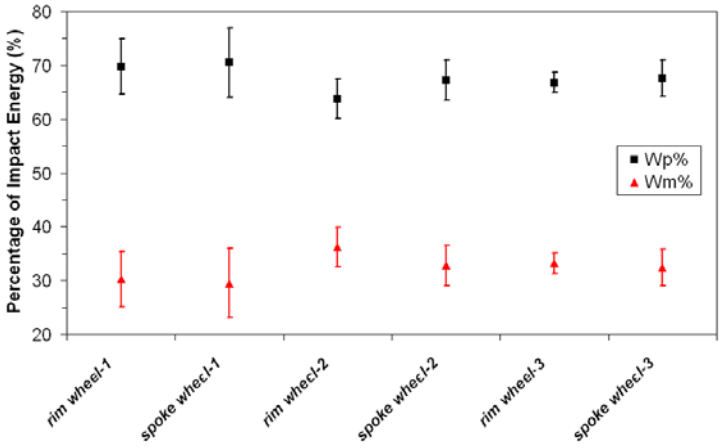

Fig. 8. Percentage of energy absorbed during crack nucleation and propagation and measured at different positions of the wheels analysed. The standard deviations are shown as error bars.

Considering the position of samples, it is necessary to note that the spokes are generally thicker (~15 mm) than the rim (~10 mm), which is the first zone to solidify, while the spoke and the hub zones are the last ones. Therefore, the microstructure in the rim region is finer, with higher mechanical properties. This is confirmed by higher F_m values in the zone of the rim. Increasing the maximum load, the load-time curves shifts towards shorter times to fracture with lower percentage of propagation energy. The samples taken from the spokes show W_p values higher than the ones drawn from the rim.

The ductility of the material depends on the hardening treatment and also on the size and the morphology of silicon particles. The highest ductility of the specimens drawn from as cast wheel-1 can be attributed to the lower amount of hardening precipitates, leading to a reduction in stresses. The strontium modification is likely to have modified the size and the shape of the silicon particles, increasing the volume fraction of the plastic aluminium matrix.

While in wheels-2 and -3 the modification of the cast alloy with strontium and the solution treatment changed the silicon particles size and morphology, the highest density of β'-Mg_2Si precipitates with their needle-like shapes and brittle behaviour, increased the micro stresses. This resulted in the reduction of α-Al matrix deformation, thus decreasing ductility [10,11]. These precipitates are brittle and may fracture at very low strains during deformation, accelerating the growth of the crack. Worth to mention, casting defects have a deleterious effect on mechanical properties and their distribution could not be uniform throughout the whole casting, consequently creating a non-uniform distribution of mechanical properties [3,20]. This could explain the different scattering level in impact properties observed in the Charpy specimens drawn from the same wheel.

3.2.1. Relationship between impact properties and SDAS

In table 2, SDAS and impact energy values for the wheels analysed are reported. SDAS measurements were correlated to the impact energy values with the aim to investigate the microstructural effect on impact properties. As it was possible to

understand from table 2, there exists an inverse correlation between SDAS and impact energy, a finer microstructure corresponds to an higher impact energy [5].

Table 2: SDAS and impact energy values in the wheels analysed. Average values and standard deviation are given.

Location	Wheel-1		Wheel-2		Wheel-3	
	SDAS (μm)	Impact Energy (J)	SDAS (μm)	Impact Energy (J)	SDAS (μm)	Impact Energy (J)
Hub	59±5	-	59±6	-	57±7	-
Spoke	35±5	1,53±0.11	42±7	2,24±0.20	39±4	2,75±0.32
Rim	23±7	1,55±0.10	28±4	2,55±0.22	26±4	2,41±0.29

In figure 9, the crack propagation energy (W_p) has been correlated to SDAS values for the as cast and the T6 heat treated wheels. A direct correlation has been found, not depending on the wheel's temper [5].

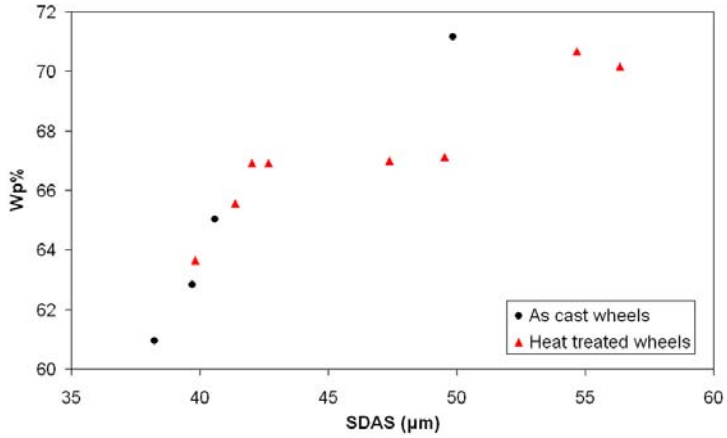

Fig. 9. Correlation between SDAS and W_p% (percentage of energy absorbed during crack propagation.

3.2.2. Microstructural analysis of fracture profiles

The crack crosses the interdendritic eutectic region, where a significant fraction of cracked eutectic silicon and intermetallic particles is found, following the dendritic profile of the α-Al solid solution. In figures 10a-c the fracture profiles of samples taken from the different wheels can be seen. Secondary cracks, parallel to the principal crack and normal to the tensile stress induced by the presence of the V-notch, can be observed [23]. The crack path follows regions where there are hard and brittle eutectic silicon and intermetallic particles.

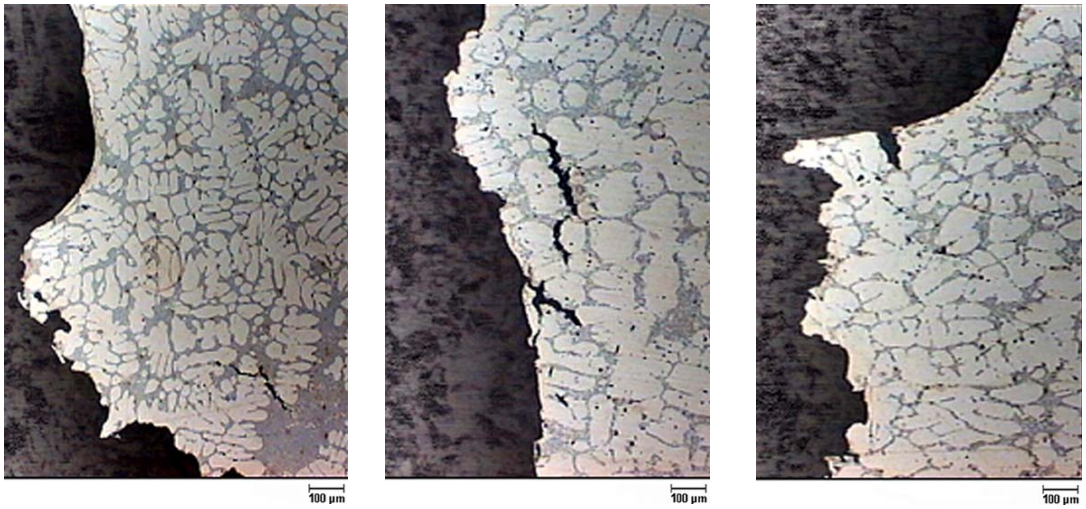

(a) (b) (c)

Fig. 10. Optical micrographs of the fracture profiles of samples drawn from (a) the rim of wheel-1 and from (b) the spoke of wheel-2 and (c) wheel-3. Secondary cracks are evident.

3.2.3. SEM analysis of fracture surfaces

As it can be seen in figure 11a the SEM analysis of the fracture surface of a sample taken from the spoke of wheel-2 reveals a transcrystalline fracture of medium-developed surface; regions of cleavage facets are visible in the silicon precipitates and brittle intermetallic phases [24]. In figure 11b the fracture surface of a sample drawn from the rim of wheel-1 reveals the presense of shrinkage porosity and the interdendritic path of the crack, that is the fracture profile follows the interdendritic eutectic zone. The edges of the deformed and fractured micronecks in α-Al solid solution with visible traces of microdeformation (dimples) are shown in figure 11c.
Fractures in the two-phase region were found, as put in evidence in figure 11d where the early stages of decohesion are visible on the interface between α-Al and silicon. In the microregion of the α-Al solid solution, the dimples have been formed around the cracked silicon particles as a result of plastic deformation of the matrix.

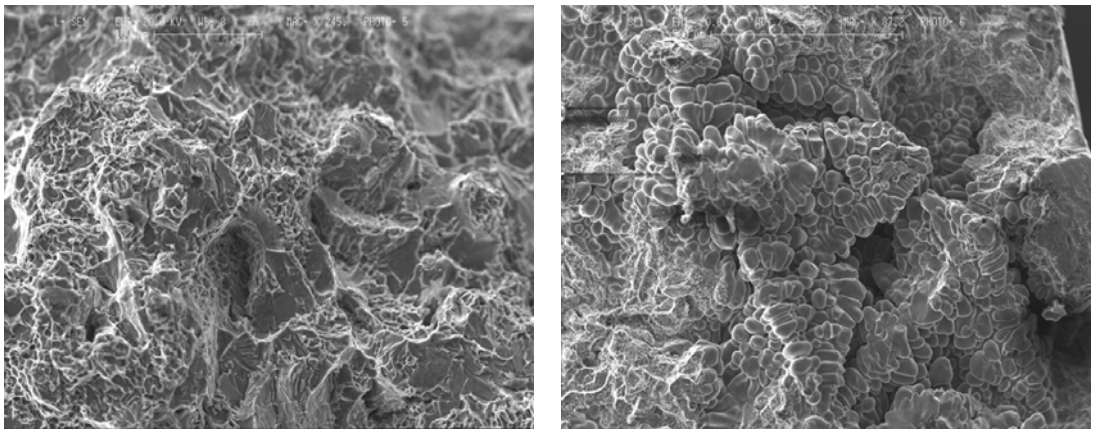

(a) (b)

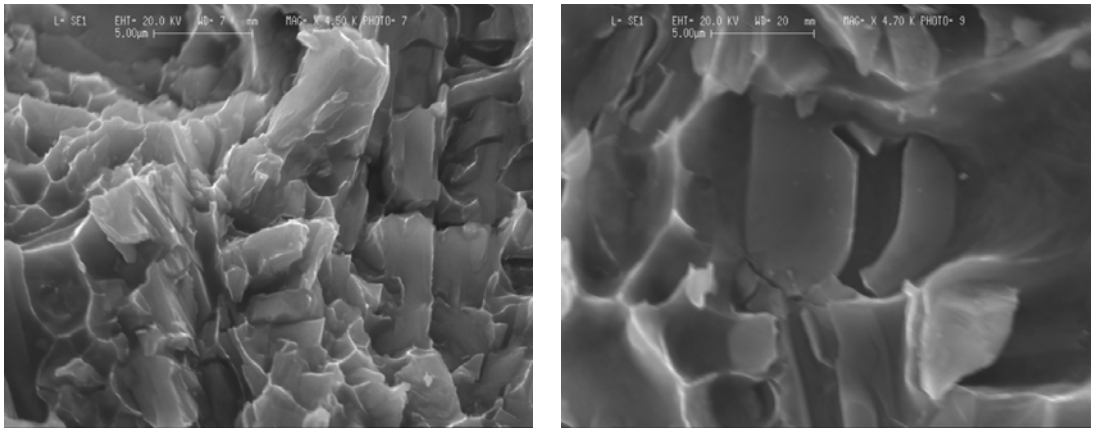

(c) (d)

Fig. 11. Features of the fracture surfaces of the Charpy specimens drawn from the wheels analysed as revealed by SEM. (a) Transcrystalline and ductile fracture from the spoke of wheel-2; (b) interdendritic fracture from the rim of wheel-1; (c) micronecks and dimples from the rim of wheel-1; (d) cleavage fracture in the silicon precipitate from the rim of wheel-3.

The presence of secondary phases were revealed on the fracture surfaces of the samples analysed. An example is shown in figure 12 for a sample drawn from the spoke of wheel-3. The EDS analysis indicated the nature of the precipitate as brittle *β*-AlFeSi platelets (figure 12).

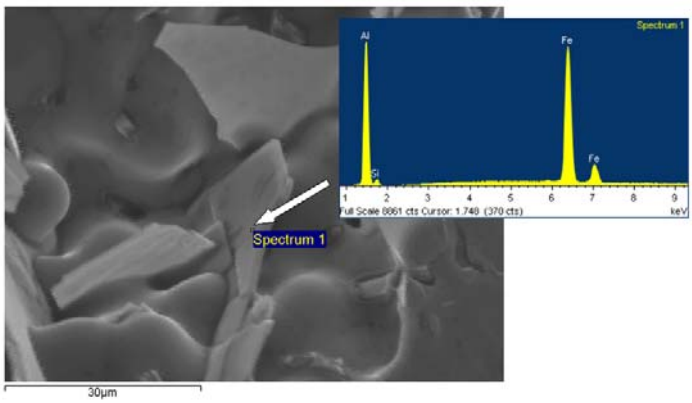

Fig. 12. SEM micrograph of β-AlFeSi platelet, on the fracture surface of sample drawn from the spoke of wheel-3, with EDS spectra.

3.3. Porosity measurement

The preliminary X-ray analysis, carried out on each wheel, revealed the presence of macro porosity both in the spokes and in the rim. The qualitative results obtained with the X-ray equipment were quantitative confirmed by density measurements of Charpy samples drawn from wheels-2 and -3. Figure 13 shows the percentage porosity of wheels-2 and -3 in different positions and the standard deviations as error bars. Wheel-3 presents the highest porosity content, mainly concentrated in the zone of the spoke, while the percentage porosity in wheel-2 appears lower, revealing good casting quality. The elevated standard deviation demonstrates a non-homogeneous

distribution of porosity inside the casting and consequently inside the Charpy specimens.

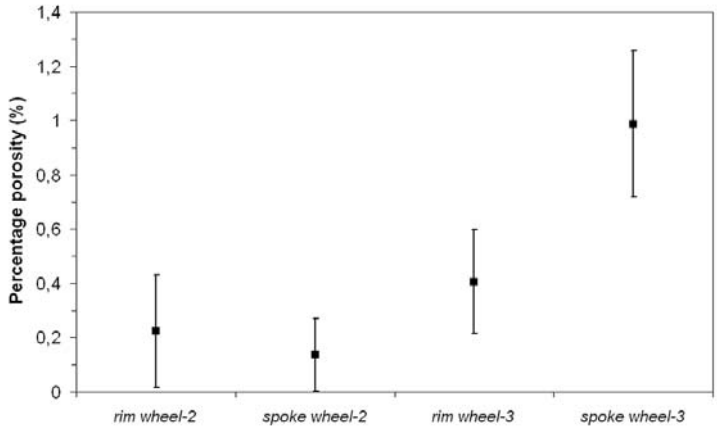

Fig. 13. Percentage porosity measured at different positions of the wheels analysed. The standard deviations are shown as error bars.

In order to individuate the macro porosity distribution, the Charpy samples were mapped with micro focus X-ray equipment. While in some samples the presence of defects extends throughout the specimen, involving also the zone around the notch (figure 14), other samples did not show defects close to the V-notch. To demonstrate the influence of defects' distribution on impact properties, the impact energy of some samples, drawn from the spoke of wheel-3, is sorted in figure 15, where some representative X-ray images, taken in the zone around the V-notch, are also shown. The X-ray images refer to a high (a), medium (b) and low (c) defect content. This is to demonstrate how the distribution of defects is not uniform in the region of the spoke of wheel-3, consequently creating a non-uniform distribution of impact properties, and how casting defects become critical when concentrated around the notch where they reduce the load bearing area of Charpy specimens. Therefore, the presence of porosity is critical on impact properties and can overcome the effect of the microstructure.

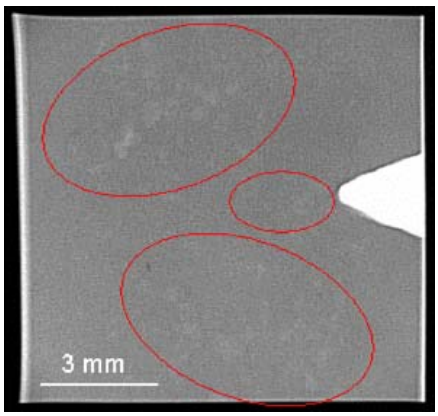

Fig. 14. Micro focus X-ray image of Charpy sample showing the presence of porosity around the notch.

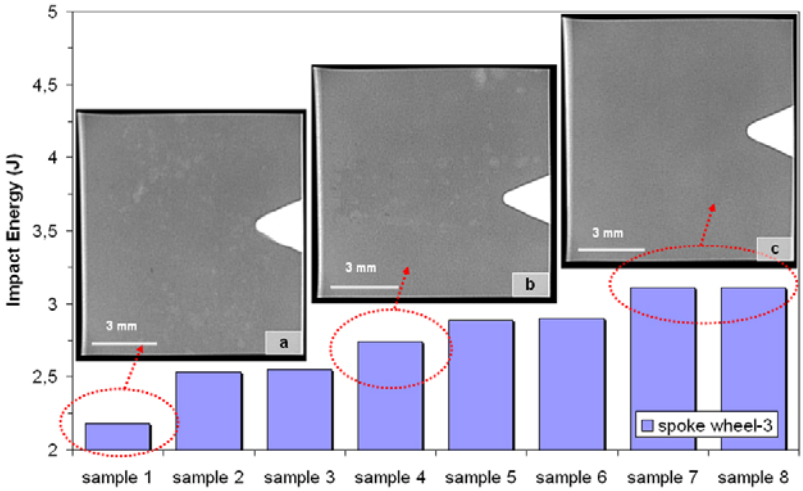

Fig. 15. Impact energy of some samples drawn from the spoke of wheel-3 associated with respective X-ray images, taken in the zone around the V-notch. The X-ray images refer to a high (a), medium (b) and low (c) defect content.

3.4. Computer simulation results

An important requirement for good casting quality of an aluminium wheel is optimal die filling, avoiding turbulence of the melt [25]. Figure 16 shows the melt velocity at 20% and 70% of die filling of 7-spoke wheel-1. The results are displayed for half the casting. At the start of die filling the flow speeds increase with an increase in the build-up pressure, increasing the risk of turbulence. Previously tests showed that a flow speed higher than 0.5 m/s results in breaking up of the melt front, leading to oxidation of the melt, inclusion of oxide films and air entrapment [25-27]. As previously seen, impact properties are strongly influenced by the presence of defects. An important feature is the different magnitude of the high melt speed and the point of time of its occurrence. With the reduction of the feed cross-section in the relatively thin spokes the melt locally accelerates in this region (Figure 16a), with a maximum melt velocity of 0.27 m/s. On reaching the larger volume with entry into the rim, the speed of the melt reduces until the wheel is completely filled (Figure 16b). The maximum melt velocity is about 0.04 m/s in the region of rim. From numerical simulation results it was possible to demonstrate how a good compromise between laminar filling and decreasing melt temperature was obtained. Too slow die filling increases the risk of freezing by decreasing the melt temperature below the alloy-dependent coherence temperature [1,3,4,28]. Numerical calculations showed a melt temperature higher than 617°C during the filling and no evidence of solidification cavities caused by a premature freezing of the melt. The 5-spoke wheels-2 and -3, even with a different geometry, reflect similar filling behaviour of wheel-1, i.e. a mean melt velocity lower than 0.3 m/s.

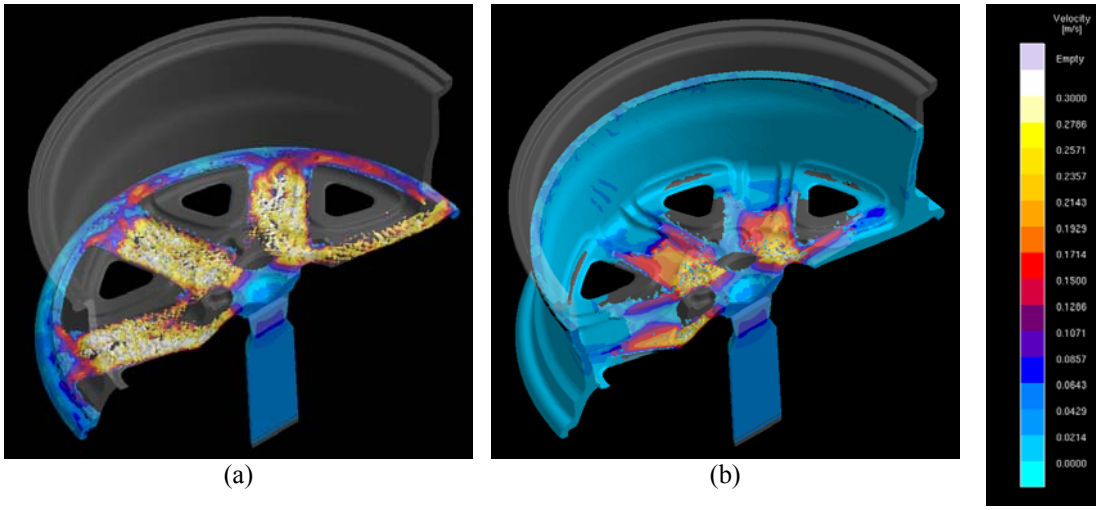

(a) (b)

Fig. 16. Calculated melt velocity at (a) 20% and (b) 70% of die filling of wheel-1.

After completion of die filling the wheel starts to solidify. Figure 17 presents calculated solidification times, from numerical simulation, with the corresponding microstructure within wheel-2. Solidification times were also estimated by means of SDAS measurements [17,29]. A comparison between calculated and estimated solidification times was carried out (Figure 17). As it is possible to observe the relationship is good, testifying the ability of numerical simulation codes to predict the local solidification conditions and the characteristics of casting components. Wheels-1 and -3, even with different geometries, reflect similar solidification behaviour, as previously evidenced by SDAS measurements.

Ideally, solidification should occur directionally, starting from the rim, via the spokes to the hub. Simulation of casting solidification revealed problem areas in the junction zone between the spoke and the rim within wheel-2, specifically, a hot spot caused by increased thickness. Longer solidification time in this zone is opposed to that of the spoke and the rim. Therefore, the hot spot in the junction zone between the spoke and the rim is a critical region for feeding. The casting shrinkage is indicated by a feeding criterion in figure 18, where, in addition to the shrinkage porosity in the junction zone between the spoke and the rim, smaller solidification cavities are present in the rim area. The presence of defects was confirmed by means of X-ray inspections and metallographic analysis (Figure 18).

The feeding criterion was applied to wheels-1 and -3 and revealed an higher content of shrinkage porosity in the rim zone and in the junction zone between the spoke and the rim. This could confirm the highest porosity amount from the density measurements of Charpy samples taken from wheel-3 even if, as previously said, the presence of defects is critical when concentrated around the notch.

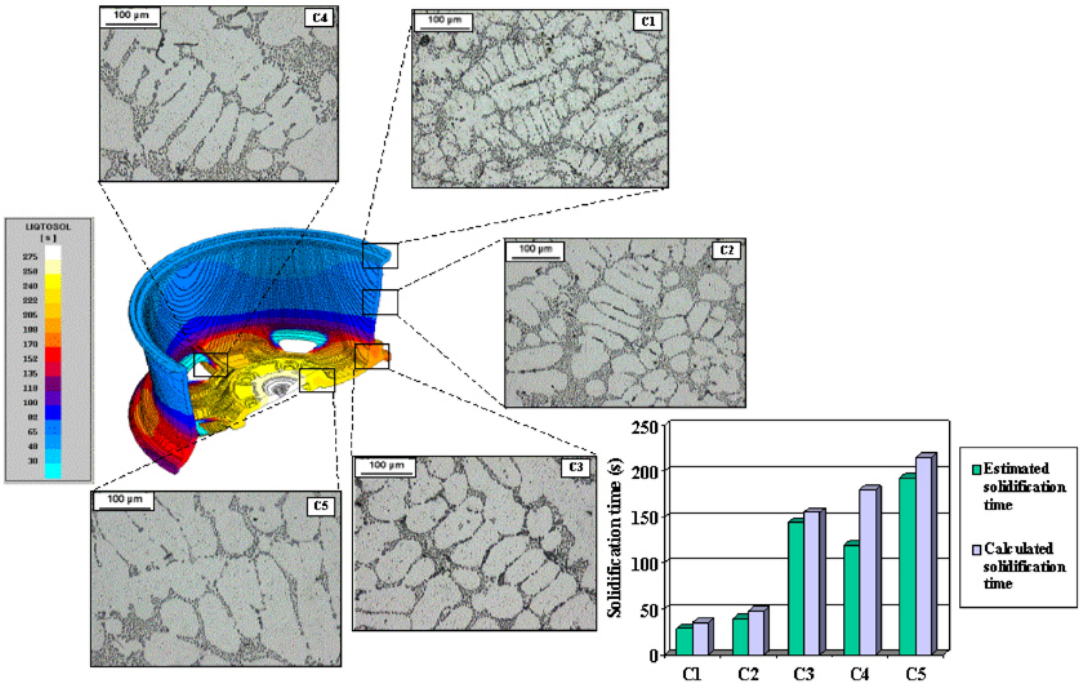

Fig. 17. Calculated solidification times with corresponding microstructure within wheel-2. Solidification times, estimated by means of SDAS measurements and calculated with a numerical simulation approach, were compared.

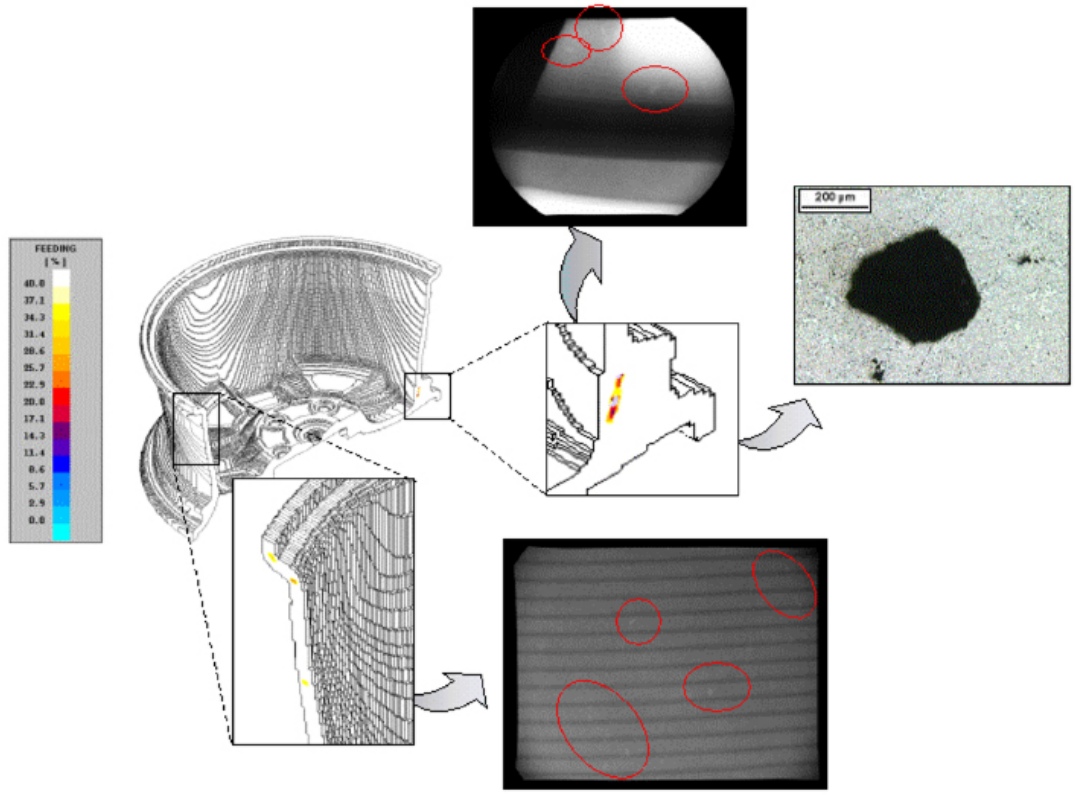

Fig. 18. Shrinkage porosity in the rim area and in the junction between the spoke and the rim within wheel-2. These zones are critical for feeding. The casting shrinkage is indicated by a feeding criterion.

4. CONCLUSIONS

Impact strength tests have been performed on Charpy V-notch specimens drawn from three different A356 17-inch wheels, produced by low pressure die casting. While one wheel is a 7-spoke wheel in the as cast temper, the other two wheels, which are 5-spoke wheels in the same T6 condition, differ on the geometry and thickness of the spokes. Based on the results obtained in the present study, the following conclusions can be drawn:

- Impact energy values are lower in the as cast wheel than in the T6 heat treated wheels.
- A finer microstructure always corresponds to higher impact strength.
- The resistance to crack propagation values (W_p) are in the range of 60-75% of the total absorbed energy and the highest values are shown by the as cast wheel.
- In every wheel a direct correlation between W_p and SDAS is found.
- Microstructural analysis has revealed the presence of microshrinkage porosity in the spoke and in the rim region of each wheel, the different size and morphology of eutectic silicon in the as cast and in the T6 heat treated wheels, the presence of brittle secondary phases.
- The crack crosses the interdendritic eutectic region where a significant fraction of cracked eutectic silicon and intermetallic particles is found.
- The preliminary X-ray analysis, carried out on each wheel, has revealed the presence of porosity both in the spokes and in the rim. The qualitative results obtained with the X-ray equipment are quantitative confirmed by density measurements of Charpy samples. The elevated standard deviation of density measurements demonstrates a non-homogeneous distribution of porosity inside the casting and consequently inside the Charpy specimens.
- Casting defects become critical when concentrated around the V-notch where they reduce the load bearing area of Charpy specimens. Therefore, the presence of defects is critical on impact properties and can overcome the effect of the microstructure.
- A mean melt velocity value lower than 0.3 m/s is calculated by means of numerical simulation for each type of wheel; the results shows a good compromise between laminar filling and decreasing melt temperature.
- Solidification times, estimated by means of SDAS measurements and calculated with a numerical simulation approach, are compared and a good correspondence is found.
- Simulation of casting solidification reveals critical areas, as concern hot spots and shrinkage porosities, generally in the zone of the wheels between the spoke and the rim, as well as in the rim area.

ACKNOWLEDGEMENTS

The Authors acknowledge for the experimental contribution to this research dr. E. Capatti, dr. F. Piasentini, dr. F. Massari and dr. N. Tomanin. Many thanks are also due to dr. E. Della Rovere and G. Mazzacavallo. Many thanks are also due to dr. N. Gramegna for helping with MAGMASOFT® simulations.

REFERENCES

1. Flinn, R.A., 1963. Fundamentals of metal casting, first ed., Addison-Wesley Publishing Company, Massachusetts.
2. Sicha, W.E., 1971. Properties of commercial casting alloys. In: Kent, R., Van Horn, Aluminum vol. I – Properties, Physical Metallurgy and Phase Diagram, fourth ed., American Society for Metals, Metals Park, OH, pp. 277-302.
3. Blackmun, E.V., 1968. Casting. In: Kent, R., Van Horn, Aluminum vol. III – Fabrication and Finishing, third ed., American Society for Metals, Metals Park, OH, pp. 43-80.
4. Street, A.C., 1986. The diecasting book, second ed., Portcullis Press, London.
5. Li, Z., Samuel, A.M., Samuel, F.H., Ravindran, C., Doty, H.W., Valtierra, S., 2004. Parameters controlling the performance of AA319-type alloys Part II. Impact properties and fractography. Mater. Sci. Eng. A 367, 111-122.
6. Paray, F., Kulunk, B., Gruzleski, J.E., 2000. Impact properties of Al-Si foundry alloys. Int. J. Cast Met. Res. 13, 17-37.
7. Srivastava, M.C., Lohne, O., Arnberg, L., Laukli, H.I., Gjestland, H., 2006. Energy absorption of HPDC aluminium and magnesium alloys. In: Proc. High Tech Die Casting 2006, Vicenza, Italy, paper 10.
8. Murali, S., Raman, K.S., Murthy, K.S.S., 1992. Effect of magnesium, iron (impurity) and solidification rates on the fracture toughness of Al-7Si-0.3Mg casting alloy. Mater. Sci. Eng. A 151, 1-10.
9. Shivkumar, S., Wang, L., Keller, C., 1994. Impact properties of A356-T6 alloys. J. Mater. Eng. Perform. 3, 83-90.
10. Zhang, D.L., Zheng, L.H., StJohn, D.H., 2002. Effect of a short solution treatment time on microstructure and mechanical properties of modified Al-7wt.%Si-0.3wt.%Mg alloy. J. Light Met. 2, 27-36.
11. Pedersen, L., 1999. Solution heat treatment of AlSiMg foundry alloys, PhD thesis, Norwegian University Of Science and Technology (NTNU), Trondheim.
12. Wang, Q.G., Cáceres, C.H., 1998. The fracture mode in Al-Si-Mg casting alloys. Mater. Sci. Eng. A 241, 72-82.
13. Cáceres, C.H., Davidson, C.J., Griffiths, J.R., 1995. The deformation and fracture behaviour of an Al-Si-Mg casting alloy. Mater. Sci. Eng. A 197, 171-179.
14. Zhang, B., Cockcroft, S.L., Maijer, D.M., Zhu, J.D., Phillion, A.B., 2005. Casting defects in low-pressure die-cast aluminium alloy wheels. JOM 57, 36-43.
15. Cáceres, C.H., Selling, B.I., 1996. Casting defects and the tensile properties of an Al-Si-Mg alloy. Mater. Sci. Eng. A 220, 109-116.
16. Rooy, E.L., 1992. Nonferrous casting alloys – Aluminum and aluminum alloys. In: American Society of Metals (ASM), Casting - ASM Handbook vol. 15, ninth ed., ASM International, Materials Park, OH, pp. 743-770.
17. MAGMASOFT® v.4.2, 2002. MAGMAlpdc Module Manual, MAGMA Giessereitechnologie GmbH.

18. Stevens, R.H., 1995. Metallographic techniques and microstructures: specific metals and alloys – Aluminum alloys. In: American Society of Metals (ASM), Metallography and Microstructures - ASM Handbook vol.9, ninth ed., ASM International, Materials Park, OH, pp. 351-388.
19. Di Russo, E., 1993. The Atlas of microstructures of aluminium casting alloys, first ed., Edimet, Brescia.
20. Brown, R., 1999. Foseco non-Ferrous foundryman's handbook, eleventh ed., Butterworth-Heinemann, Oxford.
21. Vedani, M., Mapelli, C., 2001. Effect of thermal treatments on microstructure and impact toughness of die-cast Mg-Al-Mn alloys. Mat. Sci. Tech. 17, 938-944.
22. De Marco P.P., Cerri E., Effetto della pressocolata sulla struttura di un componente in lega di magnesio, in: Proceedings 30° National Conference AIM, Vicenza, Italy, 2004, AIM, paper 92.
23. Berto, F., Lazzarin, P., Wang, C.H., 2004. Three-dimensional linear elastic distributions of stress and strain energy density ahead of V-shaped notches in plates of arbitrary thickness. Int. J. Fract. 127, 265-282.
24. Warmuzek, M., 2004. Aluminium-Silicon Casting Alloys: Atlas of Microfractographs, first ed., ASM International.
25. Campbell, J., 2003. Castings, second ed., Elsevier Butterworth-Heinemann, Oxford.
26. Kuo, J.-H., Hsu, F.-L., Hwang, W.-S., 2001. Development of an interactive simulation system for the determination of the pressure-time relationship during the filling in a low pressure casting process. Sci. Technol. Adv. Mater. 2, 131-145.
27. Schroth, A., Schemme, D., 2003. Simulation in modern quality management systems – Simulation assists the implementation of quality management systems in foundries. Casting Plant and Technology 19, 8-18.
28. Bonollo, F., Gramegna, N., Odorizzi, S., 1999. La pressocolata delle leghe di alluminio: simulazione numerica del processo, first ed., Edimet, Brescia.
29. Kurz, W., Fisher, D.J., 1998. Fundamentals of solidification, fourth ed., Trans. Tech. Publications, Switzerland.

ARTICLE 5

QUALITY MAPPING OF ALUMINIUM ALLOY DIECASTINGS

G. Timelli*, F. Bonollo*

* Department of Management and Engineering – DTG
University of Padova
I-36100 Vicenza
ITALY

Presented at the 3rd International Conference High Tech Die Casting, Vicenza, Italy, September 21-22, 2006.
Submitted for publication in: Metallurgical Science and Technology, 2007

ABSTRACT
The effect of casting defects on mechanical properties was investigated for a high-pressure die-cast aluminium alloy. A series of U-shaped components were cast using a fully controlled cold chamber high-pressure die-casting machine with different process parameters. Defects existed in gas and shrinkage pores as well as oxide inclusions. An X-ray equipment was used for a preliminary quality control but showed its limits in detecting defects. The castings were sectioned and tensile bars extracted from different locations in the castings in order to map the distribution of the mechanical properties. The decrease in mechanical properties correlated with the area fractions of defects revealed on the fracture surface of the tensile specimens. A quality mapping approach showed how the final properties depend on the position of the casting and the process parameters adopted.

Keywords: High-pressure die-casting; Aluminium alloy; Defects; Oxide inclusions; Porosity; Fractography; X-ray radiography; Mechanical properties.

1. INTRODUCTION

High-pressure die-casting (HPDC) is widely used for the possibility of obtaining net to shape components of complex geometry and thin wall thickness at high production rates [1,2]. However, a number of parameters exists, which, if not adequately determined and adjusted, result in a decadence of quality of the die cast part. Common defects in manufactured parts are shrinkage cavities, cold fills, oxide films, dross, entrapped air bubbles. One of the major source of defects in HPDC is air entrapment in the melt during the filling stage of the die, but a detrimental effect can also come from defects generated in the shot sleeve before and during the injection process [3,4]. The influence of casting defects on the mechanical properties of cast aluminium alloys has been investigated by a number of researchers, with the common conclusion that defects can make the tensile behaviour of casting alloys unpredictable. Castings with thin sections, like those produced by HPDC technology, are vulnerable to the effect of defects since a single macrodefect can cover a significant fraction of the cross-section area. Even high integrity castings are expected to contain defects and thus it is important to predict their effect on final mechanical properties of the material. Campbell [5] and Dai *et al.* [6,7] showed that improper design of the filling system results in higher turbulence so that oxide films are generated and entrapped into the bulk liquid metal. Ingate velocities significantly affect the number and distribution of the oxide film defects generated from filling stage. Cáceres *et al.* [8] and Gokhale *et al.* [9] demonstrated how the mechanical properties decrease monotonically with an increase in the area fraction of defects revealed on the fracture surface of gravity cast aluminium specimens. Avalle *et al.* [2] and Wang *et al.* [10,11] studied the effect of defects on fatigue behaviour of cast aluminium alloys showing how casting defects have a detrimental effect by shortening not only fatigue crack propagation, but also initiation period, which is influenced by defects' size. They showed also how castings with defects have at least an order of magnitude lower fatigue life compared to defect-free materials and how porosity is more detrimental to fatigue life than oxide films. In literature data, static strength appears to be modestly influenced by casting defects compared to the elongation to fracture [2,3,8,9].

Generally, the effect of porosity on mechanical properties is studied through the measurement of the defect volume fractions or X-ray analysis, but these methods have the disadvantage to not reveal the presence of detrimental oxide films [12]. Therefore, quantitative fractography became a useful tool for such study because the fracture surface of tensile bars contains the part of the microstructure and defects that affect and govern the fracture mechanism. If the fracture surface is large enough, there is a likely to be a discernible pattern of chevron marks that leads to the point at which fracture was initiated [13]. Examination of this initiation point or region can reveal if fracture was initiated from a structural defect or a microstructural feature. Non-destructive methods are also adopted, such as acoustic microscope, which are able to detect cold flakes, especially the oxide layers, better than X-ray radiography [12,14]. A better correlation and reduced scatter is then obtained if the decrease in tensile strength and elongation to fracture are plotted against the projected area of defects on the fracture surface, instead of defect volume fractions.

Almost all the above mentioned researches were based on gravity cast testing specimens separately poured in sand/chill mold, where the amount of defects was generated avoiding degassing, vigorously stirring the melt, or controlling the feeding and pouring temperature. On industrial HPDC production it is more difficult to control the amount and type of defects due to the complexity of the casting shape or

to variable parameters such as the mold temperature, dosing volume, slow and fast shots, commutation points, injection and upset pressure. Therefore, quality mapping could be a right path to lead to the quantitative extended prediction of HPDC properties.
In this work a HPDC component was analysed and a combination of injection parameters and pouring temperatures were adopted in order to generate different type and amount of casting defects. The material was EN AC-46000–UNI EN 1706 (European designation, equivalent to the US designation A380), widely used in load-bearing components in automotive field. X-ray inspection was preliminary carried out in different zones of the casting and in tensile bars extracted from the components, while fractography analysis was carried out to detect the projected area of defects on fracture surface to quantify their effect on the mechanical behaviour.

2. EXPERIMENTAL PROCEDURE

2.1. Casting Experiment

For R&D purposes, a die for casting U-shaped of aluminium alloys has been made. The CAD model of aluminium casting with runners, gating and overflow system is displayed in figure 1a. The U-shaped casting was coupled with ribs, which are generally a location with high defect concentration. Figure 1b shows an example of an interrupted filling of the die with the arrow indicating a location where two metal flows met. The die-castings, with wall thickness ranging from 2.5 mm through 6 mm, were produced in a Müller-Weingarten 750 ton cold chamber die-casting machine, with a shot chamber length of 580 mm and diameter of 70 mm. The fill fraction of the shot sleeve was kept constant at 0.56 and every shot was documented with its shot profile. Temperature measurements were performed regularly, both using an infrared camera and temperature probes and the furnace temperature was checked frequently. Manual spraying and blowing process were used in order to cool down properly the die material and aid the release of the casting after complete solidification. After-pressure was also adopted to ensure the proper ejection of the parts.

(a) (b)

Fig. 1. a) The U-shaped CAD geometry (Length: 260 mm, height: 110 mm, width: 70 mm, outer wall thickness: 2.5 mm, rib thickness: 4-6 mm); b) Interrupted filling of the die. The arrow indicates a location where two metal flows meets.

In the present work an EN AC-46000 alloy (European designation, equivalent to the US designation A380), according UNI EN 1706, with standard composition listened in table 1, was cast. This alloy has a liquidus-solidus temperature range of approximately 593-538°C [15].

Table 1: Chemical composition of the casting alloy (wt.%).

Alloy	Standard	Al	Cu	Fe	Mg	Mn	Ni	Si	Sn	Zn
EN AC-46000	EN 1706	bal.	3-4	max 1.3	max 0.1	max 0.5	max 0.5	7.5-9.5	max 0.35	max 3

The U-shaped investigated was produced with the process parameters indicated in table 2. The shot profiles can also be seen in figure 2. Throughout this paper, the different process parameters will be termed P1,..., P4 and T2 respectively.

Table 2: Process parameters.

Shot profile	Filling phase plunger velocity slow shot (ms^{-1})	Filling phase plunger velocity fast shot (ms^{-1})	Commutation point slow-fast shot (mm)	Commutation point to upset pressure (mm)	Pouring temperature (°C)
P1	0.4	3	428	552	690
P2	0.4-0.6	3	447	562	690
P3	0.4-0.7	2	373	544	690
P4	0.4-0.6	2	451	547	690
T2	0.4	3	428	552	640

In the profile P1, the plunger speed was kept constant in the first phase and a rapid acceleration was applied in the second phase, i.e. at the beginning of die filling. The same profile was adopted for T2 but the pouring temperature was 50°C lower. For the other shot profiles the plunger was accelerated slowly also in the first phase, trying however to minimize air entrapment in the slow shot. The main differences regarded the variations of the switch point between the first and second phase, where the commutation point was anticipated (P3) and postponed (P2 and P4), and the reduction of the plunger velocity in the second phase for the profiles P3 and P4.

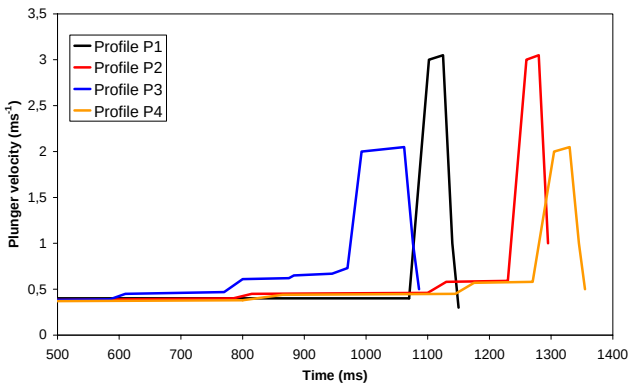

Fig. 2. Different shot profiles adopted in the present work.

The shot sleeve and the die were preheated but reached a quasi-steady state temperature after some shots, thus the first several castings were scrapped. Figure 3 shows the cooling system adopted to stabilise the temperature of the die and of the shot sleeve.

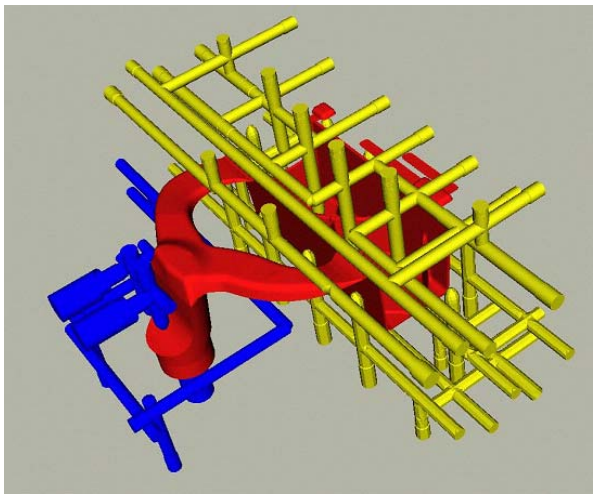

Fig. 3. Thermal management of the die.

2.2. X-ray, Tensile Tests and Microstructural Investigations

The U-shaped die-castings were mapped throughout with a macro-focus X-ray equipment for a preliminary analysis and comparison.

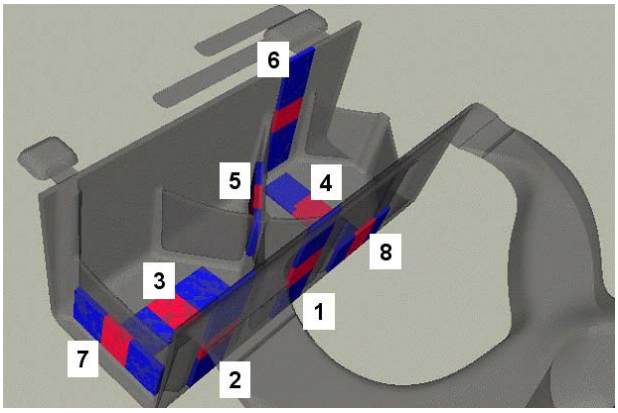

Fig. 4. U-shaped die casting with investigated locations.

Table 3: Tensile bars dimension.

	zone 1,2 (mm)	zone 3,4,7 (mm)	zone 5 (mm)	zone 6 (mm)	zone 8 (mm)
Gauge length	60	30	26	60	30
Thickness	2.5	3.1	6	4.1	2.4
Width	10	10	10	10	10

Tensile test bars with a rectangular cross section were extracted from eight different locations of the castings and the gauge length examined, pre and after the tensile testing, with a micro-focus X-ray equipment, which can magnify an image several times while still offering a better definition than a conventional X-ray tube. Throughout this paper, the different locations will be termed zones 1,...,8 respectively. The locations and the main dimensions of the tensile specimens are indicated in figure 4 and table 3. The X-ray images were then analysed using a commercial image-analysis software package. The defect area of each image was evaluated by counting the image pixels in each defect (figure 5). Every defect was counted indifferently.

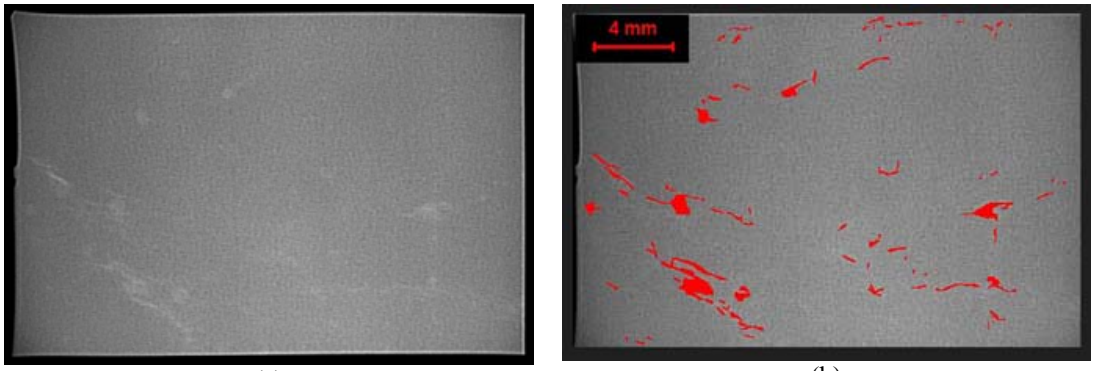

(a) (b)

Fig. 5. (a) X-ray image; (b) the same X-ray image binarized to determine the amount of defects.

The tensile strength, *UTS* (MPa), and the engineering elongation to fracture, s_f, of each sample were converted to true tensile strength (σ_f) and true elongation to fracture (ε_f) through equations [16,17]:

$$\sigma_f = UTS(1+s_f) \quad (1)$$

$$\varepsilon_f = \ln(1+s_f) \quad (2)$$

The true stress (σ)-true plastic strain (ε) flow curves of each specimen were approximated with a constitutive equation of the form [16,17]:

$$\sigma = K\varepsilon^n \quad (3)$$

where K is the alloy's strength coefficient and n the strain hardening exponent. The Quality Index, Q (MPa), defined [16-18] as

$$Q = UTS + 0.4K\log(100 \cdot s_f) \quad (4)$$

was then considered.

The fractured surfaces after testing were then observed under an optical stereomicroscope at a magnification of about x10. The acquired images were then transferred into a single photograph and the area of defects was measured by using an image analyser. The total measured defect area was then divided by the initial

cross section of the sample to find the defect area fraction. A scanning electron microscope was also used as support for the fractographic analysis.
At least three different castings from every shot profile were chosen to be analysed according the described procedure.

3. RESULTS AND DISCUSSION

3.1. X-ray analysis

The X-ray images in figure 6 are taken from zone 2 of three consecutive U-shaped castings poured according the profile P4. The size and the distribution of defects is different in spite the same process parameters were adopted. It is evident how the formation of defects is sensitive to small variations in the casting conditions and the causes cannot be only connected to the process profile adopted, even if this variable results the main source of defects.

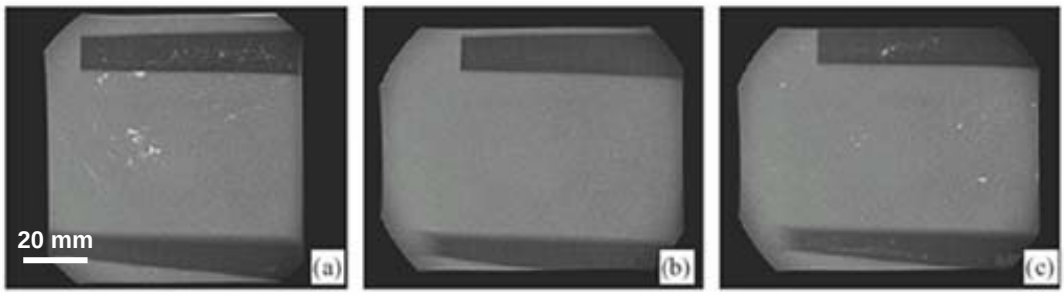

Fig. 6. Macro-focus X-ray images taken from zone 2 of three different castings consecutively poured with shot profile P4.

Figure 7 shows X-ray pictures, taken with macro- and micro-focus, from a tensile bar extracted from zone 2 of a casting poured according the profile P4. The micro-focus pictures show defects and details not appreciable with conventional X-ray tube. The defects seem to result from local die filling condition, i.e. a vortex, as indicated by arrows, was generated in the zone 2, entrapping and dragging air bubbles.

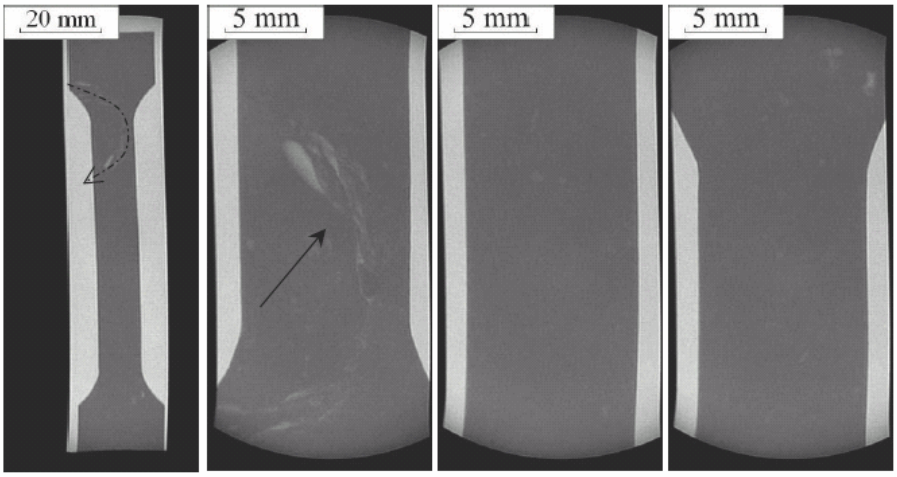

Fig. 7. Macro- and micro-focus X-ray images taken in a tensile bar extracted from zone 2 of a casting poured with shot profile P4.

The results of the X-ray image analysis of zones 1 and 2 are shown in figures 8 and 9. While figure 8 shows the defect distribution in zones 1 and 2 of castings poured with different shot profiles, evidencing the influence of process parameters in the amount of defects, figure 9 demonstrates how, in three consecutive castings poured with process P4, the defect reproducibility is sensitive to small uncontrolled variations in the casting conditions and how the amount of defects cannot be controlled only by changing shot profiles.

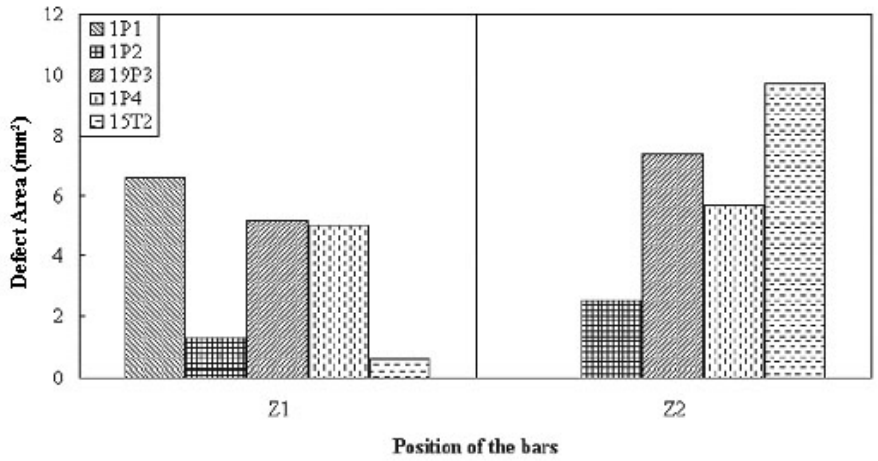

Fig. 8. Distribution of defects in zones 1 (Z1) and 2 (Z2) of castings poured with different process parameters.

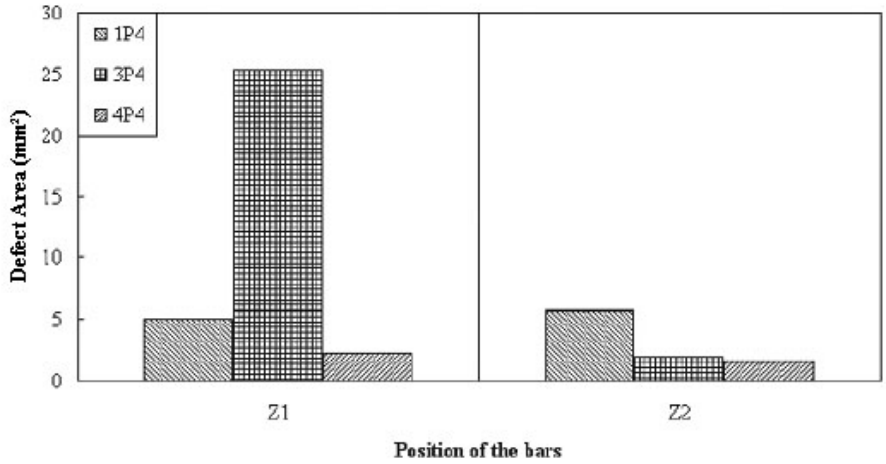

Fig. 9. Distribution of defects in zones 1 (Z1) and 2 (Z2) of three different castings consecutively poured with shot profile P4.

The same X-ray analysis was then repeated in the fractured tensile bars to characterize the position of the fracture into the whole bar. The analysis underlined how the fracture developed in the presence of defects (figure 10), but sometime the fracture path took place in a zone where the X-ray radiography didn't show any defect (figure 11). In these cases, the following fractographic inspection revealed a high amount of oxide inclusions, which represent surfaces of discontinuity in the

material and point for crack initiation. The oxide films were not revealed by X-ray inspection because the difference of density between the aluminium alloy and the aluminium oxide skins is minimum and thus not detectable through conventional X-ray technique [12].

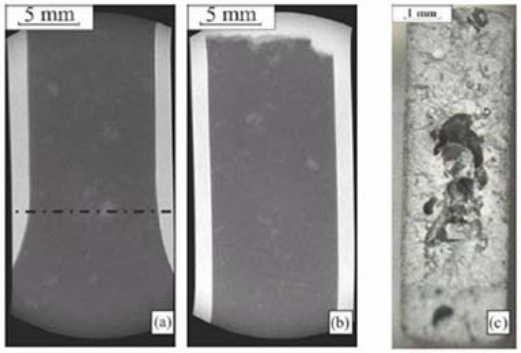

Fig. 10. X-ray images of a tensile bar (a) before and (b) after testing; (c) fracture surface. The line in (a) represents the fracture path in the specimen. Defects were detectable by X-ray inspection.

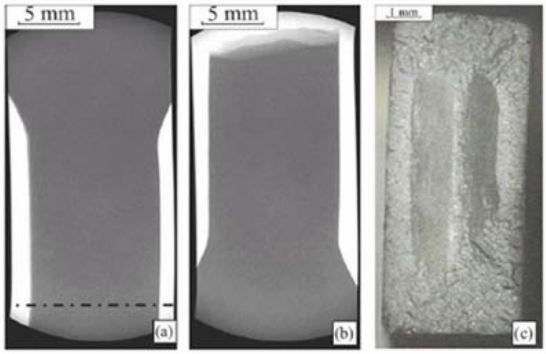

Fig. 11. X-ray images of a tensile bar (a) before and (b) after testing; (c) fracture surface. The line in (a) represents the fracture path in the specimen. Defects were not detectable by X-ray inspection.

3.2. Mechanical properties

From the tensile test results, it was possible to observe how the amount of defects influenced considerably the *UTS* and the elongation to fracture (s_f), which ranged from 129 to 307 MPa and from 0.29% to 2.89% respectively. Wide scattering was also shown by the alloy's strength coefficient (K) and the strain hardening exponent (n). If elastic properties of the material, as the Young modulus (E) and the Yield Strength ($YS_{0.2\%}$), were considered, all data arranged around constant values, (72 GPa and 180 MPa respectively) independently from the zone of extraction, the process parameters, but above all the amount of defects. Plotting the true stress-true plastic strain flow curves of each specimen and the mean flow curve (figure 12), according eq. (3), it is possible to observe how all the curves followed a similar trend and the difference consisted in the break point, i.e. the fracture. Considering the same graph with the mean flow curve but plotting the true tensile strength (σ_f) and the true elongation to fracture (ε_f) values obtained according eqs. (1) and (2), a better view of what previously said is shown (figure 13). The scattering of data from the mean flow curve

$$\sigma = 755\varepsilon^{0.23} \tag{5}$$

is low, as shown by the coefficient of determination, R^2, equal to 0.95.

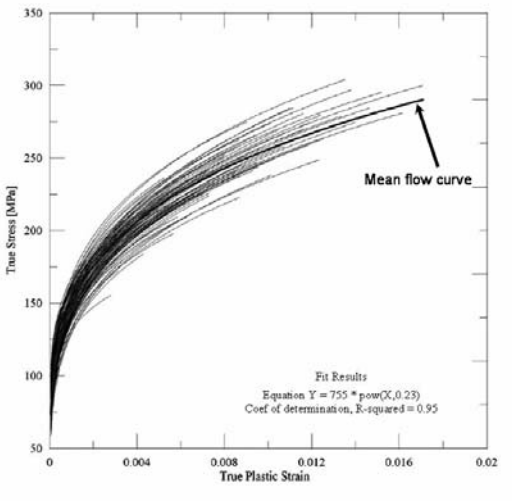

Fig. 12. The true stress-true plastic strain flow curves of each specimen and the mean flow curve, according eq. (3).

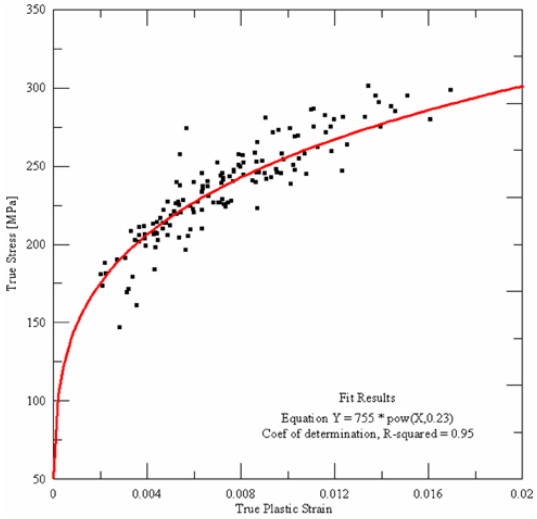

Fig. 13. The true tensile strength (σ_f) and true elongation to fracture (ε_f) values of each sample obtained according eqs. (1) and (2) are plotted together with the mean flow curve.

Therefore, eq. (5) can be considered constitutive of the uniform plastic behaviour of the alloy analysed. To understand the correlation between the fracture and the amount of defects, the bubble plot in figure 14 can be considered where each bubble represents the true tensile strength (σ_f) and the true elongation to fracture (ε_f) and the diameter of the bubble is proportional to the defect area fraction. Increasing the distance from the origin, the diameter of the bubbles and therefore the defect area fraction decreases, indicating the fundamental role of defect on fracture mechanism. A similar graph can be seen in figure 15 where the diameter of each bubble is instead proportional to the Quality Index, defined by eq. (4). Quality Index has the advantage to consider both tensile and strain properties of the material at the same time. As expected, the general trend of the graph is opposite to the previous one, showing thus the strict relationship with the defect amount.

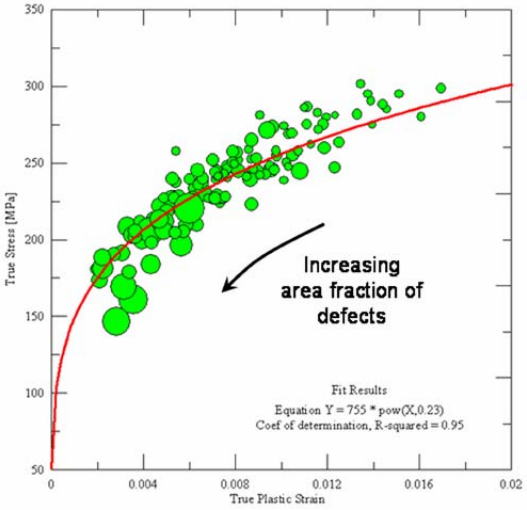

Fig. 14. Bubble plot of the true tensile strength (σ_f) and true elongation to fracture (ε_f) values of each sample where the diameter of each bubble is proportional to the defect area fraction.

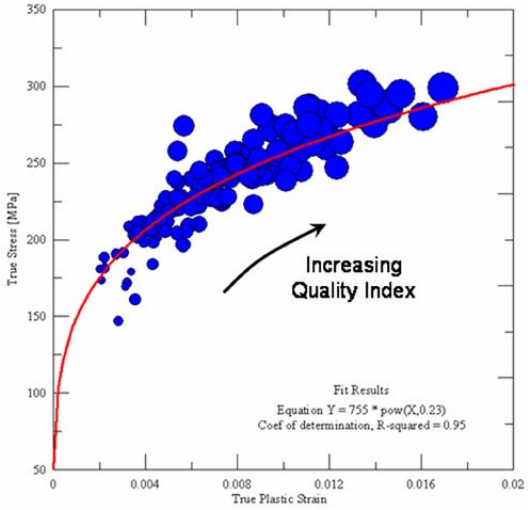

Fig. 15. Bubble plot of the true tensile strength (σ_f) and true elongation to fracture (ε_f) values of each sample where the diameter of each bubble is proportional to the Quality Index.

The final quality maps can be seen in figures 16 and 17 where the mean mechanical properties, together with the scattering bands (minimum and maximum values), are plotted versus the different positions (Z1,...,Z8) and process parameters adopted. In general, it can be seen how, considering the same position, the *UTS* and the engineering plastic strain show different values changing the process parameters; while, fixing the process variables, the mechanical properties change with changing location. Therefore, from these considerations it is possible to understand the difficulty in optimising the whole casting and the HPDC process parameters.

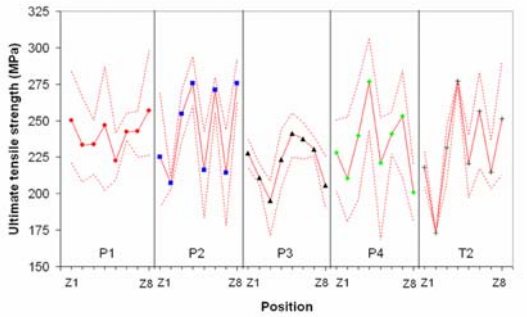

Fig. 16. The mean UTS, together with the scattering bands, is plotted versus the different positions (Z1,...,Z8) and process parameters adopted.

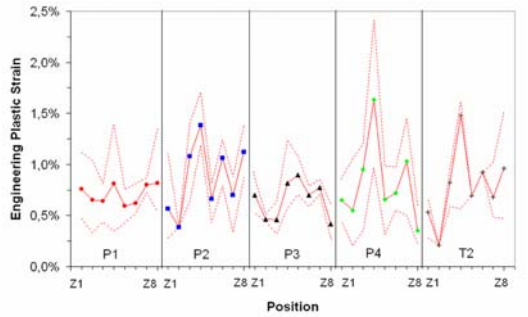

Fig. 17. The mean engineering plastic strain, together with the scattering bands, is plotted versus the different positions (Z1,...,Z8) and process parameters adopted.

4. CONCLUSIONS

The primary objective of this work has been to characterize the influence of casting defects on mechanical properties of a high-pressure aluminium U-shaped casting. From the experimental findings it can be concluded that:

1. The amount and type of defects changes by changing the process parameters.
2. The size and distribution of defects are different inside the casting in spite the same process parameters are adopted.
3. An X-ray technique reveals its limit in detecting the presence of oxide inclusions.
4. The amount of defects influences considerably the plastic properties of the material but not the elastic characteristics.
5. A constitutive equation, $\sigma = K\varepsilon^n$, can be considered as representative of the uniform plastic behaviour of the alloy, independently of the presence of defects.
6. The defect area fraction, detected on the fracture surface of tensile test specimens, can be used to establish the fracture point along the constitutive equation.
7. A quality mapping approach can be used in high-pressure die-casting to demonstrate how the amount and type of defects, and the mechanical properties are distributed in a casting by changing the process parameters.

ACKNOWLEDGMENTS

This work was developed inside "IDEAL" Project (Integrated Development Routes for Optimised Cast Aluminium Components – Contract n. GRD2-2001-50042), supported by European Union inside Growth Programme. The authors would like to thank Ing. Mauro Sadocco for helping with the preparation and conduction of the experimental activities. Many thanks are also due to Dr. E. Blümcke and Dr. S. Nisslé for their help in the experimental work as well as to Audi Spa.

REFERENCES

1. G.O. Verran, R.P.K. Mendes and M.A. Rossi. Influence of injection parameters on defects formation in die casting Al12Si1,3Cu alloy: Experimental results and numeric simulation. *J. Mater. Process. Technol.*, 179 (2006), 190-195.
2. M. Avalle, G. Belingardi, M.P. Cavatorta and R. Doglione. Casting defects and fatigue strength of a die cast aluminium alloy: A comparison between standard specimens and production components. *Int. J. Fatigue*, 24 (2002), 1-9.
3. F. Faura, J. López and J. Hernández. On the optimum plunger acceleration law in the slow shot phase of pressure die casting machines. *Int. J. Mach. Tools Manuf.*, 41 (2001), 173-191.
4. H.I. Laukli. In *High pressure die casting of aluminium and magnesium alloys – Grain structure and segregation characteristics*. PhD thesis, Norwegian University Of Science and Technology (NTNU), Trondheim, 2004.
5. J. Campbell. *Castings*, second ed., Elsevier Butterworth-Heinemann, Oxford, 2003.
6. X. Dai, X. Yang, J. Campbell and J. Wood. Effects of runner system design on the mechanical strength of Al-7Si-Mg alloy castings. *Mater. Sci. Eng. A*, 354 (2003), 315-325.

7. X. Dai, X. Yang, J. Campbell and J. Wood. Influence of oxide film defects generated in filling on mechanical strength of aluminium alloy castings. *Mater. Sci. Technol.*, 20 (2004), 505-513.

8. C.H. Cáceres and B.I. Selling. Casting defects and the tensile properties of an Al-Si-Mg alloy. *Mater. Sci. Eng. A*, 220 (1996), 109-116.

9. A.M. Gokhale and G.R. Patel. Origins of variability in the fracture-related mechanical properties of a tilt-pour-permanent-mold cast Al-alloy. *Scripta Mater.*, 52 (2005), 237-241.

10. Q.G. Wang, D. Apelian and D.A. Lados. Fatigue behavior of A356-T6 aluminum cast alloys. Part I. Effect of casting defects. *J. Light Met.*, 1 (2001), 73-84.

11. Q.G. Wang, D. Apelian and D.A. Lados. Fatigue behavior of A356/357 aluminum cast alloys. Part II - Effect of microstructural constituents. *J. Light Met.*, 1 (2001), 85-97.

12. S. Fox and J. Campbell. Visualisation of oxide film defects during solidification of aluminium alloys. *Scripta Mater.*, 43 (2000), 881-886.

13. J.A. Francis and G.M.D. Cantin. The role of defects in the fracture of an Al-Si-Mg cast alloy. *Mater. Sci. Eng. A*, 407 (2005), 322-329.

14. A.K.M. Aziz Ahamed, H. Kato, K. Kageyama and T. Komazaki. Acoustic visualization of cold flakes and crack propagation in aluminum alloy die-cast plate. *Mater. Sci. Eng. A*, 423 (2006), 313-323.

15. E.L. Rooy. Nonferrous casting alloys – Aluminum and aluminum alloys. In: American Society of Metals (ASM), *Casting - ASM Handbook vol. 15*, ninth ed., ASM International, Materials Park, OH, 1992, pp. 743-770.

16. C.H. Cáceres, A phenomenological approach to the quality index of Al-Si-Mg casting alloys. *Int. J. Cast Metals Res.*, 12 (2000), 367-375.

17. C.H. Cáceres, A rationale for the quality index of Al-Si-Mg casting alloys. *Int. J. Cast Metals Res.*, 12 (2000), 385-391.

18. M. Drouzy, S. Jacob, M. Richard, Interpretation of tensile results by means of quality index and probable yield strength. *AFS Int. Cast Metals J.*, 5 (1980), 43-50.

ARTICLE 6

EFFECT OF SOLUTION HEAT TREATMENTS ON THE MICROSTRUCTURE AND MECHANICAL PROPERTIES OF A DIE-CAST AlSi7Mg ALLOY

G. Timelli*, O. Lohne**, L. Arnberg**, H.I. Laukli***

* Department of Management and Engineering – DTG
University of Padova
I-36100 Vicenza
ITALY

** Department of Materials Science and Engineering
Norwegian University of Science and Technology – NTNU
N-7491 Trondheim
NORWAY

*** Research & Technology Development
Hydro Aluminium Metal
N-6601 Sunndalsøra
NORWAY

Submitted for publication in: Metallurgical and Materials Transactions A, 2007

ABSTRACT
The influence of solution heat treatment time and temperature on the microstructure and mechanical properties, and mode of fracture of a high-pressure die-cast AlSi7Mg0.3 alloy is reported. Metallographic and image analysis techniques have been used to quantitatively examine the microstructural changes occurring during solution heat treatment. A solution heat treatment of 15 minutes at 475°C, or even more at 525°C, is sufficient to spheroidise the eutectic Si, as well as coarsen and increase the interparticle distance of the eutectic Si. Increasing the solutionising temperature from 475 to 525°C improves the mechanical properties.

Keywords: Aluminium alloys, AlSi7Mg, Al-Si eutectic, High-pressure-die-casting (HPDC), Heat treatment, Mechanical properties, Microstructure

1. INTRODUCTION

High-pressure die-casting (HPDC) is an efficient and economical process. When used to its maximum potential, an aluminium die-cast component may replace an assembly composed of a variety of parts produced by e.g. extrusion. Consolidation into a single die casting can significantly reduce cost and labour [1-4]. While the high velocity allows for production of thin-walled castings, the associated turbulent conditions remain the major source of interior and surface casting defects, which may have deleterious effects on the mechanical properties [5,6]. Defect-containing regions in a tensile sample reduce the load bearing area and, therefore, produce a concentration of the strain. Castings with thin sections, like those produced by HPDC technology, are vulnerable to the effect of defects since a single macro-defect can cover a significant fraction of the cross-section area. Defects, commonly found in conventional die cast components, are porosity due mainly to the entrapment of gases such as air, nitrogen, hydrogen or vapours formed by decomposition of organic die wall lubricants [1-4,7,8]. These pores, particularly those located close to the casting surface, may expand during conventional solution heat treatment, which results in unacceptable surface blisters. Therefore, the application of aluminium die-castings are often limited to non-structural components that do not require such a heat treatment. New technical evolutions of the traditional HPDC process, such as vacuum technique, pore-free and semi-solid processes, lead to the production of high integrity thin walled castings [1-4]. However, recent works have revealed a process window in which HPDC components may be heat treated without encountering blistering phenomena [7-9]. These refer to a general reduction of solution heat treatment cycle, influencing also productivity and manufacturing cost.

Various efforts have been made to investigate the effect of solution temperature and time on microstructure and mechanical properties of gravity cast AlSiMg alloys [10-16]. It was established that the magnesium and silicon contents in α-Al phase reach the maximum equilibrium level according to the alloy composition and that the distribution of magnesium and silicon becomes homogeneous within less than 1 hour of solution heat treatment. The mathematical model proposed by Rometsch *et al.* also evidences that dissolution of primary Mg_2Si particles and homogenisation of α-Al solid solution are strongly influenced by the scale of microstructure [11].

It has been reported that the solution heat treatment changes the morphology of eutectic silicon from polyhedral to globular structure and the kinetics of spheroidization and coarsening processes happen much more rapidly in the modified structure [10,12,13]. These microstructural transformations (to some extent) have an effect on ductility of the alloy, *i.e*. they increase the fracture strain, as they make it more difficult for the silicon particles to fracture [17-21].

In this study, the combined effect of solution temperature (475 and 525°C) and time (in the range 15-480 minutes) on the microstructure, tensile properties, hardness and fracture mode of a Sr-modified die cast AlSi7Mg0.3 alloy was investigated. A comparison between a short (15-60 minutes) and prolonged solution heat treatment (240-480 minutes) was then carried out, describing how the aluminium alloy diecastings may be solution heat treated at high temperature without encountering problems with blistering.

2. EXPERIMENTAL METHODS

In the present work an AlSi7Mg0.3 alloy, with chemical composition as shown in Table 1, has been used. The liquidus temperature of the alloy was determined by the

solidification model program Alstruc [22], T_{liq}= 617°C. Cast to shape specimens were produced using a multicavity die in Hydro Aluminium's Bühler SC42D cold chamber die casting machine with a locking force of 4.1 MN (Figure 1).

Table 1: Chemical composition of the AlSi7Mg alloy studied in the present work [wt.%].

Alloy	Al	Si	Fe	Mn	Mg	Ti	Sr	B
Al7SiMg	bal.	6.97	0.136	0.68	0.30	0.107	0.0280	0.0004

A detailed description of the HPDC machine, casting procedure and process parameters is given elsewhere [23,24]. Briefly, a number of 15-20 castings were scrapped after the start up to reach a quasi-steady state temperature in the shot chamber and die. Oil circulation channels in the die served for stabilising the temperature (at ~200^{o}C). Table 2 summarizes the process parameters. By means of a dynamic shot control system in the HPDC machine, every casting was documented with its shot profile to monitor the final quality and repeatability.

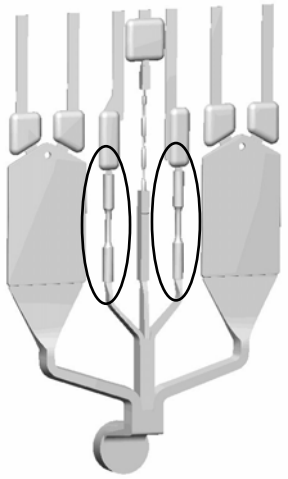

Fig. 1. Test multispecimen casting; the investigated tensile test specimens are encircled.

Table 2: Process parameters.

Parameter (piston)	Value
First phase velocity (v_1) [ms^{-1}]	0.5
Filling phase velocity (v_2) [ms^{-1}]	4.2
After pressure (P_3) [MPa]	60

The investigated round tensile test specimens are shown in Figure 1. The specimens possess a 32.5 mm gauge length and 6.4 mm diameter. Figure 2 shows the dimensions of a tensile specimen in detail. The as cast surface finish of samples was considered to be sufficiently accurate to avoid machining and only excess flash along the parting line of the die was manually removed.

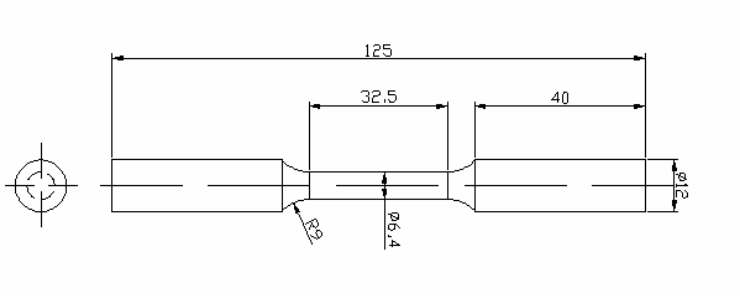

Fig. 2. Tensile test bar (dimensions in mm).

The tensile test specimens were solution heat treated in an electric resistance heated air circulating box type muffle furnace at 475°C or 525°C for 15, 60, 240 and 480 minutes (including heat up time of the specimens) and immediately quenched in water at room temperature. The temperature of the electric furnace was set and when it was stable for at least 30 minutes the tensile specimens were inserted inside the furnace. While some samples were tensile tested in the as quenched condition (T4), other specimens were artificially aged at 170°C for 8 hours after solutionising and water quenching (T6). Additional specimens were tested in T1 condition. While the T4 treated specimens were stored one day in a freezer (at ~-18°C) before conducting tensile test, the T6 treated specimens were immediately tested.

The tensile tests were done on a MTS 880 tensile testing machine. The cross-head speed used was 2 mm/min ($\dot{\varepsilon} \sim 10^{-3}$ s^{-1}). The strain was measured by using a 25 mm extensometer. At least two specimens were tested for each condition. When experimental data differed by more than 5%, another tensile specimen was tested.

Samples for microhardness measurements were ground and polished. Vickers microhardness measurements were carried out using a load of 0.05 and 0.005 kgf and 30 s dwell period according to the standard ASTM E-384. The measurements were done at 8 different locations over the cross-section of the sample and the typical standard deviation was 5 HV.

The samples were mechanically prepared to a 1 μm finish with diamond paste and finally polished with a commercial fine silica slurry (Struers OP-S) for metallographic investigations. Microstructural analysis was carried out using an optical microscope and a scanning electron microscope (SEM) equipped with an energy dispersive spectrometer (EDS), and quantitatively analysed using an image analyser (Kontron KS300). To quantify the microstructural changes during solution heat treatment, the image analysis was focused on the size, aspect ratio and interparticle spacing of the eutectic silicon particles. Size is defined as the equivalent circle diameter (d) and the aspect ratio (α) is the ratio of the maximum to the minimum Ferets. To obtain a statistical average on the distribution, a series of at least 15 photos of each specimen were taken and each measurement included more than 1000 particles. The secondary phases, such as Mg_2Si particles, and the iron-rich intermetallics were excluded from the measurements. To quantitatively calculate the eutectic area fraction in the entire cross section of tensile specimens in T1-condition, the polished specimens were etched in a modified Murakami etchant (60 ml H_20, 10 g NaOH and 5 g $K_3Fe(CN)_6$) [25]. At low magnification the α-Al phase, and the Al-

Si eutectic and intermetallics appeared white and black respectively and therefore distinguishable by quantitative metallography.

In order to study the damage after plastic strain and surface slip bands under various strength levels and strains, tensile test bars with a rectangular cross section (10 x 3 mm^2) were obtained from the central zone of the die-cast plates (included in Figure 1) and one face was metallographically polished. Figure 3 shows the dimensions of the flat tensile specimens.

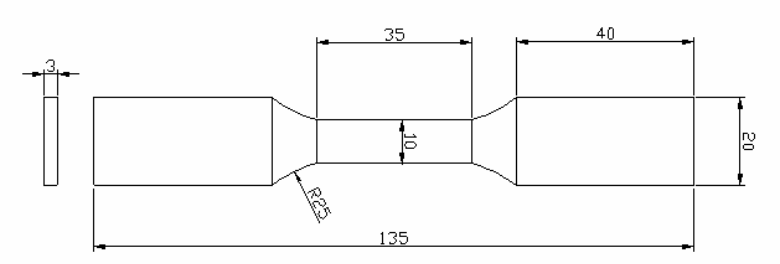

Fig. 3. Tensile test bar with rectangular cross section (dimensions in mm).

Specimens in T1-condition, as well as those solution heat treated 15, 60, 240 and 480 minutes at 525°C and aged 8h at 170°C (T6), were strained to different displacements (usually between 1 and 7%). When the total engineering strain was equal to the pre-set value, loading was immediately stopped. The specimen was then removed and observed under an optical microscope using Nomarski interference contrast to reveal the slip bands.

3. RESULTS AND DISCUSSION

3.1. Microstructural observations

A typical macrostructure in the cross-section of as die-cast samples is shown in Figure 4. The characteristic dark band follows the contour of the casting surface. Recently, Gourlay *et al.* [26] explained the formation of banded defects in solidifying high-pressure die-cast alloys applying the principles developed for cohesionless granular materials. Partially solidified alloys in HPDC conditions, i.e. under large pressures (≤ 100 MPa) and with a large number of small crystals (~10 μm), can exhibit the characteristics of a cohesionless granular material, including Reynolds' dilatancy and strain localization in dilatant shear bands. Generally in die-cast Al-Si alloys, these bands contain a segregated eutectic fraction, and their position and appearance are influenced by silicon content and solidification history [23,26,27]. In order to study how the local eutectic amount varies over the cross-section of as die cast samples, the eutectic area fraction was calculated by quantitative optical microscopy. The distribution of eutectic area fraction is overlapped to the macrostructure of a sample (Figure 4). Each data point represents the eutectic fraction in a 397x537 μm area, depicted by horizontal bars in the figure. The low eutectic area fraction, in the range of 0.25-0.35, can be due to the high solidification rate in HPDC; the system behaves as though the eutectic point is shifted to higher silicon content and the eutectic temperature is depressed [28]. The average silicon composition (at%) along the radius of a cross-sectioned sample was also measured

by means of EDS analysis in SEM (FEI Quanta 400) and plotted in Figure 4. The average silicon content was calculated in a 180x130 µm area of material. The different techniques reflect similar results and evidence a peak in the region of ~1.4 mm from the surface of casting. The arrows in the figure indicate the central position of the segregation band. These findings are in agreement with results reported in [23,26,27].

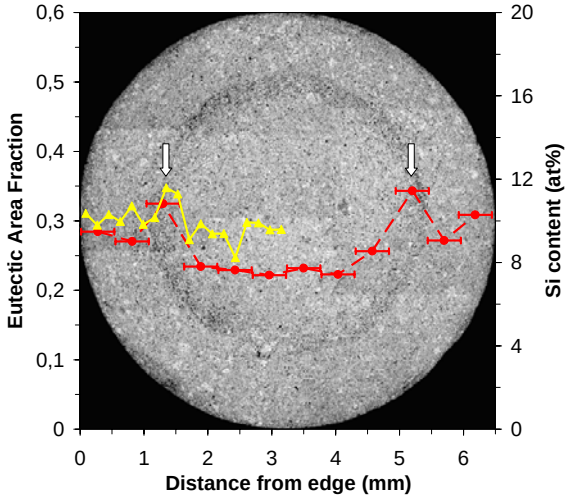

Fig. 4. Area fraction of eutectic (dashed line) and at.% Si (solid line) over the cross-section of a round tensile specimen in T1-condition. The arrows indicate the segregation band.

ESCs are observed in the cross-section of castings and their amount varies along the main axis of tensile bars. In generic die-castings a higher fraction of ESCs was observed near the gate and a lower amount was observed farther from the gate [29,30]. In a study of die-cast tensile specimens [23] it was assumed that a great fraction of ESCs did not flow into the cavity and remained in the biscuit and runner system.

Figure 5 shows typical microstructures obtained from different positions in the cross-section of die-cast samples in T1-condition. The micrographs refer to the layer near the surface of the sample (Figure 5a), the region of defect band (Figure 5b) and the centre of the casting (Figure 5c). Throughout this paper, the three different locations will be termed zones 1, 2 and 3 respectively. The grain size, characterized by means of the electron backscattered diffraction (EBSD) technique, is in the range of 10-25 µm and the primary α-Al crystals show a globular/rosette morphology. Some coarse ESCs with an elongated trunk-like morphology are present. Coarser grains are observed in the central region than in the layer near the surface of castings.

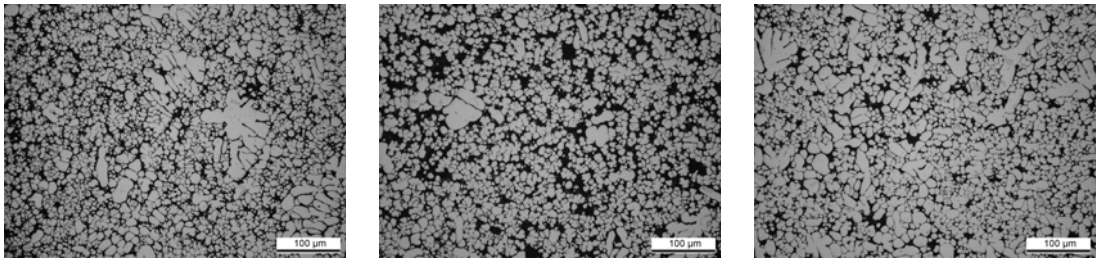

(a) (b) (c)

Fig. 5. Typical microstructures obtained from different positions in the cross-section of die-cast samples in T1-condition. a) Zone 1 (near the surface); b) zone 2 (in the segregation band); c) zone 3 (in the central region).

As expected the eutectic Si can be observed in the interdendritic regions (Figure 6). The EDS analysis revealed coarse α-Al(FeMnSi) intermetallic particles in the microstructure (Figure 7).

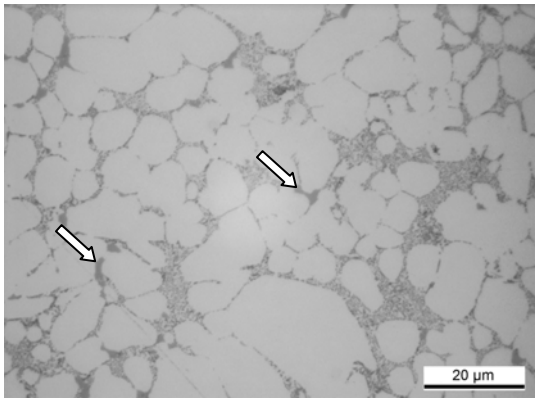

Fig. 6. Microstructure of die-cast AlSi7Mg alloy taken from zone 1 of a round tensile specimen in T1-condition. The arrows indicate α-Al(FeMnSi) intermetallic particles.

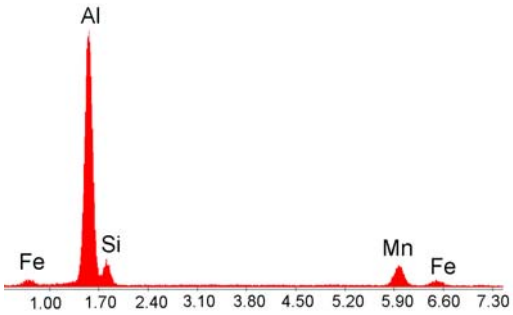

Fig. 7. EDS spectra of Fe-rich particles indicated in Figure 6.

As expected, the eutectic Si exhibits a fibrous morphology in T1-condition (Figure 8). The fineness is caused by the Sr modification and the high solidification rate. It is well established that rapid solidification changes the eutectic Si shape similar to chemically modified eutectic Si [28].

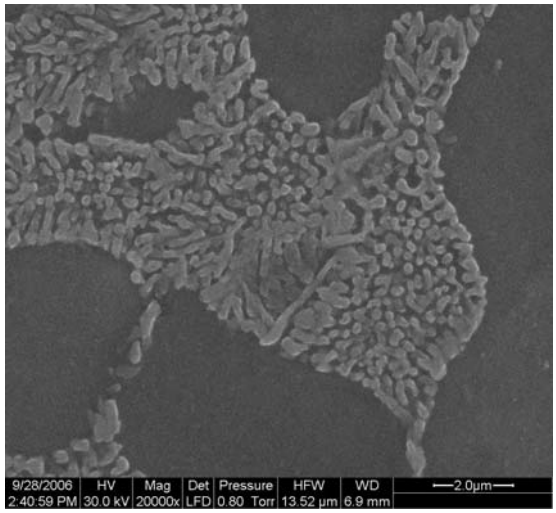

Fig. 8. Silicon crystals in the eutectic region of die-cast AlSi7Mg alloy in T1-condition. SEM micrograph in lightly etched condition.

The influence of solution heat treatment time and temperature on the microstructure of die-cast round bars is shown in Figure 9. After 15 min of solution heat treatment at 475°C, the silicon particles become coarser and the interparticle distance increases (Figure 9a). Rayleigh instability [31] occurs and silicon particles undergo necking and are broken down into fragments. Due to the instability of interfaces between two different phases and a reduction in the total interface energy, the spheroidisation and coarsening processes occur. Prolonged solution treatment of 480 min at 475°C leads to extensive coarsening of the particles with small effect on spheroidisation level (Figure 9b). The interparticle spacing increases significantly. As the coarsening and spheroidisation are diffusion controlled processes, they are directly proportional to the solution temperature. In the present investigation, heat treatment at 525°C leads to coarser silicon than the heat treatment at 475°C for every given solution time (Figure 9c-d). The α-Al(FeMnSi) intermetallic particles are not significantly affected by the solution heat treatment in the range of time and temperature used in the present work [32].

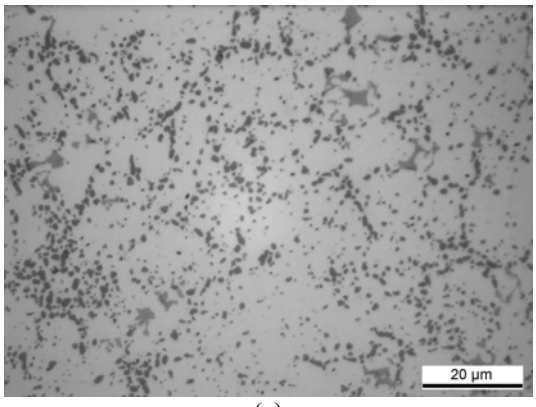

(a)

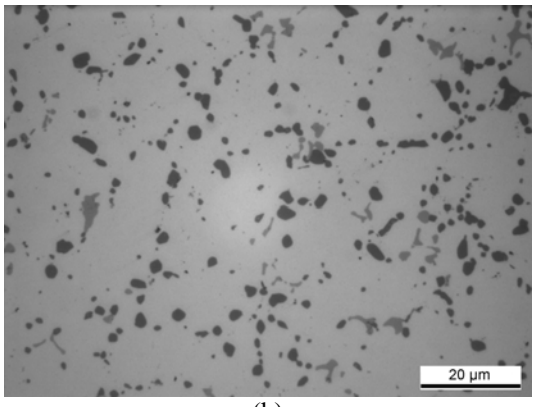

(b)

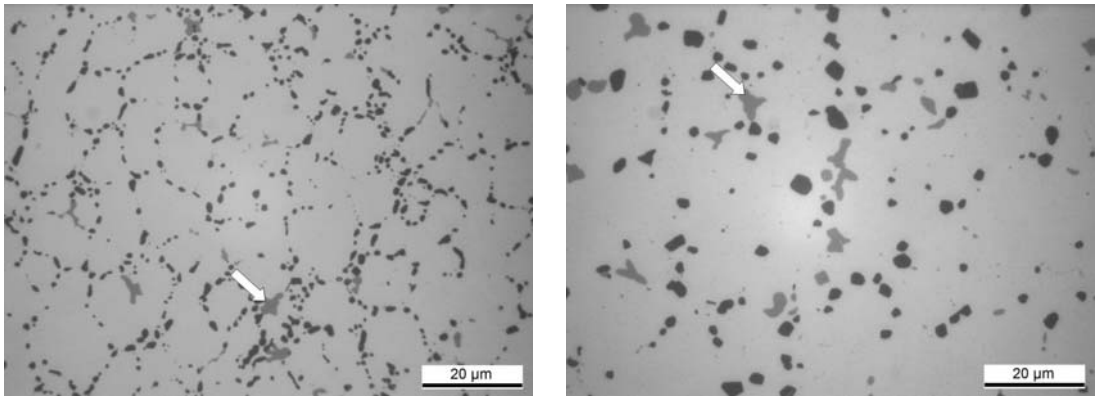

(c) (d)

Fig. 9. Microstructure of die-cast AlSi7Mg alloy after solution heat treatment. The alloy have been solutionised at 475°C for (a) 15 min and (b) 480 min, at 525°C for (c) 15 min and (d) 480 min. The arrows indicate α-Al(FeMnSi) intermetallic particles.

As demonstrated by Lumley *et al.* [7], surface blistering and discoloration of HPDC components diminish when the solution heat treatment time is reduced and/or the temperature lowered. Moreover, unacceptable distortions or cracking of complex-shaped castings can be controlled. In the present work, only the tensile test specimens solution treated 240 and 480 min at 525°C showed surface blisters (only a few), while no samples experienced significant dimensional distortions which is reasonable to expect from their geometry.

Figures 10a and b show the quantitative variation in the average Si particle diameter and the average aspect ratio as a function of solution time at 475 and 525°C. The point zero in the time axis represents the T1-condition. The analysis is focused in zones 1 and 2. Generally, the average diameter of silicon particles increases rapidly within the first 15 min at the solution temperature. Then they increase slowly with increasing solution time. Shivkumar *et al.* [13] reported a decrease in average silicon diameter after short solution treatment, before the average size increases. A similar reduction is not observed in the present work in accordance with [10,31]. As previously observed, an increased solution heat treatment temperature results in increased diffusivity of Si and therefore a rapid coarsening mechanism, where dissolution of small particles leads to growth of larger ones [33]. While Si particles show similar size in the region near the surface and in the central zone of tensile bars, the highest silicon concentration (~12 at%) in the region of segregation band leads to coarser silicon particles. Thus, the final microstructure will display a layered structure, with a different coarseness level in the distinct zones of the casting.

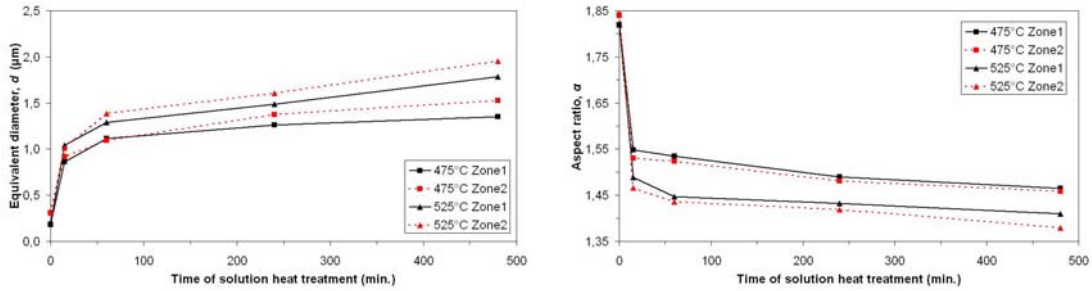

(a) (b)

Fig. 10. (a) Average diameter and (b) aspect ratio of the eutectic Si particles as a function of the solution heat treatment time at 475 and 525°C. Data refer to zones 1 and 2.

Typical growth rates have been estimated for gravity die-castings to be in the range of 0.02-0.07 μm/h. Silicon growth takes place according to the ordinary Lifshitz-Slyozow-Wagner equation [34]:

$$R^3 - R_0^3 = \frac{8}{9}\frac{DC_0\gamma V^2}{R_{gas}T}t \qquad (1)$$

Where T and t is the temperature and time, respectively, R is the radius of the particle, R_0, the initial radius at t=0, R_{gas} is the gas constant, V the molar volume, C_0 the equilibrium concentration of structures in matrix, γ the surface energy of the particle and D the diffusion coefficient [34]. In the present work this relashionship has been estimated by regression analysis, where the equivalent diameter was transformed into equivalent radius and a linear regression analysis was carried out with respect to $t^{1/3}$, using the coefficient of determination R^2 to evaluate the quality of the least-square fitting (Table 3). When R^2 equal to 1, the fit is perfect. As can be observed in Table 3, the fit is good for any solution temperature and at every position in the cross-section of samples.

Table 3: Coefficients of determination, R^2, from regression analysis of eutectic silicon equivalent radius with $t^{1/3}$. The analysis was carried in zones 1 and 2.

Position in the sample	Solution temperature (°C)	R^2
Zone 1	475	0.992
	525	0.994
Zone 2	475	0.994
	525	0.977

Up to 15 minutes of solution heat treatment there is a rapid decrease in the aspect ratio of the Si particles. The decrease is approximately 16 and 19% at solutionising temperatures of 475°C and 525°C respectively. By increasing the solutionising time from 15 to 480 minutes, there is a relatively small decrease in the aspect ratio (~5%), independently of solution temperature. The average aspect ratio values are steady in the range of 1.4-1.5, indicating a good spheroidisation level supporting the

micrographs in Figure 9. This demonstrates that a higher solutionising temperature promotes spheroidisation of eutectic Si but that solution heat treatments beyond 15 minutes at the investigated temperature have a minor effect on the extent of spheroidisation. Generally, the aspect ratios in zones 1 and 2 are quite similar.
Figures 11a and b show the distribution of Si particles in zone 1 as a function of the combined parameter *αd* for samples heat treated at various temperatures and times. Cáceres *et al.* [20] demonstrated that the eutectic Si particles in AlSiMg gravity cast alloys crack progressively with increasing applied plastic deformation and the crack is favourable for the larger and longer particles, even if the progression of particle cracking is more gradual in finer microstructure. Further, it was observed that the population of cracked particles is distributed according to the *αd* parameter, and characterised by its average *αd* value. In the present work, the particles undergo great changes in *αd* distribution after short times (15 minutes) of solution heat treatment; the fraction of particles with smaller *αd* parameter is immediately reduced while the amount of particles with greater *αd* parameter is increased. Similar changes in particle distribution are not observed by increasing the solution times, even if the distribution curves flatten with solution time and their peaks move to the right towards higher *αd* values. A comparison of the effect of temperature shows significant differences between the particles' distributions. For a given solution treatment time, increasing the solution temperature from 475 to 525°C clearly increases the fraction of Si particles with higher *αd* values.
The distributions of silicon particles in the segregation band reflect similar behaviour as in Figure 11. Comparing the results with those obtained in zone 1, the distribution curves of Si particles in zone 2 as a function of the parameter *αd* for samples heat treated at various temperatures and times shift to higher *αd* values. This can be explained with the eutectic Si behaviour. Since the Si particles in zone 2 show similar aspect ratio values as those obtained in zone 1 but higher average diameter (Figure 10), the final result is the increment of the combined parameter *αd*.

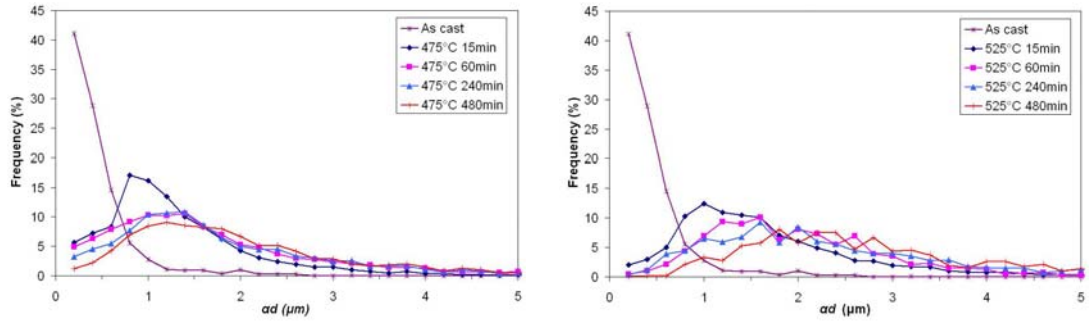

(a) (b)

Fig. 11. Frequency distribution of the combined parameter αd for eutectic silicon particles in zone 1. Data refer to solution heat treatments at (a) 475°C and (b) 525°C for different times.

In the present work the mean *αd* value of particles in zones 1 and 3 increases from ~0.36 μm, in the T1-specimens, to ~1.36 and ~2.07 μm in the specimens heat treated at 475°C for 15 and 480 min respectively. In zone 2 the increment of *αd* value is more than 130% in the first 15 min but only 57% extending the solution treatment up to 480 min. The mean *αd* value is a function of the *αd* distribution and, since the distribution curves in zone 2 shift to higher *αd* values, the average *αd* parameter

increases. Further, the αd variable is a dimensional/morphological parameter, made by the combination of the size and the aspect ratio of silicon particles, i.e. two parameters which show a different behaviour with solution temperature and time (Figure 10). In general, higher solution temperature increases the average αd parameter by more than 15%. Thus, it is reasonable to expect that the cracks initiate within the segregation bands, where the mean αd value of Si crystals is higher and coarser intermetallics [23] are observed, and the fracture then propagates in the adjacent zones 1 and 3 following a "path" of cracked finer silicon and intermetallic particles.

The measured changes of the average interparticle spacing (λ) in zones 1 and 2 during solution heat treatment at 475 and 525°C are observed in Figures 12a and b. In the present work the mean ratio Si-particle spacing to the equivalent particle diameter (λ/d) is also considered. Both of these parameters increase with increasing solution heat treatment time and/or temperature in all the examined locations of the specimens. The great increase within the first 15 min at the solution temperature of the interparticle distance confirms that the small particles are dissolved rapidly. The reduction of interparticle spacing with increasing Si content in the segregation band is observed in the present work. This is consistent with data reported in [35], where, for gravity cast AlSi alloys, at any one time of heat treatment, the interparticle distances diminished with rising silicon content and increased as the solutionising time proceeded .

The λ/d parameter considers the combined effect of increasing interparticle spacing and coarsening of neighbouring Si particles with solutionising temperature and time. Particles with small λ/d values are characterised by higher aspect ratio and fibrous morphology. Thus, high stress concentration in the α-Al matrix around the particles is expected, as well as the linking of voids nucleated at Si particles occurs at a low strain. In contrast, the increase in λ/d parameter is associated to globular Si particles, so that low stress concentration in the matrix and better load carrying capacity occurs after the void initiation [17,19,20].

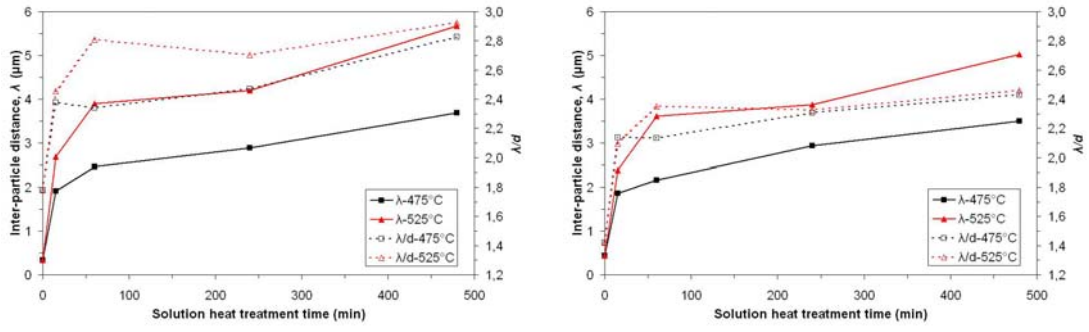

Fig. 12. Variation in average interparticle spacing (λ) and the combined parameter λ/d of eutectic silicon particles after solution treatment at different temperatures and times. Data refer to (a) zone 1 and (b) zone 2.

To investigate the influence of the amount, size and shape of eutectic Si on the variation in hardness, Vickers microhardness measurements were performed on samples in T1- and T4-condition. The indentations with a load of 0.005 kgf were positioned in the eutectic regions and in the α-Al crystals. A load of 0.05 kgf was

used to characterise the at-large hardness of zones 1 and 2. Figure 13 shows results from specimens solution heat treated at 475°C for various times. In general, the microhardness is higher in the eutectic regions than in the α-Al crystals and, due to the highest eutectic fraction, the segregation band shows higher values than the region close to the casting surface. The microhardness of the α-Al increases from ~51 $HV_{0.005}$, in T1-condition, to ~63 $HV_{0.005}$, after 15 min of solution treatment, and it remains constant with increasing solutionising time. This profile of microhardness in α-Al can be referred to the equilibrium concentration in solid solution of magnesium and silicon with solution temperature and time. Therefore, assuming that the Si and Mg concentrations in the eutectic Al remain constant (approximately equal to that of α-Al crystals), the microhardness of zones 1 and 2 is determined by the hardness of the eutectic Si. The microhardness in the eutectic regions decreases rapidly within the first 15 min of solution treatment due to the increased interparticle distance of eutectic Si. By increasing the solutionising time, the curves referred to the eutectic regions decrease with a different gradient. The different microhardness behaviour in zones 1 and 2 supports the measurements on the different coarsening level and interparticle distance of Si particles.
Generally, by increasing the solution heat treatment temperature from 475 to 525°C, the hardness in the eutectic regions and in the α-Al crystals increases markedly on samples in T4-condition; further, the microhardness profiles in these zones, as a function of solutionising time, show similar trends as in figure 13, but higher values.

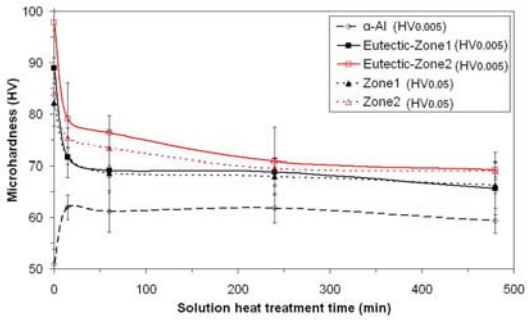

Fig. 13. Vickers microhardness measured in zones 1 and 2 of samples solution heat treated at 475°C for different times. The microhardness was measured in the α-Al crystals, the Al-Si eutectic and, at-large, in zones 1 and 2. Data refer to T4 heat treated specimens. Standard deviations are given as error bars.

3.2. Tensile testing

Figure 14 shows the mean yield strength (YS), ultimate tensile strength (UTS) and elongation to fracture as a function of solution heat treatment times at 475 and 525°C. The point zero in the time axis represents the T1-condition. The reference T1-specimens show values of 130 and 264 MPa for YS and UTS respectively, and ~10% as elongation to fracture.
With a short or long solution time at 475°C, the YS and UTS of T4-specimens are lower while at a solutionising temperature of 525°C, the strength is close to as die cast data. In the first 15 min, the average elongation to fracture reaches 11 and 16% at 475 and 525°C respectively. With increasing solution treatment time, the average elongation to fracture increases monotonically, reaching values of 19 and 21% at solution time of 480 min at 475 and 525°C respectively.

Considering the T6-condition, the YS of the specimens solution treated at 475°C slightly decreases after 15 min. The YS increases up to 208 MPa after solution time of 240 min and it is steady with extending solutionising time. The specimens solution treated at 525°C show a different YS behaviour, with an increment of ~75% in the first 15 min and maximum value (~246 MPa) reached after 60 min of solution heat treatment. Long solution treatment times do not affect the UTS of the alloy, as can be observed in figure 14b. In the first 15 min, the UTS of the specimens solution heat treated at 475°C shows similar behaviour as YS property. After 60 min of solution heat treatment at 475 and 525°C, the maximum UTS is obtained. As shown in figure 14c, while the average elongation to fracture of specimens solution treated at 475°C fluctuates slightly around 11%, it increases monotonically up to 13% for solution heat treatment of 480 min at 525°C.

As expected, the improvement of strength after the controlled precipitation of small matrix-strengthening precipitates during artificial ageing is consistent [14,36]. The reason for the increase in strength is primarily due to the precipitation of metastable β'-Mg_2Si precipitates from the supersaturated solid solution, which obstruct the movement of dislocations. Generally, from as quenched condition where the mechanical properties are principally controlled by supersaturated solid solution, the average YS and UTS increase by more than 70 and 20% in fully T6 heat treated specimens respectively. The impact is greater over YS, which is an essentially matrix-controlled parameter [36]. The strength and the hardness of the alloy after artificial ageing increase markedly when the solid solution temperature increases from 475 to 525°C, and the different Mg and Si solubility cannot explain such difference. It is reported that, while the maximum solubility of Mg is 0.3 wt% and 0.5 wt% at 475 and 525°C respectively [16,31], the solubility of Si equals to 0.7 wt% at 475°C and 1.1 wt% at 525°C [22,31]. As observed by Langsrud *et al.* [16] and Pedersen [31] for gravity cast AlSiMg alloys, an explanation can be referred to the equilibrium solubility of vacancies, which increases exponentially with temperature. Higher quenched-in vacancy concentration probably causes higher density of clusters of Si atoms, more effective clustering of Si-Mg atoms and a more efficient age hardening. The different solubility of Si at 475 and 525°C may also contribute positively.

The elongation to fracture of fully T6 heat treated specimens is lower than the corresponding T4- specimens. The increment in tensile properties of T6 treated samples is accompanied by higher amount of hardening coherent precipitates which results in increased microstresses. In turn, this factor causes lower ductility of the material which is moreover influenced by the size and the morphology of the eutectic Si [12,14,31]. Zhang *et al.* [10], Shivkumar *et al.* [13] and Pedersen [31] showed that, in T6 treated gravity cast aluminium alloys, there exists a region during the early stage of solution treatment, where the elongation to fracture of alloy reaches minimum values. This is due to a timing mismatch between an increase in strength and the changes of the characteristics of the Si particles [10]. In the present work, the maximum YS in T6-condition seems to be reached after 240 and 60 min of solution heat treatment at 475 and 525°C respectively, and the ductility of the alloy is controlled by the features of eutectic Si with extending solution time.

Similar considerations could be done for the T4-specimens. In detail, the average YS shows almost constant values (~107 and ~126 MPa at solutionising temperature of 475 and 525°C respectively) independently from solution heat treatment time and therefore the elongation to fracture continually increases due to the size and morphological changes of Si particles.

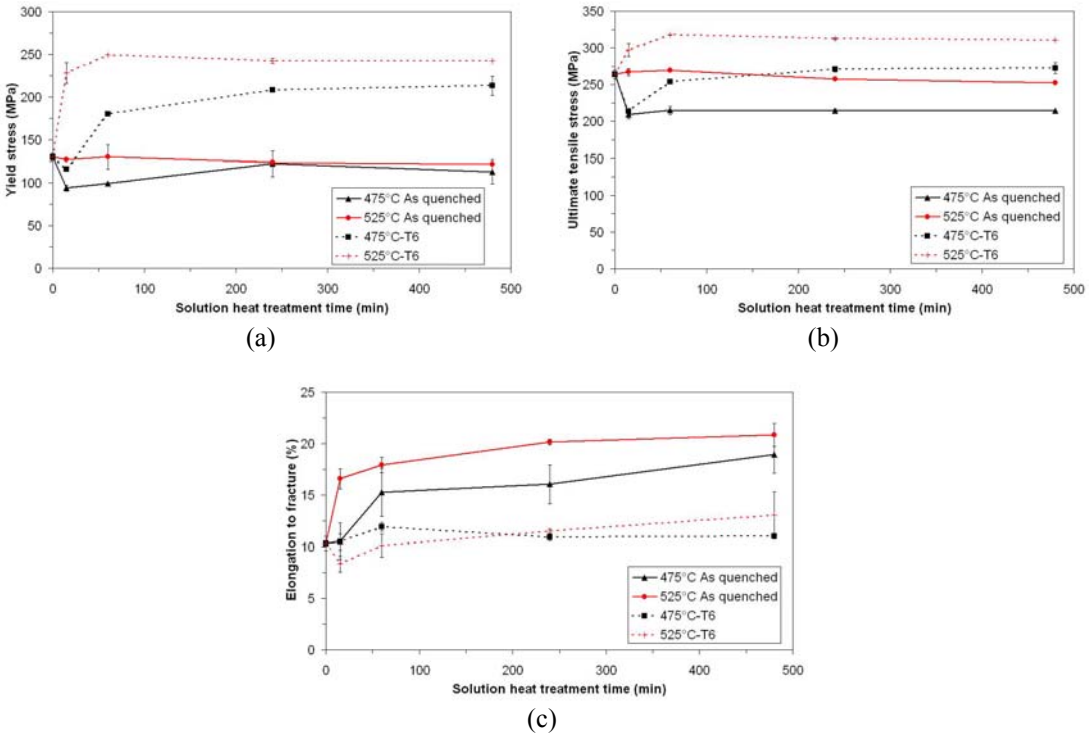

Fig. 14. Average (a) ultimate tensile stress, (b) yield stress and (c) elongation to fracture as a function of solution treatment time at 475 and 525°C. Data refer to T4- and T6 heat treated specimens. Standard deviations are given as error bars.

Figures 15 and 16 illustrate the interaction between the fracture path and the α-Al grain boundaries. The α-Al globules are defined by a high density of Si particles (Figure 8). In T1-specimens, the grain size is in the range of 10-25 μm and the α-Al globules show similar or lower dimensions (Figure 15). The grain boundaries are obstacles to slip (Figure 15). In T6 heat treated specimens, by increasing solution time or temperature, the cell structure fades and does not interrupt the slip bands, which are much longer than the α-Al cells. The eutectic silicon particles interact with the slip bands individually rather than collectively as in the case of distinct cell boundaries. Therefore, the most significant obstacles to the slip bands are again the grain boundaries (Figure 16). The grain boundaries in Figures 15 and 16 are identified by different directions in the slip traces under Nomarski interference contrast, even at high magnification observations. As demonstrated by Cáceres *et al.* [20] and Wang *et al.* [21], the interaction between grain boundaries and slip bands have consequences for cracking of eutectic Si particles during plastic straining. Brittle fracture by cleavage of Si particles is known to start at plastic strains of about 1-2% in AlSiMg cast alloys and continuing up to final fracture [20]. Plastic incompatibility between adjacent grains and, with increasing strain, the build-up of a forest of dislocations near the grain boundaries [17,20-22] make stress relaxation more difficult for silicon and intermetallic particles located at or near the grain boundaries than for isolated particles away from the grain boundaries. Particle stresses are therefore more likely to be higher near the grain boundaries, increasing the local probability of particle cracking and consequently favouring an intergranular type of fracture [22].

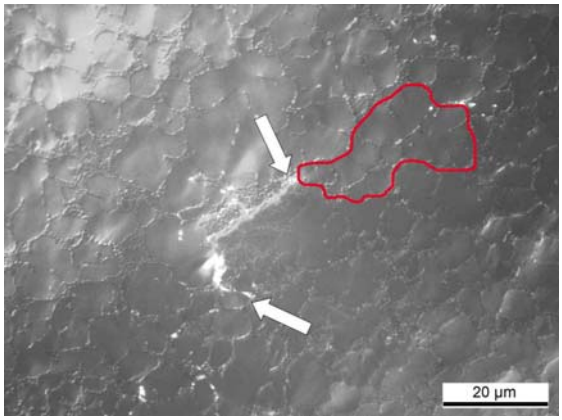

Fig. 15. Nomarski interference-contrast micrograph showing the interaction between the crack path and the grain boundaries (identified by the arrows) in a T1-specimen. A grain is marked up with a continuous red line, while the dashed arrows mark the lines separating the α-Al cells. Applied strain: 7.1%.

In general, it is observed that silicon and intermetallic particle cleavage is mainly perpendicular to the loading direction and it is easier for coarser and longer particles to crack. It has been demonstrated that the average interparticle spacing increases with solution heat treatment time and/or temperature in all the examined locations of the specimens. Therefore, in heat treated specimens, the fracture follows a path of "isolated" Si and intermetallic particles (Figure 16) rather than in T1-specimens (Figure 15) where the average interparticle spacing is lower. Decohesion at low strain on the Al matrix/α-Al(FeMnSi) and the Al matrix/Si particle interface takes also place (Figure 17). Figure 17 shows nucleation of cracks through the coalescence of adjacent microcracks created during the fracture of Si and intermetallic particles. Slip bands appear between adjacent cracks. As reported by Mishnaevsky *et al.* [18], the necking along the slip bands between the microcracks is the main mechanism for their coalescence and the microcrack coalescence is the origin of the reduction of the load-bearing area. Microcrack coalescence is observed only after slip bands have formed between them and not due to their expansion or growth.

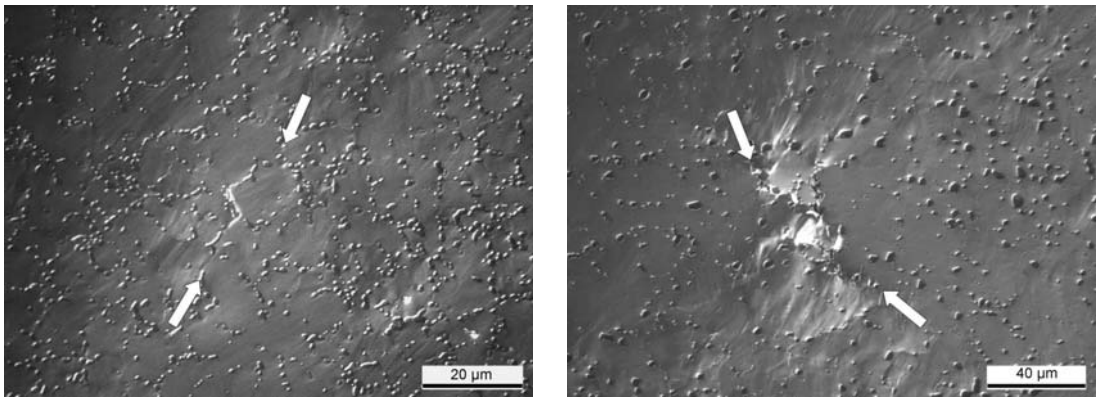

(a) (b)

Fig. 16. Nomarski-contrast micrographs showing the interaction between the crack path and the grain boundaries (identified by the arrows) in samples solutionised at 525°C for (a) 15 min and (b) 480 min, and aged at 170°C for 8h. Applied strain: 1.4%.

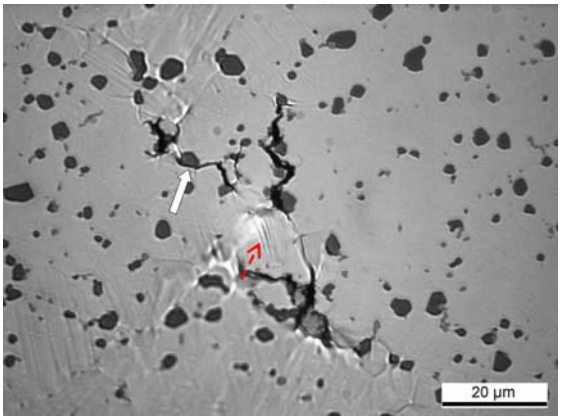

Fig. 17. Micrograph showing cracked particles in a sample deformed to 1.4% tensile strain, solution treated at 525°C for 480 min and aged at 170°C for 8h. The arrow indicates the decohesion on the Al matrix/Si particle interface. The dashed arrow shows the slip bands between adjacent cracks.

4. CONCLUSIONS

The effect of solution heat treatment time and temperature on the microstructure, tensile properties and mode of fracture of a high-pressure die-cast AlSi7Mg0.3 has been investigated. Based on the results obtained in the present study, the following conclusions can be drawn:

- A solution heat treatment of 15 min at 475°C, or even more at 525°C, causes spheroidisation, coarsening and an increase in interparticle distance of the eutectic silicon particles leading to substantial changes in the microstructure and mechanical properties.
- The distribution of the combined parameter αd of silicon particles is significantly affected by a short solution heat treatment time. The fraction of eutectic Si with smaller αd parameter is immediately reduced after a solution treatment of 15 min, while the amount of particles with greater αd parameter is increased. Similar changes in particle distribution are not observed by increasing solution times.
- Considering the T4-condition, with a short or long solution time at 475°C, the YS and UTS are lower than the as die cast values, while at solution temperature of 525°C, the strength is close to T1-data. With increasing solution treatment temperature or time, the average elongation to fracture increases monotonically.
- In the T6-condition, the YS reaches its maximum at 240 and 60 min of solution treatment at 475 and 525°C respectively. Long solution treatment times do not affect the UTS of the alloy. The improvement of strength after the controlled precipitation of small matrix-strengthening precipitates during artificial ageing is consistent.
- From as quenched condition where the tensile properties are principally controlled by supersaturated solid solution, the average YS and UTS increase by more than 70 and 20% in fully T6 heat treated condition respectively. The impact is greater over YS, which is an essentially matrix-controlled parameter.
- The strength and the hardness of the alloy after artificial ageing increase markedly when the solutionising temperature increases from 475 to 525°C.

- The ductility of T6 heat treated alloy is determined both by the size and morphology of eutectic silicon crystals and by the effect of precipitation hardening.
- The fracture mode is predominantly intergranular in T1- and T6-condition.

ACKNOWLEDGEMENTS

This work was developed inside "Marie Curie Training Sites" Project (Fellowship Contract n. HPMT-CT-2001-00305), supported by European Union inside Human Potential Programme – 5th FW Programme.

REFERENCES

1. A.C. Street, The Die Casting Book, 1986, Portcullis Press, 2ed
2. L. Andreoni, M. Case, G. Pomesano, "Quaderni della colata a pressione delle leghe di alluminio", 1995, Edimet, Brescia
3. E.J. Vinarcik, High Integrity Die Casting Processes, 2003, John Wiley & Sons, New Jersey
4. D. Apelian, M.M. Makhlouf, High Integrity Aluminium Die Casting: Alloys, Processes and Melt Preparation, North American Die Casting Association, Des Plaines, IL, 2004
5. C.H. Cáceres, B. I. Selling, Mater. Sci. Eng. A220 (1996) 109-116
6. X. Dai, X. Yang, J. Campbell, J. Wood, Mater. Sci. Technol. 20 (2004) 505-513
7. R.N. Lumley, R.G. O'Donnell, D.R. Gunasegaram, M. Givord, Mater. Sci. Forum 519-521 (2006) 351-358
8. C. Mapelli, C. Mus, M. Vedani, Metall. Ital. 7 (1999) 45-53
9. M. Vedani, C. Mapelli, Mater. Sci. Technol. 17 (2001) 938-944
10. D.L. Zhang, L.H. Zheng, D.H. StJohn, J. Light Met. 2 (2002) 27-36
11. P.A. Rometsch, L. Arnberg, D.L. Zhang, Int. J. Cast Metals Res. 12 (1999) 1-8
12. L. Pedersen, L. Arnberg, Metall. Mater. Trans. A32 (2001) 525-532
13. S. Shivkumar, S. Ricci, C. Keller, D. Apelian, J. Heat Treat. 8 (1990) 63-70
14. D.K. Dwivedi, R. Sharma, A. Kumar, Int. J. Cast Metals Res. 19 (2006) 275-282
15. J.A. Taylor, D.H. StJohn, J. Barresi, M.J. Couper, Mater. Sci. Forum 331 (2000) 277-282
16. Y. Langsrud, S. Brusethaug, ICAA6 2 (1998) 733-738
17. Jien-Wei Yeh, Wen-Pin Liu, Metall. Mater. Trans. A27 (1996) 3558-3568
18. L.L. Mishnaevsky Jr, N. Lippmann, S. Schmauder, P. Gumbsch, Eng. Fract. Mech 63 (1999) 395-411
19. C.H. Cáceres, C.J. Davidson, J.R. Griffiths, Mater. Sci. Eng. A197 (1995) 171-179

20. C.H. Cáceres, J.R. Griffiths, Acta mater. 44 (1996) 25-33
21. Q.G. Wang, C.H. Cáceres, Mater. Sci. Eng. A241 (1998) 72-82
22. A.L. Dons, E.K. Jensen, Y. Langsrud, E. Tromborg, S. Brusethaug, Metall. Mater. Trans. A30 (1999) 2135-2146
23. H.I. Laukli, C.M. Gourlay, A.K. Dahle, O. Lohne, Mater. Sci. Eng. A413-414 (2005) 92-97
24. M.C. Srivastava, O. Lohne, L. Arnberg, H.I. Laukli, H. Gjestland, Proc. High Tech Die Casting 2006, Vicenza (2006), AIM, Milano
25. G.F. Vander Voort, Metallography Principles and Practise, 1984, McGraw-Hill, New York
26. C.M. Gourlay, A.K. Dahle, Nature 445 (2007) 70-73
27. C.M. Gourlay, H.I. Laukli, A.K. Dahle, Metall. Mater. Trans. A35 (2004) 2881-2891
28. M.M. Makhlouf, H.V. Guthy, J. Light Met. 1 (2001) 199-218
29. H.I. Laukli, C.M. Gourlay, A.K. Dahle, Metall. Mater. Trans. A36 (2005) 805-818
30. H.I. Laukli, L. Arnberg, O. Lohne, Int. J. Cast Metals Res. 18 (2005) 65-72
31. L. Pedersen, PhD Thesis, Norwegian University Of Science and Technology, Trondheim, 1999
32. L. Anantha Narayanan, F.H. Samuel, J.E. Gruzleski, Metall. Mater. Trans. A26 (1995) 2161-2174
33. G.W. Greenwood, Acta Metall. 4 (1956) 243-248
34. I.M. Liftshitz, V.V. Sloyozov, J. Phys. Chem. Solids 19 (1961) 35-47
35. F.N. Rhines, M. Aballe, Met. Trans. 17A (1986) 2139-2152
36. J.A. Taylor, D.H. StJohn, J. Barresi, M.J. Couper, Int. J. Cast Metals Res. 12 (2000) 419-430